DEVELOPMENT OF SURFACE PROTEIN PATTERNS TO MODIFY ASTROCYTE RESPONSE AND REACTIVITY

by

Tony Wentai Hsiao

A dissertation submitted to the faculty of
The University of Utah
in partial fulfillment of the requirements for the degree of

Doctor of Philosophy

Department of Bioengineering

The University of Utah

May 2015

The University of Utah Graduate School

STATEMENT OF DISSERTATION APPROVAL

The dissertation of **Tony Wentai Hsiao**

has been approved by the following supervisory committee members:

Vladimir Hlady	, Chair	**03/17/2015** Date Approved
Kuberan Balagurunathan	, Member	**03/18/2015** Date Approved
Maureen Condic	, Member	**03/18/2015** Date Approved
Jindrich Kopecek	, Member	**03/18/2015** Date Approved
Patrick Tresco	, Member	**03/18/2015** Date Approved

and by **Patrick Tresco**, Chair of

the Department of **Bioengineering**

and by David B. Kieda, Dean of The Graduate School.

ABSTRACT

Spinal cord injury is debilitating and patients have historically had little hope for functional recovery. Astrocytes forming the scar tissue and producing chondroitin sulfate proteoglycan (CSPG) were often identified as the chief culprits for inhibiting neuronal regeneration. However, as the complex role of astrocytes in spinal cord injury are increasingly understood, the benefits they provide for healing have become valuable tools towards promoting recovery. Inducing aligned astrocyte populations in the wound site may promote functional recovery outcomes. Many approaches have been researched for restoring signaling after spinal cord injury, but artificial nerve guidance devices are particularly interesting as they can provide lasting directional cues to the injury site.

The goal of this research was to demonstrate and measure the impact of surface protein patterns on astrocyte reactivity in an effort to reduce their neuron-inhibitory CSPG production. By quantifying CSPG expression as measure of astrocyte reactivity, no change in reactivity was seen with varying amounts of fibrinogen surface coverage. However, astrocytes were found to selectively remove adsorbed fibrinogen from glass surfaces from amongst other proteins and also secrete CSPG onto surfaces. To mitigate protein pattern removal, a cross-linked patterning method based on microcontact printing was developed to attach protein patterns to collagen gels. Protein patterns were first created on

glass and transferred to collagen by gelling collagen directly on top of the pattern. This construct was then peeled off from glass to create free standing collagen sheets with one patterned surface. Stripe patterns of various extracellular matrix molecules were thus patterned and found to align astrocytes on collagen gel surfaces and reduced astrocyte CSPG expression. To understand how astrocytes interact with surface patterns, astrocyte morphology was measured in real time. This revealed that astrocytes prefer adhesion to laminin over aggrecan and will shift their cell bodies accordingly. Astrocytes initially extend multiple processes upon attachment and span the largest distances when presented with mixed adhesion cues, up to 150 micrometers. Collectively, this research demonstrates the importance of surface protein patterns in biasing astrocyte behavior and provides a new technique for further modifications of collagen hydrogels for use as nerve guidance materials.

For my family.

TABLE OF CONTENTS

LIST OF ABBREVIATIONS

AGG.....Aggrecan

ANOVA ..... Analysis of variance

BBB..... Blood–brain barrier

BDNF .....Brain-derived neurotrophic factor

BSA.....Bovine serum albumin

BSB.....Blood–spine barrier

CAD .....Computer-aided design

CCD ..... Charge-coupled device

ChABC.....Chondroitinase ABC

CNS ..... Central nervous system

CS..... Chondroitin sulfate

CSF..... Cerebrospinal fluid

CSPG.....Chondroitin sulfate proteoglycan

DAPI .....4',6-Diamidino-2-phenylindole

DDI..... Double-distilled deionized water

DIC..... Differential interference contrast

DMEM/F12.....Dulbecco's modified eagle medium: nutrient mixture F-12

DRG.....Dorsal root ganglion

ECM.....Extracellular matrix

EGFR ..... Epidermal growth factor receptor

FBG ..... Fibrinogen

FBS ..... Fetal bovine serume

FDA ..... Food and Drug Administration

FGF ..... Fibroblast growth factor

FN ..... Fibronectin

FWHM ..... Full-width half-maximum

GAG ..... Glycosaminoglycan

GDNF ..... Glial cell-derived neurotrophic factor

GFAP ..... Glial fibrillary acidic protein

GRP ..... Glial restricted precursor

IgG ..... Immunoglubulin G

LN ..... Laminin

LPS ..... Lipopolysaccharide

MSC ..... Mesenchymal stem cell

NCAM ..... Neural cell adhesion molecule

NGC ..... Nerve guidance conduit

NGF ..... Nerve growth factor

NT-3 ..... Neurotrophin-3

NO ..... Nitrous oxide

PBS ..... Phosphate buffered saline

PCL ..... Poly(caprolactone)

PDMS ..... Polydimethylsiloxane

PFA.....Paraformaldehyde

PGA ..... Poly(glycolic acid)

pHEMA ..... Poly(hydroxyethylmethacrylate)

PLA.....Poly(lactic acid)

PLGA ..... Poly(lactic acid-co-glycolic acid)

PNS .....Peripheral nervous system

PTPσ.....Protein tyrosine phosphatase

SCI..... Spinal cord injury

TGF-β ..... Transforming growth factor β

TNF-α..... Tumor necrosis factor α

μCP.....Microcontact printing

ACKNOWLEDGEMENTS

I would like to thank my advisor Dr. Vladimir Hlady for his guidance and providing the opportunity to do this research. I would also like to thank Dr. Patrick Tresco for allowing me to use his laboratory. I would like to thank all the members of my committee for their suggestions and advice for completing this work. I am grateful to the numerous fellow students and scholars I have worked alongside for their help along the way.

I would like to thank my family for their support and love. Most importantly, I would like to thank my wife and dearest friend, Margaret, for supporting me in this endeavor while gracefully handling the demands of career, education, and motherhood.

CHAPTER 1

INTRODUCTION

1.1. Spinal Cord Injury and Inflammation

The mammalian central nervous system (CNS) is largely ineffective at repairing or regenerating functional tissue after injury. Due to the role of the CNS in signaling and sensing, this loss of motor and sensory function leads to dramatic detriment to the quality of life of affected individuals. Spinal cord injury (SCI) is particularly impactful as individuals may require lifelong medical aids to compensate for the loss of control of basic physiologic functions, including respiration, bladder and bowel function, and ambulation. According to the National SCI Statistical Center, an estimated 12,500 SCIs occur each year and 276,000 people are living with SCI in the United States. Vehicular accidents and falls account for 68% of all SCI, with violent acts and sports collisions accounting for another 23% of cases. Males account for 79% of SCI patients. The average patient will incur treatment costs ranging from $300,000 to $1,000,000 for the first year of treatment and $40,000–$180,000 per subsequent year depending on injury severity. Around 30% of SCI patients must be rehospitalized in a given year. Ultimately, life expectancies for SCI patients are dramatically reduced, with

complications from pneumonia and septicemia being the most common[1]. To date, no treatment has proven completely successful in restoring full spinal cord functionality after SCI[2].

Poor regenerative ability was once thought to be intrinsic to CNS neurons themselves, but even adult neurons retain some regenerative ability, albeit less than younger cells[3,4]. The unique cellular responses that occur in the CNS wound environment contribute to the lack of neuronal repair. The process of wound healing in the mammalian CNS has several well-documented stages. Initial injury is similar to that of other tissues with the first processes being tissue trauma, ischemia, blood vessel compromise, and local hemorrhage. This is the acute phase of the injury. The CNS is normally immune privileged and separated from general blood exposure with the blood–brain barrier (BBB) or analogous blood–spine barrier (BSB). Once damage has occurred, the infiltration of blood molecules and cells triggers cascades of behavioral changes in each of the major cell types in the CNS. Figure 1.1 summarizes the timing of these wound healing events after SCI occurs, which are separated into three periods: acute (seconds to minutes after SCI), secondary or sub-acute (minutes to weeks after SCI), and chronic (lasting from months to years after SCI)[5].

Neurons that are severed form a retractive endball proximal to the injury and severed distal portions of axons degenerate. Furthermore, neurons associated with the wound undergo apoptosis and Wallerian degeneration[6,7]. Without axons making synaptic connections, signaling ceases, which leads to the primary symptoms of SCI. Neuronal death continues after hemostasis has been

established as macrophages begin the work of clearing cellular debris. This signals the beginning of the secondary or sub-acute response. It is during this secondary phase that the most damage is done to CNS tissue and macrophages mediate much of this secondary injury[8]. These phagocytotic cells have been shown to come from two sources: derived from monocytes in circulating blood and from a resident population in CNS tissue, known as microglia[9]. Microglia become activated immediately along with neutrophils from leaked blood. Monocytes are then recruited to the site. Both of these cell groups begin producing cytokines, proteases, free radicals, and neurotoxic enzymes[5,10].

Microglia and macrophages are also capable of neuroprotective behavior in addition to neurotoxicity. Therefore, the complexity of macrophage reactivity is difficult to compartmentalize. A single stimulus, zymosan or lipopolysaccharide (LPS), injected into the spinal cord can cause macrophages to simultaneously damage and protect neurons[11]. To distinguish between macrophage actions, there have been efforts to characterize cell populations. Macrophages have been historically categorized into M1 and M2 groups of activation for classic and alternative pathways, respectively. Some have suggested further divisions to further clarify the spectrum of macrophage behavior[12–14], but research on the impact of macrophages on the CNS has largely relied on M1/M2 characterizations. In general, M1 activated macrophages present a more proinflammatory phenotype and inhibit cell proliferation typified by nitrous oxide (NO) production; M2 macrophages are thought to promote tissue repair via ornithine expression[15]. These roles have also been distinguished in the

recovering CNS[16]. Additionally, M2-macrophage-conditioned media had a demonstrated influence on promoting neurons to overcome growth barriers[17]. M1 microglia and macrophages tend to dominate the secondary phase of SCI healing[18]. By inducing a greater amount of M2 activated microglia, more nerve tracts were preserved after SCI[19].

The origin of the macrophages also plays a role in their response to SCI. Macrophages entering the region from blood have been identified as instigators of the inflammatory injury to neurons[20]. Another detrimental effect of non-resident macrophages is their promotion of fibrous scar formation[21]. However, there is also evidence that blood-origin macrophages and their secretion of interleukin-10 in the wound site is helpful in reducing inflammation and promoting some motor recovery[22]. One potential factor for the multiple roles of monocyte-derived macrophages is the timing at which they enter the injury site as they respond to differing signals from resident cells[23]. Migrating M2 macrophages were shown to enter the wound milieu through cerebrospinal fluid (CSF) and blocking their ability to enter led to impaired motor recovery[24]. As reviewed by Oyinbo, secondary injury has numerous mechanisms for damaging CNS cells, including the triggering of apoptosis, ionic imbalance, neurotransmitter excess, and free radical and reactive oxide production[25]. Likewise, the onset of secondary injury is most likely the earliest period where interventions may be clinically staged. In humans, initial activation of microglia occurs 1–3 days after injury as evidenced by acquisition of amoeboid phenotypes and coincides with monocyte infiltration. Evidence of elevated macrophage levels via CD68 staining

persists from weeks to months post-injury[26]. Microglia from adult human cortex were compared to those in mice and were found to have very similar morphological characteristics, suggesting that these may be well conserved across species[27]. Once the chronic stage of the injury response is reached, macrophage activity is reduced and neurons begin to resprout axons[5].

The myelin sheathing cells of the CNS, oligodendrocytes, are also susceptible to secondary damage and have been observed to undergo apoptosis after SCI; their remnants are largely phagocytosed by macrophages[28]. This loss of oligodendrocytes is concomitant with neuronal death[29] and has a detrimental effect on the ability of neurons to transmit action potentials. Oligodendrocyte precursors residing in the CNS have the ability to remyelinate neurons, but this activity is inhibited by a class of molecules known as chondroitin sulfate proteoglycans (CSPGs) produced after injury[30,31]. Neurotrophin-3 (NT-3) and brain-derived neurotrophic factor (BDNF) were both found to promote oligodendrocyte remyelination after SCI[32]. M2 macrophages have also been shown to promote oligodendrocyte differentiation and remyelination[33].

1.2. Astrocytes and the Glial Scar

The most abundant cells in the CNS, astrocytes, undergo a process known as astrogliosis or reactive gliosis where cells begin profound morphological and physiological changes after injury[34]. In the prechronic phases of SCI response, astrocytes begin to reestablish the BSB and are able to

reduce the extravasation of larger blood products although some leakage of smaller molecules remains up to 4 weeks later[5]. Astrocytes do not proliferate immediately after injury, but do so rapidly after the acute phase of injury has passed. This proliferation only persists for around 1 week, after which the expression of cell-cycle markers is limited[35]. Many resident astrocytes also die as a result of the inflammatory environment produced by macrophages[8,36], although human astrocytes do not demonstrate caspase-3-mediated apoptosis after SCI[28]. The loss of tissue leads to the formation of a necrotic cavity, which is then either encircled or infiltrated by reactive astrocytes[8,37]. These reactive astrocytes persist into the chronic phases of healing, and eventually these hypertrophied, reactive astrocytes are the dominant cell type present in the wound site[36]. In humans, reactive astrogliosis exhibits only slight glial fibrillary acidic protein (GFAP) upregulation, which peaks around 4 months after injury and is reduced to baseline levels after 1 year[26].

The stable meshwork of reactive astrocyte tissue is known as the glial scar[38,39]. The disorganized glial scar stands in stark contrast to the well-organized and aligned astrocytes found in intact spinal cord tissue. It has been shown that neurons follow these longitudinal astrocyte processes in healthy spinal cord[40]. It is thought that the random, disorganized state of astrocytes in the glial scar is a contributing culprit to failed neuronal regeneration, as neurons are known to be sensitive to topographical cues[41]. The extent of the scar has been historically identified via GFAP, an intermediate filament of the cytoskeleton, and vimentin expressed in reactive astrocytes[34,42]. The glial scar has been

found to delimit the extent of axonal processes around injury sites and this inhibition has been attributed to both its lack of physical, directional support as well as upregulation of CSPGs[43]. Chondroitin sulfate (CS) proteoglycans are composed of a core protein molecule with CS sugar chains attached. CSPGs are another hallmark of astrocyte reactivity and astrocytes have been shown to express multiple types of CSPGs after SCI, including neurocan, phosphacan, brevican, versican, and aggrecan[44–48]. While macrophages, oligodendrocytes, and oligodendrocyte precursors also produce some CSPG in the SCI wound site[48,49], astrocytes are the key producers of these molecules.

The CSPGs expressed by astrocytes have been viewed as the chief components of the extracellular matrix (ECM) responsible for neuron inhibition in the glial scar[50]. The functions of CSPGs, however, are not always inhibitory and are still being explored[51,52]. Astrocyte CSPG production has been shown to be triggered by transforming growth factor β (TGF-β) available from blood fibrinogen (FBG). As the BBB is compromised after injury, the influx of FBG initiates the creation of this neuron inhibitory ECM[53]. An additional function of CSPG expressed by astrocytes in the glial scar may be influencing macrophage activation[54]. By inhibiting CSPG synthesis with a xyloside immediately after injury, macrophage cytokine expression favored necrosis and led to more tissue loss. Conversely, by applying xyloside 2 days after injury to inhibit CSPG production after the initial burst led to improved neuronal recovery[54].

It is clear astrocytes are a very heterogeneous population, and, like macrophages in the inflammatory response, it is overly simplistic to characterize

astrocyte reactivity solely as positive or negative for wound healing[55–57]. Astrocytes have been found to exhibit differing forms of reactivity in response to different triggers[35], thus astrocytes are capable of a spectrum of behaviors during astrogliosis.

The mere presence of astrocytes in the scar does not cause the failure of neurons to regenerate. In fact, reactive astrocytes have been shown to be vital in protecting CNS tissues from further damage after injury[58]. This protective nature of astrocytes is due to their ability to secrete neurotrophic factors as well as their ability to balance other signaling molecules[59]. For example, astrocytes scavenge excess glutamate and prevent excitotoxicity[60,61]. It has been shown that in the brain, newly differentiated astrocytes migrate to wound sites to perform neuroprotective functions after injury from the subventricular zone in the brain[62]. Thus, the relationships between astrocytes and the wound environment are still not fully understood. Since astrocytes do play beneficial roles, the effort to reduce inhibitory effects while maintaining the positive influence of astrocytes is a promising approach to improving SCI repair.

1.3. SCI Treatments

There are multiple approaches to treating SCI. The injection of methylprednisolone soon after acute injury to combat some of the impact of secondary inflammation has been approved by the Food and Drug Administration (FDA), but the efficacy of this treatment has been criticized[63,64]. To improve outcomes, there are currently 668 clinical trials in the United States aimed at

improving SCI recovery (clinicaltrials.gov, December 2014). The goals for supporting regeneration and repair after SCI include protecting remaining neurons, decreasing inhibition in the injury ECM, increasing permissive signals to augment growth, providing physical support, and reinforcing cell populations[2,65]. Growth-promoting biomaterials, stem cell transplants, tissue engineered constructs, tissue grafts, pharmaceutical agents, and drug-delivery devices may all potentially improve SCI recovery. In the present work, I focus on the application of prefabricated biomaterials. The benefits of this approach include better control over material properties, increased potential for off-the-shelf availability, and reduction in processing time compared with more complex and cell-based systems. However, artificial biomaterials lack the signals and structures found in either natural tissue or with native cells as well as the continued, dynamic support that can occur with living tissues. Ideally, the utilization of such materials could be combined with other available techniques in the future, as the largest likelihood for success comes from combinatorial tactics[66]. While regrown nerve tracts are not always necessary for improved function[67], evidence indicates that directional neuronal growth that spans the injury can contribute positively to functional recovery[68–70].

Pharmaceutical applications have been promising. As CSPG was identified as the chief inhibitory culprit in the glial scar, the use of chondroitinase ABC (ChABC), an enzyme that digests the CS side chains off of the protein cores in CSPGs, has been used extensively[71,72]. Rats that had ChABC administered after spinal cord hemisection above the diaphragm were able to

recover respiratory function[73]. The application of this enzyme presents challenges as well. The optimal delivery method, timing, and stability will need to be resolved. Thermal stability of ChABC is also a challenge for sustained activity[74,75]. Likewise, the core proteins of proteoglycans left behind after ChABC digestion have also been shown to contribute to neuronal inhibition[44,76]. The alternative approach for mitigating CSPG inhibition has been to interfere with neuronal receptors for CSPG, including Nogo receptors[77] and protein tyrosine phosphatase (PTPσ)[78]. Recently, a PTPσ–mimetic peptide was developed and shown to improve neuronal recovery with systemic delivery[79].

Cell therapies have also been appealing as cells can provide appropriate growth factors, binding molecules, and physical guidance cues necessary for neurons to allow directional regrowth. Many cell types have been pursued, including nerve grafts, stem cells, Schwann cells, and precursors[2,65]. However, application of stem cells carries inherent ethical concerns regarding cell sourcing and the potential for tumorigenesis[80,81]. Interestingly, one potential reason progenitor and precursor cells are effective is actually an induced increase in astrocyte activity[82]. Recent progress in a human patient has been reported where olfactory ensheathing cells were implanted into a spinal cord transection. The implantation surgery removed the resident glial scar and also added autologous nerve grafts in conjunction with the olfactory cells. After 19 months, evaluation showed improvement in muscle mass, stability, and partial recovery of sensation and voluntary movement below the injury[83].

Of particular note, astrocytes have also been an attractive cell population to treat SCI due to their positive effects towards tissue repair. An early experiment demonstrated that applying embryonic astrocytes on cellulose supports aided dorsal root axon growth back into astrocyte grey matter[84]. Neonatal astrocytes seeded within collagen gels also increased neuronal fibers that were associated with the transplanted cells. This led to modest improvements in locomotion[85]. Astrocytes differentiated with BDNF from precursors were found to be beneficial to functional recovery after SCI in adult rats. These cells were seeded in collagen gels without any particular directional bias. Their presence led to a net positive increase in neuronal outgrowth. While likely still producing CSPG and other potentially inhibitory molecules, their supportive aspects allowed for 60% of severed axons to regrow[68]. These results have also been supported using astrocytes derived from human precursor cells[86,87]. Differentiated human astrocytes without any scaffold have also been used, but showed no increased motor recovery after injection into spinal cord contusion. There was, however, some improvement in sensory function and reduction in scar formation as the cells migrated and proliferated to fill in the wound cavity[88]. A key feature as to the success of younger or differentiated astrocytes could be in a decrease in their inhibitory nature. The injection of differentiated astrocytes in medium into a contusion wound in the spinal cord led to a reduced amount of GFAP and CSPG expression[89]. Another potential benefit of using young cells is their plasticity and ability to reverse phenotypes[87]. As Chu et al. reviewed, astrocyte transplantation is a

multifaceted problem and details regarding cell population and transplantation timing must be considered to understand the efficacy of astrocytes as a therapeutic treatment[90].

Cell therapy has also been coupled with implantable devices with directional channels to provide trophic and physical support for nerve repair[91,92]. Another enticing alternative implantable device is microelectrodes. Recent work with the use of implanted electrodes for epidural stimulation has allowed four human males to control voluntary motor functions in the lower extremities distal to the injury site. As this approach has demonstrated, there may be spared nerve tracts after SCI even with complete loss of motor and sensory functions[93].

1.4. Nerve Guidance Device Design

Inspired by the success of artificial guidance devices in aiding neuronal regeneration in peripheral nervous system (PNS) injuries, nerve guidance devices have been tested to repair SCIs. Most human SCIs are of a contusion nature, meaning some spinal cord tissue is potentially undamaged as opposed to damage to all nerve tracts in a complete transection. Thus, the application of nerve guidance devices may be an overly invasive clinical procedure depending on the severity of injury. Any device interventions used to improve neuronal regeneration will also unavoidably cause surgery-associated damage to CNS tissues. A subsequent concern after intervention is then the mediation of the CNS inflammatory response triggered by the insertion and the presence of these

foreign bodies. However, the application of such devices provides a unique potential benefit as currently no pharmaceutical or injectable material can provide cellular-level directional information during the healing process. They also serve as valuable tools for researching the behavioral mechanisms of CNS cells to injury and correlating tissue regrowth to functional outcomes.

In addition to restarting the CNS injury cascade, an additional complication for an implanted support device arises from the fact that device surfaces will be adsorbed with fibrinogen after blood contact. As previously mentioned, this blood molecule initiates CSPG production cascades in astrocytes. It remains unclear, however, whether astrocytes respond to FBG after it has physically adsorbed to a surface with its associated conformational changes. Similarly, the presence of FBG at the device-astrocyte interface may cause astrocytes to increase CSPG expression. In Chapter 2, I investigated the astrocyte CSPG response to FBG adsorbed to glass surfaces to gain insight on these quandaries. If FBG presence causes devices to be increasingly neuron inhibitory, perhaps precoating devices with alternative proteins or designing materials to minimize FBG adsorption would improve neuronal regeneration on the device. My hypothesis was that astrocytes would still recognize FBG even after adsorption and that increasing the amount of FBG exposure would lead to a coinciding increase in CSPG expressed on astrocyte surfaces as indicated by immunocytochemistry. The CS-56 antibody has been correlated with inhibition of neuronal outgrowth and is a core contributor of the poor recovery seen in SCI[43].

The working basis of grafts and nerve guidance conduit (NGC) devices is to provide a substrate for regenerating nerves to grow upon and thereby facilitate the reconnection of severed nerve tracts. NGCs can also isolate the recovering nerve tissue from foreign cells and cytokines[94]. Application of such devices in SCI models have shown that CNS neurons can regenerate through given constructs like their PNS counterparts[95]. As mentioned earlier, timing is an important factor for glial scar maturation. NGC–based treatment will likely target individuals in the chronic phases of recovery with developed glial scars, a niche that is not well served with acute treatment methods. There has been prolific improvement on these guidance devices from basic tube shapes to those containing grooves, multiple lumens, or nanofibers. These NGCs also have been supplemented with the addition of ECM proteins (laminin [LN], fibronectin [FN], collagen)[96], growth factors (e.g. glial cell-derived neurotrophic factor [GDNF], nerve growth factor [NGF])[95], and the aforementioned cell-seeding. Cell treatments are particularly potent as the cell populations provide physical support as well as both soluble and insoluble signals to regenerating neurons. Stem cells (mesenchymal stem cell [MSC], glial-restriced precursor [GRP]), as well as support cells (Schwann Cells, astrocytes) have all been shown to improve regeneration compared with scaffold materials alone[86,97–99].

There are several key factors to consider while designing a CNS NGC which have been well reviewed. These include mechanical strength, porosity, degradation, electrical conductivity, cell interaction, growth factors, and directional cues[66,94]. As summarized in Figure 1.2, many of these design

parameters function to increase neuronal viability as well as provide directional cues.

Bioresorpable and biodegradable materials are often considered the most viable materials for NGCs as persistent devices can lead to continued cellular response and compression syndromes[100]. Popular biodegradable material choices besides collagen include the poly(α-hydroxyacids) family of polymers, which comprises poly(glycolic acid) (PGA), poly(lactic acid) (PLA), poly(lactic acid-co-glycolic acid) (PLGA), and poly(lactide-co-caprolactone) (PCL), as well as chitosan and poly(β-hydroxybutyrate)[66]. Collagen is expressed after SCI in forms I, III, and IV. While collagen may form a barrier to regrowth[101], there is evidence that collagen itself does not contribute to axonal inhibition during SCI recovery[102–105]. Fibroblasts from surrounding tissues likely contribute some of this collagen, but astrocytes themselves can produce it in many of its various types[105–107]. As a regenerative biomaterial for SCI, functional recovery and neuronal outgrowth have been shown through collagen biomaterials in in vivo SCI models[67,108–110].

There have been multiple approaches to improve bioactivity and neuronal guidance with collagen-based NGCs. Application of collagen by gelling in-situ provides more robust neuronal growth through collagen[111]. The physical alignment of collagen into nanofibers also promotes directional neuronal outgrowth[112]. The chemical addition of brain-derived neurotrophic factor (BDNF) and antagonists to epidermal growth factor receptor (EGFR) to oriented collagen fibers restored synaptic connections in rats across a 6 mm spinal cord

transection[113]. Another example of a synergistic approach to adding additional bioactivity to collagen was the addition of neurotrophin-3 and ChABC to collagen nanofibers. These devices provided topographical cues, reduced inhibition, and added growth signals all in one and were shown to sustain dorsal root ganglion (DRG) outgrowth in vitro[72]. Even when co-gelled with potentially inhibitory chondroitin-6-sulfate, collagen still supported spinal cord neuron penetration[114]. Collagen has been a popular material for numerous applications for neural guidance devices as it has demonstrated biocompatibility and the ability for local cells to remodel and degrade the material[91,115,116]. Collagen has also been extensively tested to allow for control over physical properties, including porosity and stiffness [117,118]. With such extensive research history and documented results, I chose collagen as a model biomaterial for my studies in Chapter 3.

1.5. Influence of Surface Cues

The surface of an NGC is an important factor for determining how the device interfaces with the body. As expected, macrophages are active at the surface of CNS implants. Macrophages have been shown to encapsulate conduits made from genipin-linked gelatin by 8 weeks post-implantation[119], thus giving another impetus for biodegradable materials to reduce chronic inflammatory responses. Similarly, macrophages and multinucleated cells have been found to surround and infiltrate fibrillar PLGA/PCL implants[120]. Macrophages were found to infiltrate and surround poly(hydroxyethylmethacrylate) (pHEMA) scaffolds 1 week after implantations,

though their presence was markedly decreased after 4 weeks. This corresponded with a similar trend for CSPG expression around the implant even while astrocyte GFAP levels remained relatively constant[121]. Because of this, any surface patterns or cues must resist modification or removal from the surface in order to have prolonged efficacy past the initial inflammatory response.

Importantly, neurons are highly sensitive to surface cues. In a study of DRG on collagen type I, DRG enclosed between glass with a directional pattern and the gel preferentially followed the surface pattern. It was also shown that the majority of neurons grew on the surface of the gel rather than penetrate into it[122]. The use of grooved surfaces has been shown to guide neurite extension, as neurites will follow the grooves in a parallel fashion if the grooves have sufficiently large features (around 0.2 μm)[41,123] . Similarly, incorporation of fibers on the surface has shown potent guidance of neuron outgrowth[41]. Finally, ECM protein stripes have been shown to align and direct neurons[124].

Glia are also impacted by surface properties. Oriented PCL fibers have been shown to direct oligodendrocyte migration along surfaces[125]. Astrocytes also align on surfaces with grooved topography[126]. Astrocytes and microglia decrease both rates of proliferation and migration when confronted with 4.7 μm pillars on PDMS but are not impacted by pillars that are 0.5 μm tall[127]. Interestingly, fibers have also been shown to guide astrocytes and increase their rate of migration onto NGCs. Hurtado et al. formed sheets with PLA fibers that were rolled up to produce an NGC that had surface topography to aid neurons in bridging a SCI. The authors observed improved function and neuronal outgrowth

that was correlated with increased astrocyte migration onto the device. From this observation, the authors suggest that neurons present pioneering growth cones after which astrocytes follow in their supportive role. While not necessarily causal, this in vivo finding demonstrates that astrocytes will interact with the NGC surface and that functional recovery occurs with their presence[128].

As regenerating neurons will extend growth cones to sample the environment, it will be beneficial to combine multiple cues to promote correct directional growth. This type of synergy has recently been demonstrated where the application of electrical stimulation on DRG neurons grown on aligned PLA fibers led to an increase in outgrowth compared to either the electrical or topographical stimulus alone[129]. Astrocytes are an ideal candidate for the role of neuron guide as they provide both physical and molecular surface cues for alignment. As astrocytes are the dominant cell type at chronic healing phases, the ability to establish a supportive, directive tissue in place of the glial scar could provide long-lasting information to regenerating neurons.

While surface topography has been readily applied to NGC research, aligned surface protein patterns have only begun to be explored as novel printing techniques are developed. Such protein patterns printed onto glass surfaces have been shown to align astrocytes in vitro[130,131]. Surface-based cues are particularly appealing as they can be added to existing biomaterial platforms and can eventually utilize complex patterning techniques. One particular challenge presented by using soft materials is that deformation makes microcontact printing difficult[132]. To investigate whether surface patterns that have been effective at

aligning astrocytes on glass remain so when presented on a NGC material, I developed a technique to place directional protein patterns onto the surface of collagen type I in Chapter 3. I hypothesized that utilizing a bifunctional crosslinker, I could physically attach ECM protein patterns first created on glass to collagen as it was gelled on top of the patterns. I anticipated that the spatial placement of molecules would impart similar effects on aligning astrocytes as seen on patterned glass.

Fibers often rely on the addition of ECM components to improve cell affinity and increase their efficacy[133]. This equates to aligned ECM molecules in conjunction with topography. My present work allows direct placement of ECM components in aligned patterns and, while lacking topography, creates opportunities for placement of multiple molecules in controlled amounts and variations in patterns. There have been several techniques for patterning surfaces of soft substrates with protein patterns. These include polydimethylsiloxane (PDMS), polyvinyl alcohol, and polyacrylamide[132,134–136]. Recent work has also demonstrated controlled patterning onto PCL fibers[137]. Utilizing freeze-drying, Matrigel® and gelatin can also be directly printed with proteins[138]. Several of these techniques would be amenable to patterning materials for future NGC research, including those developed in this work.

1.6. Positive Effects of Astrocyte Alignment

In addition to the myriad positive impacts of astrocytes described above, aligned astrocytes have also demonstrated the ability to guide subsequent neuronal growth beyond simple topographical contact guidance. Clearly, the presence of astrocytes with their thicker nuclear regions and extended processes provide topographical information to neurons. This effect has been successfully repeated on materials that mimic astrocyte topography by casting upon cell layers. Cell-inspired computer-aided design (CAD) patterns also provided neurons with topography-mediated guidance[139]. However, these physical cues are also accompanied by numerous chemical signals expressed by astrocytes, including laminin (LN), fibronectin (FN), neural cell adhesion molecule (NCAM), and N-Cadherin[140]. In healthy spinal cord tissue, astrocytes, which are aligned and organized, are potent directors of neuron outgrowth and are co-localized with directed nerve tracts[141,142]. Laminin has been commonly used for guidance studies and is expressed by astrocytes[143]. Fibronectin has also been shown to be important for aiding transitional binding to LN [144]. FN is also important for astrocyte-mediated guidance of regenerating neurons and is found to be colocalized with axons[130,145]. Astrocytes have been aligned in vitro using electric fields[146], topography[126], protein patterns[130], and mechanical force[147]. Intuitively, because astrocytes are pivotal to maintaining healthy cellular environments for neurons, their presence on NGCs could potentially benefit neuronal response.

It has been shown that aligned astrocytes cause neurons to follow their growth directions and also to extend longer outgrowth[126,130,147]. Even in a reactive state as evidenced by positive GFAP and CSPG staining, aligned astrocytes permit and direct robust neuron outgrowth in vitro. This behavior continues even after astrocytes have been fixed, signifying that cell-associated factors also contribute to guidance in addition to active astrocytic processes[130]. To further understand how aligned astrocytes result in increased neuron outgrowth, studies on the influence of alignment on astrocyte physiology have been performed. Culturing astrocytes on a grooved poly(methylmethacrylate) substrate led to a decrease in GFAP expression in astrocytes. While few cells adhered, there was marked alignment of astrocytes and decreased cell viability and proliferation[148]. Similarly, astrocytes cultured on PCL nanofibers had diminished GFAP reactivity, although they did demonstrate increased adhesion on these surfaces[149]. Astrocytes grown on collagen nanofibers also exhibited similar behavior with an increase in astrocyte elongation and decreased GFAP expression 3 and 7 days post-injury. When placed in vivo as a rolled NGC, these devices demonstrated little GFAP staining within the spiral lumen of the device when compared with the device borders[112]. This result indicates either little astrocyte infiltration or maintenance of less reactive phenotypes.

In vitro evidence indicates that aligned astrocytes may also aid NGC function. Artificial collagen constructs containing physically aligned astrocytes align subsequent neuronal outgrowth on those collagen gels[147]. Additionally, when associated with DRG neurons, astrocytes that are given a stimulus to

migrate away were shown to stretch, dislodge, and even tear neuronal processes during their migration[8]. Therefore, preserving an intact astrocyte structure would prevent this type of neuronal loss. When neurons were placed on astrocytes aligned by grooved PCL with features 12.5 or 25.0 μm in width, neuron outgrowth was aligned with the “buried” topography and persisted for 3 weeks. Besides this directionality, it is vital to note that neurons simply cultured on the grooved PCL surfaces did not survive longer than 1 week[150]. Therefore, stimulating a population of aligned astrocytes in the SCI wound could allow for improved neuronal survival and directional growth. There has been conflicting evidence of this based on in vivo observations of the population of NGCs by astrocytes. Collagen-based fibers planted into the spinal cord showed little infiltration of GFAP positive cells even though neurons did extend onto the device[113,151]. Conversely, a PLA–nanofiber NGC had astrocyte process extension concurrently with neuronal growth[128]. The same lab further explored the impact of their fibers on astrocyte behavior and found that astrocytes aligned by fibers had increased migration rates and neuroprotective glutamine uptake rates[133]. They also showed that aligned fibers increased astrocyte cellular extensions to 200 μm.

As mentioned above, surface patterning with directional patterns of ECM molecules such as LN and FN is effective for aligning astrocytes, although surface patterned NGCs have yet to be tested in vivo. A study varying the width of stripes in patterns for aligning confluent astrocyte layers revealed the best alignment with 50 μm stripes of laminin, the widest stripe available for their study,

with 17 μm spacing between them[152]. Additionally, 15 μm stripe and spacing patterns also aligned astrocytes and transferred directional information through multiple astrocyte layers[130]. Thus, the ability to guide initial astrocyte attachment and growth could subsequently bias the implant surface to align additional astrocyte tissue layers and be more permissive for subsequent neuronal regeneration. While such evidence indicates a general size range for astrocyte aligning patterns, I wished to observe how astrocytes interact with surface patterns and the extent of their cellular extensions to understand the size of patterns that these cells can encounter upon attachment to a surface. In Chapter 4, I observed individual astrocytes with time-lapse microscopy as they attached to surfaces. The captured images allowed quantification of astrocyte spans and migration rates. As cellular behavior will likely be dependent on underlying molecules, I used mixed gradients of laminin, which is traditionally adhesion permissive, and aggrecan, a neuron inhibitory CSPG, to test how astrocytes attached and moved on patterned substrates. I hypothesized that in the process of sampling the surface, astrocytes would prefer to attach to laminin over CSPG.

1.7. Dissertation Overview

As the roles of astrocytes in SCI are increasingly understood, the benefits they provide toward recovery have reduced the previously negative perception once held towards them. Direct injection and scaffold-based applications of astrocytes have resulted in improvement in SCI outcomes in vivo. There is also

cellular evidence that the efficacy of a neuron promoting NGC material is in part due to guidance of astrocytes that concurrently populate the devices. Numerous in vitro studies have demonstrated the ability of astrocytes to both improve neuronal outgrowth distance and provide directionality. This effect may be partly attributed to astrocytes having a reduction in reactivity when grown in a directional environment. Astrocytes will be prevalent in the glial scar that forms after injury and after implantation. By designing materials to reduce astrocyte CSPG expression, neurons may have one less barrier towards recovery.

The goal of this research was to demonstrate and measure the impact of surface protein patterns on astrocyte reactivity in an effort to reduce neuron-inhibitory CSPG production. To complete this endeavor, I first correlated CSPG expression in astrocytes as a token indicator of reactivity resultant from TGF-β exposure in Chapter 2. By inhibiting TGF-β type I activin receptor-like kinase receptors, CSPG production was decreased[153]. Interestingly, I found that astrocytes specifically identify FBG and selectively remove it from the glass surfaces from amongst other adsorbed blood proteins regardless of downstream signaling. While varying densities of FBG patterned on surfaces had no clear effect on overall CSPG production, I observed that astrocytes preferentially secreted CSPG onto FBG contacting surfaces.

As directional surface protein patterns decrease astrocyte inhibition of neurons on glass, I patterned collagen hydrogels with similar designs to investigate the impact of patterns on CSPG expression. A cross-linked patterning method based on microcontact printing was developed in Chapter 3 to prevent

astrocyte removal of patterns, as seen in Chapter 2, from the collagen. Protein patterns on glass can be cross-linked and transferred to collagen by allowing gelling on top of the pattern and then using a peel-off technique to create free collagen sheets bearing the pattern on one surface. Stripe patterns of various ECM molecules aligned astrocytes on gel surfaces and reduced overall astrocyte CSPG expression[154]. This new method allows for the translation of any protein pattern developed on glass to be transferred to collagen.

Lastly, astrocyte attachment and migration were measured in real time to understand astrocyte substrate preference and their morphological characteristics as they initially interact with patterned surfaces. Such measurements may inform future pattern designs for guiding astrocyte attachment and alignment. Random dot gradients of mixed cues were developed to assess surface protein preference for astrocyte adhesion[155]. These measurements revealed that astrocytes prefer adhering to laminin over aggrecan, a CSPG, and will shift their cell bodies to do so. These findings also showed that astrocytes initially spread multiple processes upon attachment and are capable of spanning an average of 150 micrometers to sample surface patterns. These largest spans occured when astrocytes were presented with a choice for underlying substrate.

1.8. References

[1] National Spinal Cord Injury Statistical Center. Facts and Figures at a Glance 2014.

[2] Thuret S, Moon LDF, Gage FH. Therapeutic interventions after spinal cord injury. Nat Rev Neurosci 2006;7:628–43. doi:10.1038/nrn1955.

[3] Richardson PM, McGuinness UM, Aguayo AJ. Axons from CNS neurones regenerate into PNS grafts. Nature 1980;284:264–5. doi:10.1038/284264a0.

[4] Condic ML. Adult neuronal regeneration induced by transgenic integrin expression. J Neurosci 2001;21:4782–8.

[5] Donnelly DJ, Popovich PG. Inflammation and its role in neuroprotection, axonal regeneration and functional recovery after spinal cord injury. Regen Rehabil Spinal Cord Inj 2008;209:378–88. doi:10.1016/j.expneurol.2007.06.009.

[6] Zhang Z, Guth L. Experimental Spinal Cord Injury: Wallerian Degeneration in the Dorsal Column Is Followed by Revascularization, Glial Proliferation, and Nerve Regeneration. Exp Neurol 1997;147:159–71. doi:10.1006/exnr.1997.6590.

[7] Liu XZ, Xu XM, Hu R, Du C, Zhang SX, McDonald JW, et al. Neuronal and glial apoptosis after traumatic spinal cord injury. J Neurosci 1997;17:5395–406.

[8] Fitch MT, Doller C, Combs CK, Landreth GE, Silver J. Cellular and Molecular Mechanisms of Glial Scarring and Progressive Cavitation: In Vivo and In VitroAnalysis of Inflammation-Induced Secondary Injury after CNS Trauma. J Neurosci 1999;19:8182–98.

[9] Aguzzi A, Barres BA, Bennett ML. Microglia: Scapegoat, Saboteur, or Something Else? Science 2013;339:156–61. doi:10.1126/science.1227901.

[10] Zhou X, He X, Ren Y. Function of microglia and macrophages in secondary damage after spinal cord injury. Neural Regen Res 2014;9:1787.

[11] Gensel JC, Nakamura S, Guan Z, van Rooijen N, Ankeny DP, Popovich PG. Macrophages promote axon regeneration with concurrent neurotoxicity. J Neurosci 2009;29:3956–68.

[12] Martinez FO, Sica A, Mantovani A, Locati M. Macrophage activation and polarization. Front Biosci J Virtual Libr 2008;13:453.

[13] Murray PJ, Allen JE, Biswas SK, Fisher EA, Gilroy DW, Goerdt S, et al. Macrophage Activation and Polarization: Nomenclature and Experimental Guidelines. Immunity 2014;41:14–20. doi:10.1016/j.immuni.2014.06.008.

[14] Condeelis J, Pollard JW. Macrophages: Obligate Partners for Tumor Cell Migration, Invasion, and Metastasis. Cell 2006;124:263–6. doi:10.1016/j.cell.2006.01.007.

[15] Mills C. M1 and M2 Macrophages: Oracles of Health and Disease 2012;32:463–88.

[16] David S, Kroner A. Repertoire of microglial and macrophage responses after spinal cord injury. Nat Rev Neurosci 2011;12:388–99. doi:10.1038/nrn3053.

[17] Kigerl KA, Gensel JC, Ankeny DP, Alexander JK, Donnelly DJ, Popovich PG. Identification of two distinct macrophage subsets with divergent effects causing either neurotoxicity or regeneration in the injured mouse spinal cord. J Neurosci 2009;29:13435–44.

[18] Loane DJ, Byrnes KR. Role of Microglia in Neurotrauma. Neurother J Am Soc Exp Neurother 2010;7:366–77. doi:10.1016/j.nurt.2010.07.002.

[19] Stirling DP, Cummins K, Mishra M, Teo W, Yong VW, Stys P. Toll-like receptor 2-mediated alternative activation of microglia is protective after spinal cord injury. Brain 2013. doi:10.1093/brain/awt341.

[20] Popovich PG, Guan Z, Wei P, Huitinga I, van Rooijen N, Stokes BT. Depletion of Hematogenous Macrophages Promotes Partial Hindlimb Recovery and Neuroanatomical Repair after Experimental Spinal Cord Injury. Exp Neurol 1999;158:351–65. doi:10.1006/exnr.1999.7118.

[21] Zhu Y, Soderblom C, Krishnan V, Ashbaugh J, Bethea JR, Lee JK. Hematogenous macrophage depletion reduces the fibrotic scar and increases axonal growth after spinal cord injury. Neurobiol Dis 2015;74:114–25. doi:10.1016/j.nbd.2014.10.024.

[22] Shechter R, London A, Varol C, Raposo C, Cusimano M, Yovel G, et al. Infiltrating blood-derived macrophages are vital cells playing an anti-inflammatory role in recovery from spinal cord injury in mice. PLoS Med 2009;6:e1000113.

[23] London A, Cohen M, Schwartz M. Microglia and monocyte-derived macrophages: functionally distinct populations that act in concert in CNS plasticity and repair. Front Cell Neurosci 2013;7:34. doi:10.3389/fncel.2013.00034.

[24] Shechter R, Miller O, Yovel G, Rosenzweig N, London A, Ruckh J, et al. Recruitment of Beneficial M2 Macrophages to Injured Spinal Cord Is Orchestrated by Remote Brain Choroid Plexus. Immunity 2013;38:555–69. doi:10.1016/j.immuni.2013.02.012.

[25] Oyinbo CA. Secondary injury mechanisms in traumatic spinal cord injury: a nugget of this multiply cascade. Acta Neurobiol Exp (Warsz) 2011;71:281.

[26] Fleming JC, Norenberg MD, Ramsay DA, Dekaban GA, Marcillo AE, Saenz AD, et al. The cellular inflammatory response in human spinal cords after injury. Brain 2006;129:3249–69. doi:10.1093/brain/awl296.

[27] Torres-Platas SG, Comeau S, Rachalski A, Bo GD, Cruceanu C, Turecki G, et al. Morphometric characterization of microglial phenotypes in human cerebral cortex. J Neuroinflammation 2014;11:12.

[28] Emery E, Aldana P, Bunge MB, Puckett W, Srinivasan A, Keane RW, et al. Apoptosis after traumatic human spinal cord injury. J Neurosurg 1998;89:911–20.

[29] Casha S, Yu W., Fehlings M. Oligodendroglial apoptosis occurs along degenerating axons and is associated with FAS and p75 expression following spinal cord injury in the rat. Neuroscience 2001;103:203–18. doi:10.1016/S0306-4522(00)00538-8.

[30] Siebert JR, Stelzner DJ, Osterhout DJ. Chondroitinase treatment following spinal contusion injury increases migration of oligodendrocyte progenitor cells. Exp Neurol 2011;231:19–29. doi:10.1016/j.expneurol.2011.05.002.

[31] Siebert JR, Osterhout DJ. The inhibitory effects of chondroitin sulfate proteoglycans on oligodendrocytes. J Neurochem 2011;119:176–88. doi:10.1111/j.1471-4159.2011.07370.x.

[32] McTigue DM, Horner PJ, Stokes BT, Gage FH. Neurotrophin-3 and brain-derived neurotrophic factor induce oligodendrocyte proliferation and myelination of regenerating axons in the contused adult rat spinal cord. J Neurosci 1998;18:5354–65.

[33] Miron VE, Boyd A, Zhao J-W, Yuen TJ, Ruckh JM, Shadrach JL, et al. M2 microglia and macrophages drive oligodendrocyte differentiation during CNS remyelination. Nat Neurosci 2013;16:1211–8.

[34] Sofroniew MV. Molecular dissection of reactive astrogliosis and glial scar formation. Trends Neurosci 2009;32:638–47. doi:10.1016/j.tins.2009.08.002.

[35] Zamanian JL, Xu L, Foo LC, Nouri N, Zhou L, Giffard RG, et al. Genomic analysis of reactive astrogliosis. J Neurosci 2012;32:6391–410.

[36] Dusart I, Schwab ME. Secondary Cell Death and the Inflammatory Reaction After Dorsal Hemisection of the Rat Spinal Cord. Eur J Neurosci 1994;6:712–24. doi:10.1111/j.1460-9568.1994.tb00983.x.

[37] Popovich PG, Wei P, Stokes BT. Cellular inflammatory response after spinal cord injury in sprague-dawley and lewis rats. J Comp Neurol 1997;377:443–64. doi:10.1002/(SICI)1096-9861(19970120)377:3<443::AID-CNE10>3.0.CO;2-S.

[38] Barrett CP, Guth L, Donati EJ, Krikorian JG. Astroglial reaction in the gray matter of lumbar segments after midthoracic transection of the adult rat spinal cord. Exp Neurol 1981;73:365–77. doi:10.1016/0014-4886(81)90272-7.

[39] Li Y, Raisman G. Sprouts from Cut Corticospinal Axons Persist in the Presence of Astrocytic Scarring in Long-Term Lesions of the Adult Rat Spinal Cord. Exp Neurol 1995;134:102–11. doi:10.1006/exnr.1995.1041.

[40] Davies SJA, Goucher DR, Doller C, Silver J. Robust Regeneration of Adult Sensory Axons in Degenerating White Matter of the Adult Rat Spinal Cord. J Neurosci 1999;19:5810–22.

[41] Hoffman-Kim D, Mitchel JA, Bellamkonda RV. Topography, Cell Response, and Nerve Regeneration. Annu Rev Biomed Eng 2010;12:203–31. doi:10.1146/annurev-bioeng-070909-105351.

[42] Chiu F-C, Norton WT, Fields KL. The Cytoskeleton of Primary Astrocytes in Culture Contains Actin, Glial Fibrillary Acidic Protein, and the Fibroblast-Type Filament Protein, Vimentin. J Neurochem 1981;37:147–55.

[43] Silver J, Miller JH. Regeneration beyond the glial scar. Nat Rev Neurosci 2004;5:146–56. doi:10.1038/nrn1326.

[44] Schmalfeldt M, Bandtlow CE, Dours-Zimmermann MT, Winterhalter KH, Zimmermann DR. Brain derived versican V2 is a potent inhibitor of axonal growth. J Cell Sci 2000;113:807–16.

[45] Afshari FT, Kwok JC, White L, Fawcett JW. Schwann cell migration is integrin-dependent and inhibited by astrocyte-produced aggrecan. Glia 2010;58:857–69. doi:10.1002/glia.20970.

[46] Yamada H, Fredette B, Shitara K, Hagihara K, Miura R, Ranscht B, et al. The Brain Chondroitin Sulfate Proteoglycan Brevican Associates with Astrocytes Ensheathing Cerebellar Glomeruli and Inhibits Neurite Outgrowth from Granule Neurons. J Neurosci 1997;17:7784–95.

[47] Jones LL, Margolis RU, Tuszynski MH. The chondroitin sulfate proteoglycans neurocan, brevican, phosphacan, and versican are differentially regulated following spinal cord injury. Exp Neurol 2003;182:399–411. doi:10.1016/S0014-4886(03)00087-6.

[48] Jones LL, Yamaguchi Y, Stallcup WB, Tuszynski MH. NG2 is a major chondroitin sulfate proteoglycan produced after spinal cord injury and is expressed by macrophages and oligodendrocyte progenitors. J Neurosci 2002;22:2792–803.

[49] Rhodes KE, Raivich G, Fawcett JW. The injury response of oligodendrocyte precursor cells is induced by platelets, macrophages and inflammation-associated cytokines. Neuroscience 2006;140:87–100. doi:10.1016/j.neuroscience.2006.01.055.

[50] Busch SA, Silver J. The role of extracellular matrix in CNS regeneration. Curr Opin Neurobiol 2007;17:120–7. doi:10.1016/j.conb.2006.09.004.

[51] Laabs T, Carulli D, Geller HM, Fawcett JW. Chondroitin sulfate proteoglycans in neural development and regeneration. Curr Opin Neurobiol 2005;15:116–20. doi:10.1016/j.conb.2005.01.014.

[52] Swarup VP, Hsiao TW, Zhang J, Prestwich GD, Kuberan B, Hlady V. Exploiting Differential Surface Display of Chondroitin Sulfate Variants for Directing Neuronal Outgrowth. J Am Chem Soc 2013;135:13488–94. doi:10.1021/ja4056728.

[53] Schachtrup C, Ryu JK, Helmrick MJ, Vagena E, Galanakis DK, Degen JL, et al. Fibrinogen Triggers Astrocyte Scar Formation by Promoting the Availability of Active TGF-β after Vascular Damage. J Neurosci 2010;30:5843–54. doi:10.1523/JNEUROSCI.0137-10.2010.

[54] Rolls A, Shechter R, London A, Segev Y, Jacob-Hirsch J, Amariglio N, et al. Two faces of chondroitin sulfate proteoglycan in spinal cord repair: a role in microglia/macrophage activation. PLoS Med 2008;5:e171.

[55] Anderson MA, Ao Y, Sofroniew MV. Heterogeneity of reactive astrocytes. Astrocytes Inj Brain Gliosis Adapt Mal 2014;565:23–9. doi:10.1016/j.neulet.2013.12.030.

[56] Raivich G, Bohatschek M, Kloss CUA, Werner A, Jones LL, Kreutzberg GW. Neuroglial activation repertoire in the injured brain: graded response, molecular mechanisms and cues to physiological function. Brain Res Rev 1999;30:77–105. doi:10.1016/S0165-0173(99)00007-7.

[57] Cahoy JD, Emery B, Kaushal A, Foo LC, Zamanian JL, Christopherson KS, et al. A transcriptome database for astrocytes, neurons, and oligodendrocytes: a new resource for understanding brain development and function. J Neurosci 2008;28:264–78.

[58] Faulkner JR, Herrmann JE, Woo MJ, Tansey KE, Doan NB, Sofroniew MV. Reactive astrocytes protect tissue and preserve function after spinal cord injury. J Neurosci 2004;24:2143–55.

[59] Rolls A, Shechter R, Schwartz M. The bright side of the glial scar in CNS repair. Nat Rev Neurosci 2009;10:235–41. doi:10.1038/nrn2591.

[60] Hertz L, Zielke HR. Astrocytic control of glutamatergic activity: astrocytes as stars of the show. Trends Neurosci 2004;27:735–43. doi:10.1016/j.tins.2004.10.008.

[61] Cui W, Allen ND, Skynner M, Gusterson B, Clark AJ. Inducible ablation of astrocytes shows that these cells are required for neuronal survival in the adult brain. Glia 2001;34:272–82. doi:10.1002/glia.1061.

[62] Benner EJ, Luciano D, Jo R, Abdi K, Paez-Gonzalez P, Sheng H, et al. Protective astrogenesis from the SVZ niche after injury is controlled by Notch modulator Thbs4. Nature 2013;497:369–73.

[63] Hurlbert RJ. Methylprednisolone for acute spinal cord injury: an inappropriate standard of care*. J Neurosurg Spine 2000;93:1–7.

[64] Sayer FT, Kronvall E, Nilsson OG. Methylprednisolone treatment in acute spinal cord injury: the myth challenged through a structured analysis of published literature. Spine J 2006;6:335–43. doi:10.1016/j.spinee.2005.11.001.

[65] Willerth SM, Sakiyama-Elbert SE. Cell therapy for spinal cord regeneration. Adv Drug Deliv Rev 2008;60:263–76. doi:10.1016/j.addr.2007.08.028.

[66] Straley K, Foo C, Heilshorn S. Biomaterial design strategies for the treatment of spinal cord injuries. J Neurotrauma 2010;27:1–19.

[67] Houweling DA, Lankhorst AJ, Gispen WH, Bär PR, Joosten EAJ. Collagen Containing Neurotrophin-3 (NT-3) Attracts Regrowing Injured Corticospinal Axons in the Adult Rat Spinal Cord and Promotes Partial Functional Recovery. Exp Neurol 1998;153:49–59. doi:10.1006/exnr.1998.6867.

[68] Davies J, Huang C, Proschel C, Noble M, Mayer-Proschel M, Davies S. Astrocytes derived from glial-restricted precursors promote spinal cord repair. J Biol 2006;5:7.

[69] Grill R, Murai K, Blesch A, Gage FH, Tuszynski MH. Cellular Delivery of Neurotrophin-3 Promotes Corticospinal Axonal Growth and Partial Functional Recovery after Spinal Cord Injury. J Neurosci 1997;17:5560–72.

[70] Teng YD, Lavik EB, Qu X, Park KI, Ourednik J, Zurakowski D, et al. Functional recovery following traumatic spinal cord injury mediated by a unique polymer scaffold seeded with neural stem cells. Proc Natl Acad Sci 2002;99:3024–9. doi:10.1073/pnas.052678899.

[71] Bradbury EJ, Moon LDF, Popat RJ, King VR, Bennett GS, Patel PN, et al. Chondroitinase ABC promotes functional recovery after spinal cord injury. Nature 2002;416:636–40. doi:10.1038/416636a.

[72] Liu T, Xu J, Chan BP, Chew SY. Sustained release of neurotrophin-3 and chondroitinase ABC from electrospun collagen nanofiber scaffold for spinal cord injury repair. J Biomed Mater Res A 2012;100A:236–42. doi:10.1002/jbm.a.33271.

[73] Alilain WJ, Horn KP, Hu H, Dick TE, Silver J. Functional regeneration of respiratory pathways after spinal cord injury. Nature 2011;475:196–200. doi:10.1038/nature10199.

[74] Tester NJ, Plaas AH, Howland DR. Effect of body temperature on chondroitinase ABC's ability to cleave chondroitin sulfate glycosaminoglycans. J Neurosci Res 2007;85:1110–8. doi:10.1002/jnr.21199.

[75] Lee H, McKeon RJ, Bellamkonda RV. Sustained delivery of thermostabilized chABC enhances axonal sprouting and functional recovery after spinal cord injury. Proc Natl Acad Sci 2010;107:3340–5. doi:10.1073/pnas.0905437106.

[76] Lemons ML, Sandy JD, Anderson DK, Howland DR. Intact aggrecan and chondroitin sulfate-depleted aggrecan core glycoprotein inhibit axon growth in the adult rat spinal cord. Exp Neurol 2003;184:981–90. doi:10.1016/S0014-4886(03)00383-2.

[77] Dickendesher TL, Baldwin KT, Mironova YA, Koriyama Y, Raiker SJ, Askew KL, et al. NgR1 and NgR3 are receptors for chondroitin sulfate proteoglycans. Nat Neurosci 2012;15:703–12.

[78] Shen Y, Tenney AP, Busch SA, Horn KP, Cuascut FX, Liu K, et al. PTP {sigma} Is a receptor for chondroitin sulfate proteoglycan, an inhibitor of neural regeneration. Sci Signal 2009;326:592.

[79] Lang BT, Cregg JM, DePaul MA, Tran AP, Xu K, Dyck SM, et al. Modulation of the proteoglycan receptor PTP[sgr] promotes recovery after spinal cord injury. Nature 2014;advance online publication.

[80] Amariglio N, Hirshberg A, Scheithauer BW, Cohen Y, Loewenthal R, Trakhtenbrot L, et al. Donor-Derived Brain Tumor Following Neural Stem Cell Transplantation in an Ataxia Telangiectasia Patient. PLoS Med 2009;6:e1000029. doi:10.1371/journal.pmed.1000029.

[81] Riggs JW, Barrilleaux BL, Varlakhanova N, Bush KM, Chan V, Knoepfler PS. Induced pluripotency and oncogenic transformation are related processes. Stem Cells Dev 2012;22:37–50.

[82] Lukovic D, Valdés-Sanchez L, Sanchez-Vera I, Moreno-Manzano V, Stojkovic M, Bhattacharya SS, et al. Brief Report: Astrogliosis Promotes Functional Recovery of Completely Transected Spinal Cord Following Transplantation of hESC-Derived Oligodendrocyte and Motoneuron Progenitors. STEM CELLS 2014;32:594–9. doi:10.1002/stem.1562.

[83] Tabakow P, Raisman G, Fortuna W, Czyz M, Huber J, Li D, et al. Functional regeneration of supraspinal connections in a patient with transected spinal cord following transplantation of bulbar olfactory ensheathing cells with peripheral nerve bridging 2014.

[84] Kliot M, Smith GM, Siegal JD, Silver J. Astrocyte-polymer implants promote regeneration of dorsal root fibers into the adult mammalian spinal cord. Exp Neurol 1990;109:57–69. doi:10.1016/S0014-4886(05)80008-1.

[85] Joosten EAJ, Veldhuis WB, Hamers FPT. Collagen containing neonatal astrocytes stimulates regrowth of injured fibers and promotes modest locomotor recovery after spinal cord injury. J Neurosci Res 2004;77:127–42. doi:10.1002/jnr.20088.

[86] Davies SJA, Shih C-H, Noble M, Mayer-Proschel M, Davies JE, Proschel C. Transplantation of Specific Human Astrocytes Promotes Functional Recovery after Spinal Cord Injury. PLoS ONE 2011;6:e17328. doi:10.1371/journal.pone.0017328.

[87] Haas C, Fischer I. Human Astrocytes Derived from Glial Restricted Progenitors Support Regeneration of the Injured Spinal Cord. J Neurotrauma 2013;30:1035–52. doi:10.1089/neu.2013.2915.

[88] Jin Y, Neuhuber B, Singh A, Bouyer J, Lepore A, Bonner J, et al. Transplantation of Human Glial Restricted Progenitors and Derived Astrocytes into a Contusion Model of Spinal Cord Injury. J Neurotrauma 2011;28:579–94. doi:10.1089/neu.2010.1626.

[89] Fan C, Zheng Y, Cheng X, Qi X, Bu P, Luo X, et al. Transplantation of D15A-Expressing Glial-Restricted-Precursor-Derived Astrocytes Improves Anatomical and Locomotor Recovery after Spinal Cord Injury. Int J Biol Sci 2012;9:78–93. doi:10.7150/ijbs.5626.

[90] Chu T, Zhou H, Li F, Wang T, Lu L, Feng S. Astrocyte transplantation for spinal cord injury: Current status and perspective. Brain Res Bull 2014;107:18–30. doi:10.1016/j.brainresbull.2014.05.003.

[91] Pereira Lopes FR, Camargo de Moura Campos L, Dias Corrêa Jr. J, Balduino A, Lora S, Langone F, et al. Bone marrow stromal cells and resorbable collagen guidance tubes enhance sciatic nerve regeneration in mice. Thirteen Annu Conf Am Soc Neural Ther Repair 2006;198:457–68. doi:10.1016/j.expneurol.2005.12.019.

[92] Phillips JB, Bunting SC, Hall SM, Brown RA. Neural tissue engineering: a self-organizing collagen guidance conduit. Tissue Eng 2005;11:1611–7.

[93] Angeli CA, Edgerton VR, Gerasimenko YP, Harkema SJ. Altering spinal cord excitability enables voluntary movements after chronic complete paralysis in humans. Brain 2014. doi:10.1093/brain/awu038.

[94] Schmidt CE, Leach JB. NEURAL TISSUE ENGINEERING: Strategies for Repair and Regeneration. Annu Rev Biomed Eng 2003;5:293–347. doi:10.1146/annurev.bioeng.5.011303.120731.

[95] Stokols S, Tuszynski MH. Freeze-dried agarose scaffolds with uniaxial channels stimulate and guide linear axonal growth following spinal cord injury. Biomaterials 2006;27:443–51. doi:10.1016/j.biomaterials.2005.06.039.

[96] Jiang X, Lim SH, Mao HQ, Chew SY. Current applications and future perspectives of artificial nerve conduits. Exp Neurol 2010;223:86–101.

[97] Goto E, Mukozawa M, Mori H, Hara M. A rolled sheet of collagen gel with cultured Schwann cells: Model of nerve conduit to enhance neurite growth. J Biosci Bioeng 2010;109:512–8. doi:10.1016/j.jbiosc.2009.11.002.

[98] Ketschek AR, Haas C, Gallo G, Fischer I. The roles of neuronal and glial precursors in overcoming chondroitin sulfate proteoglycan inhibition. MicroRNAs—Human Neurobiol Neuropathol 2012;235:627–37. doi:10.1016/j.expneurol.2012.03.017.

[99] Yucel D, Kose GT, Hasirci V. Tissue Engineered, Guided Nerve Tube Consisting of Aligned Neural Stem Cells and Astrocytes. Biomacromolecules 2010;11:3584–91. doi:10.1021/bm1010323.

[100] Schlosshauer B, Dreesmann L, Schaller H-E, Sinis N. Synthetic Nerve Guide Implants in Humans: A Comprehensive Survey. Neurosurgery 2006;59:740–8 10.1227/01.NEU.0000235197.36789.42.

[101] Yoshioka N, Hisanaga S-I, Kawano H. Suppression of fibrotic scar formation promotes axonal regeneration without disturbing blood-brain barrier repair and withdrawal of leukocytes after traumatic brain injury. J Comp Neurol 2010;518:3867–81. doi:10.1002/cne.22431.

[102] Weidner N, Grill RJ, Tuszynski MH. Elimination of Basal Lamina and the Collagen “Scar” after Spinal Cord Injury Fails to Augment Corticospinal Tract Regeneration. Exp Neurol 1999;160:40–50. doi:10.1006/exnr.1999.7200.

[103] Joosten EAJ, Dijkstra S, Brook GA, Veldman H, Bär PR. Collagen IV deposits do not prevent regrowing axons from penetrating the lesion site in spinal cord injury. J Neurosci Res 2000;62:686–91.

[104] Klapka N, Müller HW. Collagen Matrix in Spinal Cord Injury. J Neurotrauma 2006;23:422–36. doi:10.1089/neu.2006.23.422.

[105] Okada M, Miyamoto O, Shibuya S, Zhang X, Yamamoto T, Itano T. Expression and role of type I collagen in a rat spinal cord contusion injury model. Neurosci Res 2007;58:371–7. doi:10.1016/j.neures.2007.04.009.

[106] Hirano S, Yonezawa T, Hasegawa H, Hattori S, Greenhill NS, Davis PF, et al. Astrocytes express type VIII collagen during the repair process of brain cold injury. Biochem Biophys Res Commun 2004;317:437–43. doi:10.1016/j.bbrc.2004.03.049.

[107] Heck N, Garwood J, Schütte K, Fawcett J, Faissner A. Astrocytes in culture express fibrillar collagen. Glia 2003;41:382–92. doi:10.1002/glia.10184.

[108] Houweling D., van Asseldonk JT., Lankhorst A., Hamers FP., Martin D, Bär P., et al. Local application of collagen containing brain-derived neurotrophic factor decreases the loss of function after spinal cord injury in the adult rat. Neurosci Lett 1998;251:193–6. doi:10.1016/S0304-3940(98)00536-9.

[109] Cholas RH, Hsu H-P, Spector M. The reparative response to cross-linked collagen-based scaffolds in a rat spinal cord gap model. Biomaterials 2012;33:2050–9. doi:10.1016/j.biomaterials.2011.11.028.

[110] Liu S, Peulve P, Jin O, Boisset N, Tiollier J, Said G, et al. Axonal regrowth through collagen tubes bridging the spinal cord to nerve roots. J Neurosci Res 1997;49:425–32. doi:10.1002/(SICI)1097-4547(19970815)49:4<425::AID-JNR4>3.0.CO;2-A.

[111] Joosten EAJ, Bär PR, Gispen WH. Collagen implants and cortico-spinal axonal growth after mid-thoracic spinal cord lesion in the adult rat. J Neurosci Res 1995;41:481–90. doi:10.1002/jnr.490410407.

[112] Liu T, Houle JD, Xu J, Chan BP, Chew SY. Nanofibrous collagen nerve conduits for spinal cord repair. Tissue Eng Part A 2012;18:1057–66.

[113] Han Q, Jin W, Xiao Z, Ni H, Wang J, Kong J, et al. The promotion of neural regeneration in an extreme rat spinal cord injury model using a collagen scaffold containing a collagen binding neuroprotective protein and an EGFR neutralizing antibody. Biomaterials 2010;31:9212–20. doi:10.1016/j.biomaterials.2010.08.040.

[114] Marchand R, Woerly S, Bertrand L, Valdes N. Evaluation of two cross-linked collagen gels implanted in the transected spinal cord. Brain Res Bull 1993;30:415–22. doi:10.1016/0361-9230(93)90273-E.

[115] Kassar-Duchossoy L, Duchossoy Y, Rhrich-Haddout F, Horvat J-C. Reinnervation of a denervated skeletal muscle by spinal axons regenerating through a collagen channel directly implanted into the rat spinal cord. Brain Res 2001;908:25–34. doi:10.1016/S0006-8993(01)02554-9.

[116] Liu S, Bodjarian N, Langlois O, Bonnard AS, Boisset N, Peulvé P, et al. Axonal regrowth through a collagen guidance channel bridging spinal cord to the avulsed C6 roots: Functional recovery in primates with brachial plexus injury. J Neurosci Res 1998;51:723–34. doi:10.1002/(SICI)1097-4547(19980315)51:6<723::AID-JNR6>3.0.CO;2-D.

[117] Raub CB, Unruh J, Suresh V, Krasieva T, Lindmo T, Gratton E, et al. Image Correlation Spectroscopy of Multiphoton Images Correlates with Collagen Mechanical Properties. Biophys J 2008;94:2361–73. doi:10.1529/biophysj.107.120006.

[118] Elias PZ, Spector M. Viscoelastic characterization of rat cerebral cortex and type I collagen scaffolds for central nervous system tissue engineering. J Mech Behav Biomed Mater 2012;12:63–73. doi:10.1016/j.jmbbm.2012.03.014.

[119] Chen Y-S, Chang J-Y, Cheng C-Y, Tsai F-J, Yao C-H, Liu B-S. An in vivo evaluation of a biodegradable genipin-cross-linked gelatin peripheral nerve guide conduit material. Biomaterials 2005;26:3911–8. doi:10.1016/j.biomaterials.2004.09.060.

[120] Panseri S, Cunha C, Lowery J, Del Carro U, Taraballi F, Amadio S, et al. Electrospun micro-and nanofiber tubes for functional nervous regeneration in sciatic nerve transections. Bmc Biotechnol 2008;8:39.

[121] Bakshi A, Fisher O, Dagci T, Himes BT, Fischer I, Lowman A. Mechanically engineered hydrogel scaffolds for axonal growth and angiogenesis after transplantation in spinal cord injury. J Neurosurg Spine 2004;1:322–9.

[122] Kofron CM, Fong VJ, Hoffman-Kim D. Neurite outgrowth at the interface of 2D and 3D growth environments. J Neural Eng 2009;6:016002.

[123] Rajnicek A, Britland S, McCaig C. Contact guidance of CNS neurites on grooved quartz: influence of groove dimensions, neuronal age and cell type. J Cell Sci 1997;110:2905–13.

[124] Hodgkinson GN, Tresco PA, Hlady V. The differential influence of colocalized and segregated dual protein signals on neurite outgrowth on surfaces. Biomaterials 2007;28:2590–602. doi:10.1016/j.biomaterials.2007.01.038.

[125] Xie J, Willerth SM, Li X, Macewan MR, Rader A, Sakiyama-Elbert SE, et al. The differentiation of embryonic stem cells seeded on electrospun nanofibers into neural lineages. Biomaterials 2009;30:354–62. doi:10.1016/j.biomaterials.2008.09.046.

[126] Biran R, Noble MD, Tresco PA. Directed nerve outgrowth is enhanced by engineered glial substrates. Exp Neurol 2003;184:141–52. doi:10.1016/S0014-4886(03)00253-X.

[127] Minev IR, Moshayedi P, Fawcett JW, Lacour SP. Interaction of glia with a compliant, microstructured silicone surface. Acta Biomater 2013;9:6936–42. doi:10.1016/j.actbio.2013.02.048.

[128] Hurtado A, Cregg JM, Wang HB, Wendell DF, Oudega M, Gilbert RJ, et al. Robust CNS regeneration after complete spinal cord transection using aligned poly-l-lactic acid microfibers. Biomaterials 2011;32:6068–79. doi:10.1016/j.biomaterials.2011.05.006.

[129] Koppes AN, Zaccor NW, Rivet CJ, Williams LA, Piselli JM, Gilbert RJ, et al. Neurite outgrowth on electrospun PLLA fibers is enhanced by exogenous electrical stimulation. J Neural Eng 2014;11:046002.

[130] Meng F, Hlady V, Tresco PA. Inducing alignment in astrocyte tissue constructs by surface ligands patterned on biomaterials. Biomaterials 2012;33:1323–35. doi:10.1016/j.biomaterials.2011.10.034.

[131] Eichinger CD, Hsiao TW, Hlady V. Multiprotein Microcontact Printing with Micrometer Resolution. Langmuir 2011;28:2238–43. doi:10.1021/la2039202.

[132] Yu H, Xiong S, Tay CY, Leong WS, Tan LP. A novel and simple microcontact printing technique for tacky, soft substrates and/or complex surfaces in soft tissue engineering. Acta Biomater 2012;8:1267–72. doi:10.1016/j.actbio.2011.09.006.

[133] Zuidema JM, Hyzinski-García MC, Van Vlasselaer K, Zaccor NW, Plopper GE, Mongin AA, et al. Enhanced GLT-1 mediated glutamate uptake and migration of primary astrocytes directed by fibronectin-coated electrospun poly-l-lactic acid fibers. Biomaterials 2014;35:1439–49. doi:10.1016/j.biomaterials.2013.10.079.

[134] Polio SR, Rothenberg KE, Stamenović D, Smith ML. A micropatterning and image processing approach to simplify measurement of cellular traction forces. Acta Biomater 2012;8:82–8. doi:10.1016/j.actbio.2011.08.013.

[135] Rape AD, Guo W, Wang Y. The regulation of traction force in relation to cell shape and focal adhesions. Biomaterials 2011;32:2043–51.

[136] Alford PW, Nesmith AP, Seywerd JN, Grosberg A, Parker KK. Vascular smooth muscle contractility depends on cell shape. Integr Biol 2011;3:1063–70. doi:10.1039/C1IB00061F.

[137] Giannitelli SM, Abbruzzese F, Mozetic P, De Ninno A, Businaro L, Gerardino A, et al. Surface decoration of electrospun scaffolds by microcontact printing. Asia-Pac J Chem Eng 2014:n/a – n/a. doi:10.1002/apj.1809.

[138] Castano AG, Hortiguela V, Lagunas A, Cortina C, Montserrat N, Samitier J, et al. Protein patterning on hydrogels by direct microcontact printing: application to cardiac differentiation. RSC Adv 2014;4:29120–3. doi:10.1039/C4RA03374D.

[139] Kofron CM, Liu YT, López-Fagundo CY, Mitchel JA, Hoffman-Kim D. Neurite outgrowth at the biomimetic interface. Ann Biomed Eng 2010;38:2210–25.

[140] Neugebauer KM, Tomaselli KJ, Lilien J, Reichardt LF. N-cadherin, NCAM, and integrins promote retinal neurite outgrowth on astrocytes in vitro. J Cell Biol 1988;107:1177–87. doi:10.1083/jcb.107.3.1177.

[141] Davies SJA, Fitch MT, Memberg SP, Hall AK, Raisman G, Silver J. Regeneration of adult axons in white matter tracts of the central nervous system. Nature 1997;390:680–3. doi:10.1038/37776.

[142] Barry D, McDermott K. Differentiation of radial glia from radial precursor cells and transformation into astrocytes in the developing rat spinal cord. Glia 2005;50:187–97. doi:10.1002/glia.20166.

[143] Costa S, Planchenault T, Charriere-Bertrand C, Mouchel Y, Fages C, Juliano S, et al. Astroglial permissivity for neuritic outgrowth in neuron–astrocyte cocultures depends on regulation of laminin bioavailability. Glia 2002;37:105–13. doi:10.1002/glia.10015.

[144] Féréol S, Fodil R, Barnat M, Georget V, Milbreta U, Nothias F. Micropatterned ECM substrates reveal complementary contribution of low and high affinity ligands to neurite outgrowth. Cytoskeleton 2011;68:373–88. doi:10.1002/cm.20518.

[145] Tom VJ, Doller CM, Malouf AT, Silver J. Astrocyte-associated fibronectin is critical for axonal regeneration in adult white matter. J Neurosci 2004;24:9282–90.

[146] Alexander JK, Fuss B, Colello RJ. Electric field-induced astrocyte alignment directs neurite outgrowth. Neuron Glia Biol 2006;2:93–103. doi:10.1017/S1740925X0600010X.

[147] East E, de Oliveira DB, Golding JP, Phillips JB. Alignment of astrocytes increases neuronal growth in three-dimensional collagen gels and is maintained following plastic compression to form a spinal cord repair conduit. Tissue Eng Part A 2010;16:3173–84.

[148] Ereifej ES, Matthew HW, Newaz G, Mukhopadhyay A, Auner G, Salakhutdinov I, et al. Nanopatterning effects on astrocyte reactivity. J Biomed Mater Res A 2013;101A:1743–57. doi:10.1002/jbm.a.34480.

[149] Min SK, Kim SH, Kim CR, Paik S-M, Jung S-M, Shin HS. Effect of topography of an electrospun nanofiber on modulation of activity of primary rat astrocytes. Neurosci Lett 2013;534:80–4. doi:10.1016/j.neulet.2012.11.015.

[150] Sørensen A, Alekseeva T, Katechia K, Robertson M, Riehle MO, Barnett SC. Long-term neurite orientation on astrocyte monolayers aligned by microtopography. Biomaterials 2007;28:5498–508. doi:10.1016/j.biomaterials.2007.08.034.

[151] Han S, Wang B, Jin W, Xiao Z, Chen B, Xiao H, et al. The collagen scaffold with collagen binding BDNF enhances functional recovery by facilitating peripheral nerve infiltrating and ingrowth in canine complete spinal cord transection. Spinal Cord 2014;52:867–73.

[152] Kofron C, Hoffman-Kim D. Optimization by Response Surface Methodology of Confluent and Aligned Cellular Monolayers for Nerve Guidance. Cell Mol Bioeng 2009;2:554–72. doi:10.1007/s12195-009-0087-1.

[153] Hsiao TW, Swarup VP, Kuberan B, Tresco PA, Hlady V. Astrocytes specifically remove surface-adsorbed fibrinogen and locally express chondroitin sulfate proteoglycans. Acta Biomater 2013;9:7200–8. doi:10.1016/j.actbio.2013.02.047.

[154] Hsiao TW, Tresco PA, Hlady V. Astrocytes alignment and reactivity on collagen hydrogels patterned with ECM proteins. Biomaterials 2015;39:124–30. doi:10.1016/j.biomaterials.2014.10.062.

[155] Hsiao T, Swarup V, Eichinger C, Hlady V. Cell Substrate Patterning with Glycosaminoglycans to Study Their Biological Roles in the Central Nervous System. In: Balagurunathan K, Nakato H, Desai UR, editors. Glycosaminoglycans, vol. 1229, Springer New York; 2015, p. 457–67.

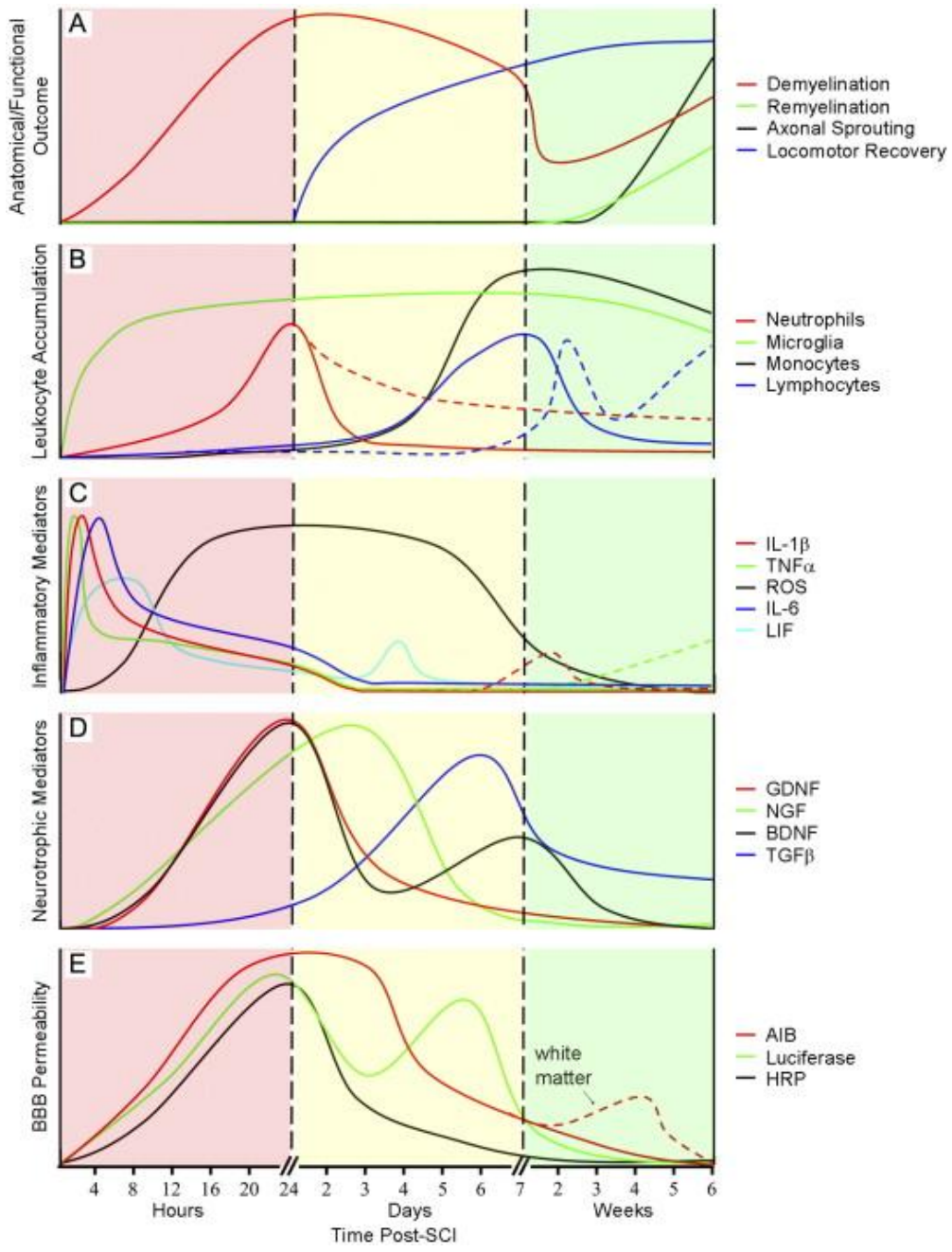

Figure 1.1. SCI recovery timing and relative inflammatory events. A) Anatomic and functional outcomes. B) Macrophage activation and accumulation. Dotted lines are for studies from mice and solid from rats when there was a discrepancy between species. C) Expression of proinflammatory markers. D) Expression of neurotrophic factors. E) BBB permeability to α-aminoisobutyric acid (AIB; 104 Da), horseradish peroxidase (HRP; 44,000 Da), and luciferase (61,000 Da). Dotted lines represent levels in white matter and solid lines report grey matter levels. Reprinted from [5] with permission from Elsevier.

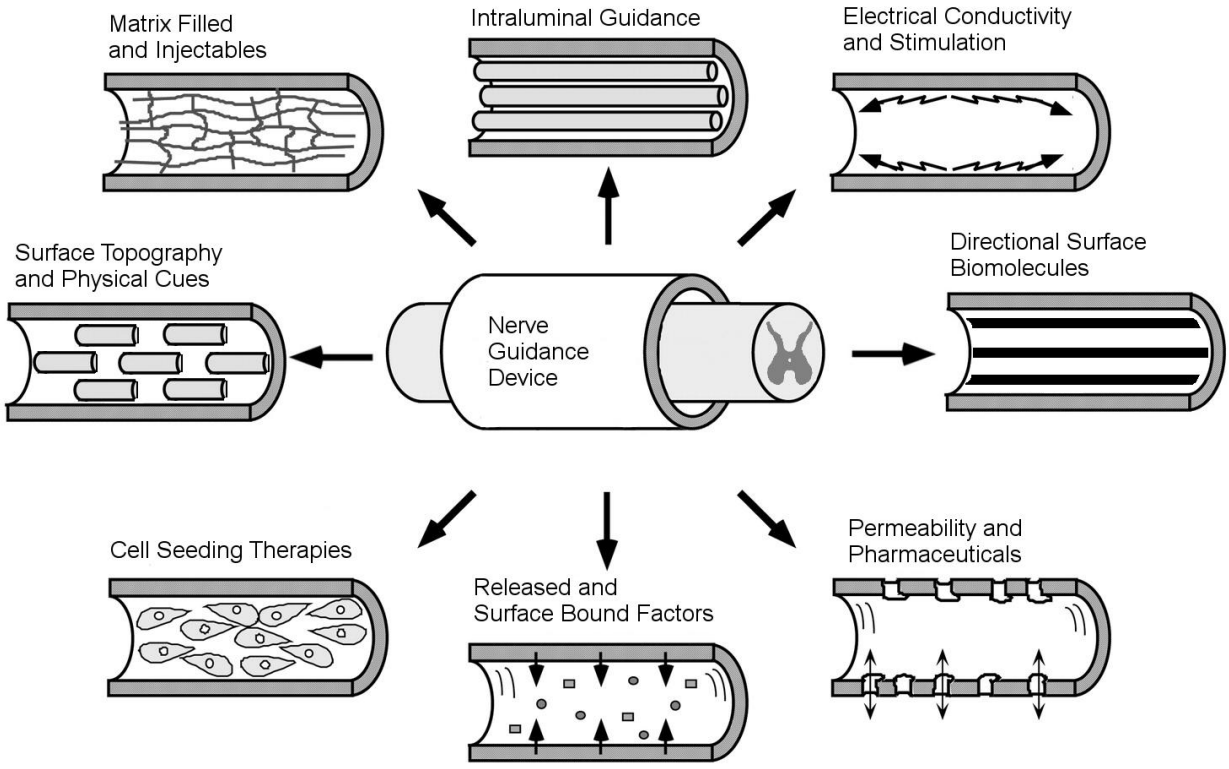

Figure 1.2. Nerve guidance device modifications and strategies to improve functional outcomes. Developments on the initial tubular design have been made to incorporate additional cues to promote neuronal recovery provide directionality. Adapted from [94].

CHAPTER 2

ASTROCYTES SPECIFICALLY REMOVE SURFACE-ADSORBED FIBRINOGEN AND LOCALLY EXPRESS CHONDROITIN SULFATE PROTEOGLYCANS[*]

2.1. Abstract

Surface-adsorbed fibrinogen (FBG) was recognized by adhering astrocytes, and was removed from the substrates in vitro by a two-phase removal process. The cells removed adsorbed FBG from binary proteins' surface patterns (FBG + laminin, or FBG + albumin) while leaving the other protein behind. Astrocytes preferentially expressed chondroitin sulfate proteoglycan (CSPG) at the loci of fibrinogen stimuli; however, no differences in overall CSPG production as a function of FBG surface coverage were identified. Removal of FBG by astrocytes was also found to be independent of transforming growth factor type β (TGF-β) receptor based signaling as cells maintained CSPG production in the presence of TGF-β receptor kinase inhibitor, SB 431542. The inhibitor decreased CSPG expression, but did not abolish it entirely. Because blood contact and subsequent FBG adsorption are unavoidable in neural implantations, the results

[*] Reprinted from Acta Biomaterialia, Vol 9, Iss. 7, pp. 7200-7208, © 2013 with permission from Elsevier.

indicate that implant-adsorbed FBG may contribute to reactive astrogliosis around the implant as astrocytes specifically recognize adsorbed FBG.

2.2. Introduction

Neural implants elicit the foreign body response of the central nervous system (CNS), leading to a loss of local neurons [1] and [2]. The CNS response to implants is characterized by acute activation of microglia and astrocytes within one day of injury. Edema and debris are lessened within 1 week; however, chronic inflammation persists around these devices, and they become encapsulated by macrophage-like cells after 4 weeks [3]. This persistent, stable sheath of tissue, termed the glial scar, is composed of astrocytes and microglia. In the case of recording or stimulating electrodes that are implanted in the brain, degradation of electric signal quality has been attributed to this foreign body response and associated neuronal loss [1].

Initial CNS response to the neural implant can provide insight into the mechanism of glial scar formation. A universal feature of neural implants is that the initial surgical intervention during implantation causes hemorrhage and/or leakage of the blood–brain barrier (BBB). This effect may be compounded if the BBB remains compromised, allowing continuous contact of the device with blood. Like all materials exposed to blood, surfaces of such implants quickly adsorb plasma proteins at the blood–implant interface. Among the dozen plasma proteins with concentrations greater than 1 mg ml^{-1}, fibrinogen (FBG, 2–3 mg ml^{-1} in blood plasma) plays a key role in hemostasis after injury and is known to

be a surface active protein that readily adsorbs to surfaces [4]. In circulation, FBG adsorbs to the surface of implants and often undergoes conformational changes that lead to adhesion and activation of platelets [5]. Fibrinogen adsorbed onto the surface of neural implants is ultimately exposed to the CNS tissue and not to blood. The question is whether CNS astrocytes recognize adsorbed FBG and react by mounting CNS inflammatory response. Such recognition could be one of the initial steps in the formation of a glial scar that ultimately results in an inhibition of neuronal activity around implants.

Astrocytes in vivo have minimal glial fibrillary acidic protein (GFAP) expression in their quiescent state [3] and [6]. In reactive astrogliosis, however, GFAP expression is increased and astrocytes display hypertrophied morphology. Interestingly, astrocytes cultured in three-dimensional (3-D) collagen gels mimic more closely their in vivo state, while in two-dimensional (2-D) cultures in vitro they appear as being reactive [7]. In addition to their morphological changes, reactive astrocytes proliferate and secrete various factors and macromolecules. Of these secreted species, chondroitin sulfate proteoglycan (CSPG) is of particular interest as it has been implicated as a potential inhibitor of neuronal regeneration [8] and [9]. The modes of astrocyte expression of CSPGs can be varied. For example, brevican CSPGs are attached to the astrocyte membrane [9] and [10] while other CSPGs, like neurocan, are shed into cell media and were also found bound to underlying substrates [11].

Soluble chemical signals are also potent contributors to astrogliosis [12] and [13]. For example, transforming growth factor type β (TGF-β) is known to

trigger astrocyte activation. In this role TGF-β has been utilized to enhance in vitro models of the glial scar for neuronal outgrowth studies [14]. It has recently been shown that soluble blood FBG is a source of latent TGF-β; BBB leakage of soluble FBG into the CNS causes an increased CSPG expression in astrocytes both in vivo and in vitro by the TGF-β-mediated smad signaling pathway [15]. While it has been demonstrated that astrocytes can become reactive without BBB leakage by addition of a neurotoxicant [16], the FBG/TGF-β/smad activation pathway seems likely to be involved when neural implants covered with adsorbed blood proteins, including FBG, interface with CNS tissue.

The objective of the present study was to find how astrocytes respond to adsorbed FBG and determine if this causes astrocytes to become more reactive and change their CSPG production. To investigate this particular scenario, we cultured astrocytes on surface-adsorbed FBG layers at different protein surface coverage. We found that the cells, after some initial incubation period, start to actively remove adsorbed FBG and locally produce CSPG. To test the role of latent TGF-β on adsorbed FBG recognition, we blocked the TGF-β receptors by an inhibitor of TGF-β receptor kinase. This blocking did not alter FBG removal by astrocytes nor completely abolish expression of CSPG in vitro, thereby indicating that signaling pathways other than TGF-β/smad may be involved.

2.3. Materials and Methods

2.3.1. Cell culture

Primary cortical astrocytes were harvested from P1 Sprague–Dawley rats according to the protocol approved by University of Utah Institutional Animal Care and Use Committee [17]. Briefly, cortical tissue with removed meninges was broken up and digested in collagenase (1.33%, Worthington) for 30 min. Cortices were then treated with trypsin (0.25%, Worthington) for 30 min, triturated, suspended and plated in 75 cm^2 tissue culture flasks. To purify astrocyte cultures, flasks were shaken overnight at 175 rpm after 1 week of culture post-dissection. After shaking, astrocytes were dissociated with 0.25% trypsin–EDTA (Gibco) and either frozen in liquid N2 or prepared for use. Cultures were verified for astrocyte populations with anti-GFAP immunostaining (1:1000, Chemicon). Cells were maintained in DMEM/F12 (Gibco) supplemented with 10% fetal bovine serum (FBS, Sigma). Astrocytes had media exchanged once every 2 days and were cultured for 1 week prior to use in experiments.

Cells were seeded onto prepared coverslips in a 12-well tissue culture plate (CellTreat) at a density of ~10,000 cells cm^{-2}. This density was used to maintain sparse culture and minimize intercellular interactions. Astrocytes were seeded and cultured in DMEM/F12 with three types of conditions: (a) 10% FBS, (b) 10% FBS with 1% DMSO (Sigma), and (c) 10% FBS with 10 mM TGF-β receptor kinase inhibitor (SB 431542, Sigma) in 1% DMSO to block TGF-β signaling. Cells were cultured on experimental substrates for 48 h and then fixed with a 4% paraformaldehyde (PFA, Sigma) solution for 15 min.

2.3.2. Substrate preparation

Human plasma fibrinogen (plasminogen depleted, Calbiochem) was fluorescently labeled with Alexa Fluor 594 (A-20004, Invitrogen) by reacting at room temperature for 2 h in 0.1 M sodium bicarbonate solution. The solution was eluted in phosphate buffered saline (PBS) through a PD-10 Sephadex column (GE Healthcare) to separate labeled protein from free dye. Collected fibrinogen solution (2 mg ml^{-1}) was then filtered through a 0.2 μm syringe filter (Sarstedt), divided into 100 μl aliquots, and stored at −20 °C until use. Laminin (L2020, Sigma–Aldrich) solution was prepared in a 100 μg ml^{-1} concentration in PBS. Laminin was fluorescently labeled using Alexa Fluor 488 (A-20000, Invitrogen). For albumin studies, bovine serum albumin (68700, Proliant) was dissolved in PBS at 4.5 mg ml^{-1} and was also labeled with Alexa Fluor 488.

Glass coverslips (Fisherbrand, 18 mm #2, Fisher) were rinsed in acetone, ethanol and DDI water before being sonicated in DDI water for 15 min. Coverslips were then dried in N_2 and autoclaved. For samples with single adsorbed protein (fibrinogen or laminin), protein solution was applied over the surface and allowed to incubate at room temperature for 1 h. Autoclaved coverslips without adsorbed proteins were used as controls. For samples with added soluble TGF-β, human TGF-β 1 (R&D Systems) was added to culture media at 20 ng ml^{-1} at time of seeding.

Microcontact printing (μCP) was used to create surfaces with different FBG coverage [18]. Patterns of randomly distributed μm-sized islands with coverage of 30% and 50% were made using soft lithography [19]. The 30% and

50% random distributions of pixels were first created in Mathematica (Wolfram). These pixels were then converted to a template for a photolithography mask where each pixel equated to a ~1 μm^2 feature. The mask served as a mold for polydimethylsiloxane (PDMS) casting. PDMS (Sylgard 184, Dow Corning) was poured over the mask and allowed to cure at 100 °C. Cast PDMS was peeled from the mask and soaked in hexane, acetone and ethanol to remove unreacted siloxane molecules, dried in an oven and cut into stamps containing the desired coverage pattern. The stamps were then sonicated in detergent solution (Alconox), rinsed with DDI water, and stored in DDI water prior to use. For use in μCP, the stamp was incubated in FBG solution (2 mg ml^{-1}) at room temperature for 20–30 min, then briefly rinsed with DDI water and dried with an N2 stream. Stamps were brought into conformal contact with sterilized coverslips for ~1 min for protein transfer. Upon stamp removal, the patterned coverslips were backfilled with laminin solution. The created FBG patterns are shown in Fig. 2.1. The coverage of proteins was 100% FBG (FBG100/LN0), 50% FBG with LN backfill (FBG50/LN50), 30% FBG with LN backfill (FBG30/LN70) or 100% LN (FBG0/LN100). This same protocol was followed to create binary FBG and albumin surfaces except that the labeled albumin solution was used for backfill after stamping. All substrates were then immediately used for cell culture.

2.3.3. Time-lapse microscopy

Astrocytes were seeded onto sterile glass-bottomed culture dishes (Fluorodish, WPI Inc.) that had been covered with micro-contact printed and/or

adsorbed proteins as described above. Cells were allowed to attach for 4 h and then imaged with an Olympus IX81 microscope on a temperature-controlled stage. Metamorph software (Molecular Devices) was used to take images of multiple stage positions once every 6 min for 20 h. Live cell images were taken with a 20× DIC objective and overlaid with corresponding fluorescence images.

Time-lapse fluorescence images were brought in register manually to compensate for sample drift and were used in calculating fibrinogen removal kinetics. Areas of 5 × 5 pixels from five different cell regions of a given cell were tracked through time for analysis and used in calculation of the FBG removal rate according to the equation:

$$\theta(t) = \theta_0 + A\, e^{\frac{(t_0 - t)}{\tau}} \quad (1)$$

where θ(t) is the surface coverage of FBG (assumed to be proportional to the fluorescence intensity) measured as a function of time t, θ_0 is a final FBG coverage at the time when rapid removal process is finished, A is a removal coefficient and τ is a characteristic time for this removal process (τ = the inverse of the FBG removal rate constant). The initial time, t0, is defined as the time when the cell began to rapidly remove FBG and was determined as the point where there was a rapid fluorescence intensity change in the θ(t) curves. Coefficients for Eq. (1) were found by fitting the θ(t) curves using Igor Pro (WaveMetrics).

2.3.4. Immunocytochemistry

Astrocytes were fixed with 4% PFA for 15 min and rinsed in PBS with 0.1% sodium azide prior to immunocytochemical staining. All procedures were carried out at room temperature. Samples were first blocked with 4% goat serum in PBS for 1 h then rinsed thrice in PBS with azide. Primary anti-chondroitin sulfate (CS-56) antibody (C8035, Sigma) was applied to the fixed astrocytes for 1 h at a 1:500 dilution in block solution. Samples were again rinsed three times in PBS/azide and the secondary goat anti-mouse IgM antibody labeled with Alexa Fluor 488 (A21042, Molecular Probes) was subsequently applied to the samples for 1 h. Following three more PBS/azide rinses, DAPI (Invitrogen) at a 1:100 dilution was added for 15 min to stain for nuclei. Samples were then rinsed in DDI water, allowed to dry and mounted onto 3″ glass microscope slides (VWR) with Fluoromount-G (Southern Biotech) for fluorescence imaging.

2.3.5. Astrocyte surface CSPG expression

Stained CSPG samples were imaged using a Nikon Eclipse E600 epifluorescence microscope with a 20× PlanApo objective and CCD camera (CoolSNAP, Photometrics) using identical exposure times with blank images subtracted. Ten sample images were taken per condition. Each image was divided into six equal regions for quantification. The fluorescence intensity in each region was quantified using ImageJ (NIH). The integrated CSPG fluorescence intensity was normalized by dividing it by the number of cells per region as identified by DAPI nuclear stain. To correct for regions where no cells

were present and also regions with high densities of cells, ten regions with the highest and five regions with the lowest CSPG per cell values were removed from the analysis. An ANOVA with a Tukey post hoc test ($\alpha = 0.05$) was used to determine the significance of data differences. To assess the 3-D distribution of CSPG fluorescence, a confocal microscope (Olympus BX61WI, 40× PlanFLN, NA 1.30) was used to image samples using multiple slices in the vertical, z-direction. Image stacks were then compiled using Olympus Fluoview software. Vertical distribution of FGB and CSPG was measured at nuclear (as confirmed by DAPI), cell periphery and regions where cells deposited CSPG and then migrated away. For each region the fluorescence intensity was averaged over an area of 25 by 25 pixels in each z-slice.

2.3.6. Expression of shed CSPG

Radioactive sulfur assay was used to determine the amount of glycosaminoglycans (GAGs) shed by astrocytes into media vs. the GAG amount present on the cell membrane [20]. Astrocytes were cultured for 48 h in F-12 nutrient mixture (Gibco) with 10% dialyzed FBS supplemented with 700 μCi of [35S] Na_2SO_4 (Perkin Elmer Life Sciences). Cells were cultured in T75 flasks on tissue-culture polystyrene (TCPS) with or without pre-adsorbed FBG layer. After the culture period, the conditioned medium was removed for GAGs analysis and the remaining cells were treated with 1 mg ml^{-1} pronase solution (Pronase Streptomyces griseuswas, Sigma–Aldrich) for endogenous GAG quantification. Each sample was purified for GAG chains using a DEAE-Sepharose (Amersham

Biosciences) column, and 35S radioactivity was measured using a scintillation counter (Beckman).

2.4. Results

2.4.1. Astrocyte removal of adsorbed fibrinogen

Astrocytes adhered to fibrinogen-covered surfaces and subsequently removed the fibrinogen, as evidenced by progressive loss of fluorescence over time. This behavior was observed in real time via time-lapse microscopy and was also evident in fixed samples (Fig. 2.2). Fig. 2.2A–C (DIC + FBG fluorescence) shows the progress of fibrinogen removal from 4 to 23 h post seeding. Astrocyte adhesion to FBG-coated surfaces was a dynamic process with cells attaching to, detaching from and migrating across the surface throughout 24 h of culture. The initial 4 h of culture were used to allow for cells to attach to the substrates prior to imaging. At the 4 h time point, however, some regions depleted of FBG were already present on the substrates. Some of these sites had astrocytes attached, while others did not have any cells remaining on the FBG depleted sites.

Adsorbed FBG removal by astrocytes was found to be a two-step process characterized by an initial gradual decrease of FBG fluorescence followed by a more rapid decay of fluorescence intensity (Fig. 2.3). The rapid FBG removal phase, when modeled as exponential intensity decrease (Eq. (1)), had a characteristic time, $\tau = 1.69 \pm 0.46$ h (mean ± standard deviation) over the five sub-areas across the cell (Fig. 2.3B and E). Similar FBG removal phases were found on patterned surfaces as well (Fig. 2.3C and D). The rapid removal only

occurred after an incubation period that varied as the cell migrated along the substrate (which contributed to dispersion in τ values). The initial slow FBG removal had an average dθ/dt slope of −0.0064 ± 0.0033 h^{-1} (mean ± standard deviation) and the duration of the slow FBG removal phase varied from cell to cell.

In fixed and stained samples, FBG was seen as being selectively removed in the areas that were frequently co-localized with adhered cells. Such astrocyte behavior was independent of blocking TGF-β receptor type I, as astrocyte cultures treated with SB 431542 showed similar substrate modification. There was also sporadic evidence of cellular uptake of FBG in fixed samples as shown by areas of increased fluorescence associated with astrocytes (Fig. 2.4A and B).

2.4.2. FBG removal is a protein-specific astrocyte response

The specificity of astrocyte recognition and removal of adsorbed FBG was tested by comparing the effect of astrocytes on laminin (LN) and albumin (ALB) coated surfaces. These two proteins also provided a test for proteins larger and smaller than FBG. Adsorbed laminin is known to present the sites for astrocytes adhesion [21], and the cells spread more readily on laminin surfaces when compared to surfaces covered with FBG or serum proteins alone. Unlike FBG, surface-adsorbed laminin remained minimally modified by astrocytes over the culture period (Fig. 2.2D). The modification of surface fibrinogen by astrocytes was therefore not merely a result of cellular adhesion.

Similarly, astrocyte culture on a mixed albumin–fibrinogen substrate with 50% ALB and 50% FBG coverage left albumin largely intact while still removing FBG (Fig. 2.4C and D). Thus astrocytes specifically removed the FBG from amongst the albumin, and left albumin in its original surface patterns. Adsorbed albumin and laminin results indicated that astrocyte did not use any nonspecific, broad-target proteolysis to remove FBG. Instead, the removal of FBG by astrocytes appeared to be a selective process that was unaffected by the presence of other proteins.

2.4.3. CSPG expression in response to surface coverage of fibrinogen

The cell-associated CSPG production was not significantly dependent on the amount of adsorbed fibrinogen presented to the cells (Fig. 2.5). Astrocytes expressed CSPG on all four substrates used for cell culture: full-coverage fibrinogen (FBG100/LN0), 50% coverage FBG backfilled with LN (FBG50/LN50), 30% coverage FBG backfilled with LN (FBG30/LN70) and full-coverage laminin (FBG0/LN100). The levels of CSPG production were comparable to those found on astrocytes cultured in culture media on glass coverslips alone (data not shown). However, astrocytes seemed to produce CSPG in a local response to adsorbed fibrinogen patterns. For example, on FBG50/LN50 and also on FBG30/LN70 substrates, astrocytes were often found to produce the higher levels of CSPG by depositing it in between the random FBG patches (Fig. 2.6A, arrows). Astrocyte production of cell-associated CSPG was largest in the areas where cell membrane made contact with FBG. This behavior was consistent

across both nuclear and peripheral regions of the cell. Confocal 3-D imaging showed that the vertical z-position of expressed CSPG coincided with the z-position of fibrinogen (Fig. 2.6B–D). Cells also produced CSPG throughout their intracellular space in addition to membranes. CSPG was also found deposited on surfaces where the cells had previously been but were no longer present, as evidenced by a footprint of removed FBG but the lack of positive DAPI staining (Fig. 2.6D). Once FBG was removed from a region, CSPG expression by the adherent cell became more uniform and was similar to CSPG expression by cells on homogenous substrates. Importantly, CSPG was not found on areas without either a footprint or a nucleus of cells, indicating that CSPG was not merely shed into the solution and then re-adsorbed to the surface from the medium.

2.4.4. TGF-β contribution to CSPG production in vitro

To clarify the role of adsorbed FBG in TGF-β signaling of CSPG production by adherent astrocytes, a small molecule inhibitor, SB 431542, was used to inhibit TGF-β receptors with superfamily type I activin receptor-like kinase [22]. These receptors have been shown to mediate CSPG expression in astrocytes when latent TGF-β was provided by soluble fibrinogen [15]. Fig. 2.7 shows that CSPG production was somewhat attenuated in cultures with added inhibitor but not eliminated. The only significant decrease in CSPG production per cell with inhibitor treatment was found on cells grown on substrates with low or no fibrinogen (i.e. on FBG30/LN70 and FBG0/LN100 substrates). In general,

the cells also maintained their ability to remove FGB from surfaces, even in the presence of the inhibitor.

Adding extraneous, soluble TGF-β to the sparse astrocyte cultures in 10% serum showed no significant differences in the overall CSPG produced per cell on fibrinogen (FBG100/LN0)- and laminin (FBG0/LN100)-covered substrates (Fig. 2.8). For a clearer understanding of how the produced CSPGs were distributed, scintillation counts of [35S] from astrocytes cultured for 48 h on TCPS coated with FBG were taken. The radioactivity counts showed that around four times as many GAGs were secreted into the culture media (206,556 counts min−1, cpm) as compared to remaining CSPGs associated with the cell (49,755 cpm on FBG-coated TCPS). Similar [35S] counts were also found for TCPS control surfaces coated with serum proteins from 10% FBS (211,977 cpm for secreted vs. 58,950 cpm for cell-bound GAGs).

2.5. Discussion

It has been shown that astrocytes respond to soluble fibrinogen leaked into the CNS by cleaving latent TGF-β that subsequently activates the smad signaling pathway leading to increased CSPG expression [15]. The present study showed that surface-adsorbed FBG is also recognized by astrocytes and removed away from surfaces as a part of the CNS inflammatory response. Furthermore, astrocytes removed adsorbed FBG both with and without TGF-β signaling inhibitor, SB 431542. Therefore, when present on the surfaces of neural implants and CNS biomaterials, adsorbed FBG is sufficient to incite astrocytes to

respond by FBG recognition and subsequent removal. The FBG removal was found to be a two-step process: an initial gradual decline followed by a more rapid phase. The rapid removal phase had a similar characteristic time constant, $\tau \sim 1–2$ h, when measured at different locations. The rapid removal only occurred after an initial period that varied as the cells migrated along the substrate[1]. No consistent evidence for cellular uptake of FBG was found in time-lapse experiments. Occasionally increased intracellular FBG fluorescence signals were seen due to cells that detached from the surface and passed through the field of view while still being suspended in medium. In studies where the cells were fixed, there were also few examples of FBG cellular uptake (Fig. 2.4A and B). At this stage, there is no information about the mechanism by which astrocytes removed and potentially digested adsorbed FBG; however, it is clear that the removal process was specific to FBG. The proteases present in the serum-containing media did not appear to influence the specific FBG removal. FBG used here was plasminogen-depleted to minimize the addition of excess plasmin. The characteristic patterns of FBG removal from the substrates were associated with astrocytes. Even if there was any removal of surface protein mediated by serum proteases, it was much less than what occurred with the cellular removal of FBG. Furthermore, the FBG removal was independent of presence of TGF-β receptor inhibitor. The phases of FBG removal indicated that the cells need some initial

[1] To reliably observe cell behavior, an initial 4 h of culture was used to allow for cells to attach to the substrates. In that initial time period, however, some regions of depleted fibrinogen but lacking cells were already present on the surface.

period for FBG recognition and mounting of the digestion apparatus for rapid FBG removal.

Serum albumin uptake by astrocytes after BBB disruption has been implicated in altering astrocyte behavior and causing pathological neuronal outcomes [23]. Astrocytes have been shown to uptake soluble albumin both in vivo and in vitro by Ivens et al. [24]. Such albumin uptake led to epileptiform activity in brain tissues. The same study also showed that both type I and type II TGF-β receptors were involved in albumin uptake into the brain. There may be a role for FBG in epileptogenesis as soluble FBG also triggers the same smad pathways [15]. In the current study, some evidence of astrocytes uptake of labeled albumin was seen when the cells were visualized by albumin fluorescence (Fig. 2.4C and D), but any uptake of adsorbed albumin from substrates was much smaller than the extent of FBG removal. This may potentially be due to cells being cultured in the presence of 10% serum and thus having an abundance of soluble albumin to uptake. Similarly, the differences in albumin conformation when adsorbed to the surface may have changed its bioavailability. However, in all samples astrocytes maintained FBG recognition and removal in the presence of serum.

The experiments showed that the responses of astrocytes to the FBG patterns were local: the cells that recognized and removed adsorbed FBG preferentially expressed CSPG on the locations of the FBG stimuli (Fig. 2.5 and Fig. 2.6). However, there was no apparent dose-dependence of CSPG expression on adsorbed FBG coverage (Fig. 2.7). On these samples, laminin

substrates had similar levels of CSPG production to the substrates with adsorbed FBG even though there was no evidence of laminin uptake by astrocytes. This was possibly due to CSPG binding to surface laminin, which is known to occur and has been well characterized in vitro [25] and [26]. The effect of such binding is likely minor in the present studies as the CSPG expression on LN substrates were not significantly greater than expression on FBS-coated glass substrates (data not shown). The binding of CSPG to LN could explain the presence of CSPG deposited in between the FBG patterns, but one would then expect that the bound CSPG would remain in such patterns even after FBG removal as the LN remains unchanged. On the contrary, CSPG expression by cells becomes more uniform after the underlying patterns are removed (Fig. 2.6). This suggests a specific deposition of CSPG in response to FBG that diminishes as the stimulus wanes. Another potential contributor to the similar levels of CSPG expression across surface types could be due to the presence of 10% serum in cell culture medium. The effects of growth factors, albumin and other blood proteins may have affected astrocyte phenotypes to the point where the influence of substrate proteins was less effective. In the CNS wound environment, however, the same serum proteins would also be present. Additionally, the effect of using SB 431542 to inhibit TGF-β could have been diminished if those same TGF-β receptors were inundated with albumin. This inhibitor treatment, however, did yield significant differences in CSPG expression for some samples (Fig. 2.7).

CSPG expression is expected to be a dynamic process in the sense that the acute CSPG response to local FBG might have been attenuated over time.

Note that in the present study CSPG production was not observed in real time, but only after 48 h of culture and subsequent cell fixing and staining. In an in vivo study of CSPG production in a stab-wound-induced glial scar in the spinal cord, it was shown that 130 kDa neurocan production actually decreased in the first 48 h post injury in the spinal cord, although this behavior was different for different types of CSPG macromolecules [27]. The peak level of RNA expression for neurocan in astrocytes in vitro occurred at 12 h after soluble fibrinogen treatment and this expression then diminished to baseline levels by 24 h though neurocan secretion into media persisted up to 7 days [15].

Astrocytes migrated while removing FBG and were even seen detaching after modifying the surface. Because of cell detachment, there likely was even higher CSPG production than what was captured after sample fixation and antibody staining. The radioactive sulfur measurements indicated that about four times as much GAGs are produced by astrocytes and released in the medium, though no differences in secreted and membrane bound CPSG were found for astrocytes exposed to adsorbed FBG vs. FBS-only proteins. It is apparent, however, that there was local, membrane bound CSPG expression in the presence of FBG. Confocal imaging indicated that CSPG vertical position was coincident with the position of surface bound FBG (Fig. 2.6). This local expression on the μm scale suggests that the astrocytic response to FBG was not a sustained, global upregulation of CSPG but rather a defined, controlled increase on membrane regions exposed to adsorbed FBG.

A significant decrease in CSPG production by blocking TGF-β receptors with SB 431542 in astrocyte cultures was only found for the substrates with predominant laminin coverage (FBG0/LN100 and FBG30/LN70). Decreases in CSPG production were found on the other substrate types but were not statistically significant (Fig. 2.7). It has been shown that astrocytes themselves produce TGF-β [28] available for intercellular signaling, which would be affected by adding of the inhibitor. This autocrine TGF-β functionality of astrocytes may potentially be more causal in determining overall CSPG production than the surface adsorbed FBG or externally added TGF-β, as these particular experiments yielded no significant changes in CSPG production. Although TGF-β contributed to CSPG production, blocking of the receptor did not abolish all CSPG production. Reducing the amount of expressed CSPG is an active area of research as potential CNS injury treatment. One approach is the digestion of CSPGs by chondroitinase, which leads to improved neuronal regeneration and function [29] and [30]. Similarly, SB 431542 might be considered for local treatment of CNS injuries and implants to reduce CSPG expression and astrogliosis, but the myriad roles of TGF-β signaling in the CNS wound environment must first be further understood [31]. The results presented here indicate that the TGF-β signaling pathway was not entirely responsible for astrocyte activation and CSPG expression in vitro on substrates with predominant fibrinogen coverage as the cells continued to produce CSPG even with SB 431542 treatment. In fact, a large fraction (>75%) of the astrocytic CSPG expression remained after inhibitor treatment on all types of substrates. In the

case of neural implants, one can infer that astrocytes will respond to the foreign stimulus and continue to present inhibitory CSPGs, even without TGF-β signaling. The impact that fibrinogen has on long term CNS implants has yet to be determined. It has been shown that BBB leakage continues 12 weeks after implantation, as demonstrated by the continued presence of IgG in brain tissue [1]. While FBG is approximately twice as large as IgG, it is likely that, if the BBB is compromised, various proteins could enter and potentially adsorb to the implant surface. However, it is important to note that after long-term implantation astrocytes are found at a distance of ~50 μm from the implant/tissue interface that is typically populated with microglia and macrophages [2]. Thus it is unclear whether astrocytes would be able to maintain long-term contact with implant surfaces. Regardless, based on the evidence presented here, astrocytes mount an initial removal of FBG from and deposition of CSPG on implant surfaces: events that may trigger the neuronal inhibition.

2.6. Conclusions

It was found that surface-adsorbed FBG is specifically recognized and removed by astrocytes. Thus, in addition to its roles in coagulation and carrying latent TGF-β in circulation, adsorbed fibrinogen also initiates cellular responses by CNS astrocytes. Astrocytes removed adsorbed FBG over the course of several hours, and such behavior was maintained regardless of the presence of a TGF-β signaling pathway inhibitor. This indicated that astrocytes maintain sensitivity to adsorbed FBG by some, yet unknown, TGF-β receptor-independent

mechanism. While the CSPG expression was not dependent on the amount of FBG presented on the substrates, there was evidence that astrocytes preferentially produce CSPG at FBG contacting parts of their cell membranes. Additionally, CSPG production was also maintained in the presence of the inhibitor. Based on the fact that blood contact and subsequent FBG adsorption is unavoidable in neural implantations, the present results indicate that implant-adsorbed FBG will trigger astrocyte removal of FBG. This alone may lead to local CSPG expression at the implant-CNS interface and thus contribute to subsequent inhibition of neuronal activity around the implant

2.7. Acknowledgements

This study was supported by the NIH Grant R01 NS057144. We thank Dr. F.W. Meng for cell culture and immunochemistry assistance, Dr. E. Budko for astrocyte isolation and Dr. C. Rodesch and K. Carney for time-lapse imaging support.

2.8. Appendix A. Figures with Essential Colour Discrimination

Certain figures in this article, particularly Figs. 2.1–2.6 are difficult to interpret in black and white. The full colour images can be found in the on-line version, at http://dx.doi.org/10.1016/j.actbio.2013.02.047.

2.9. Appendix B. Supplementary Data

Supplementary data associated with this article can be found, in the online version, at http://dx.doi.org/10.1016/j.actbio.2013.02.047.

2.10. References

[1] Winslow BD, Tresco PA. Quantitative analysis of the tissue response to chronically implanted microwire electrodes in rat cortex. Biomaterials 2010;31:1558–67.

[2] Biran R, Martin DC, Tresco PA. Neuronal cell loss accompanies the brain tissue response to chronically implanted silicon microelectrode arrays. Exp Neurol 2005;195:115–26.

[3] Polikov VS, Tresco PA, Reichert WM. Response of brain tissue to chronically implanted neural electrodes. J Neurosci Methods 2005;148:1–18.

[4] Brash JL. The fate of fibrinogen following adsorption at the blood–biomaterial, interface. Ann NY Acad Sci 1987;516:206–22.

[5] Roach P, Farrar D, Perry CC. Interpretation of protein adsorption: surface-induced conformational changes. J Am Chem Soc 2005;127:8168–73.

[6] Sofroniew MV. Molecular dissection of reactive astrogliosis and glial scar formation. Trends Neurosci 2009;32:638–47.

[7] East E, Golding JP, Phillips JB. A versatile 3D culture model facilitates monitoring of astrocytes undergoing reactive gliosis. J Tissue Eng Regener Med 2009;3:634–46.

[8] Davies SJA, Goucher DR, Doller C, Silver J. Robust regeneration of adult sensory axons in degenerating white matter of the adult rat spinal cord. J Neurosci 1999;19:5810–22.

[9] Dow KE, Wang W. Cell biology of astrocyte proteoglycans. Cell Mol Life Sci 1998;54:567–81.

[10] Yamada H, Fredette B, Shitara K, Hagihara K, Miura R, Ranscht B, et al. The brain chondroitin sulfate proteoglycan brevican associates with astrocytes ensheathing cerebellar glomeruli and inhibits neurite outgrowth from granule neurons. J Neurosci 1997;17:7784–95.

[11] Asher RA, Morgenstern DA, Fidler PS, Adcock KH, Oohira A, Braistead JE, et al. Neurocan is upregulated in injured brain and in cytokine-treated astrocytes. J Neurosci 2000;20:2427–38.

[12] Silver J, Miller JH. Regeneration beyond the glial scar. Nat Rev Neurosci 2004;5:146–56.

[13] Smith GM, Strunz C. Growth factor and cytokine regulation of chondroitin sulfate proteoglycans by astrocytes. Glia 2005;52:209–18.

[14] Kimura-Kuroda J, Teng X, Komuta Y, Yoshioka N, Sango K, Kawamura K, et al. An in vitro model of the inhibition of axon growth in the lesion scar formed after central nervous system injury. Mol Cell Neurosci 2010;43:177–87.

[15] Schachtrup C, Ryu JK, Helmrick MJ, Vagena E, Galanakis DK, Degen JL, et al. Fibrinogen triggers astrocyte scar formation by promoting the availability of active TGF-β after vascular damage. J Neurosci 2010;30:5843–54.

[16] O'Callaghan JP, Miller DB, Reinhard Jr JF. Characterization of the origins of astrocyte response to injury using the dopaminergic neurotoxicant, 1-methyl-4-phenyl-1,2,3,6-tetrahydropyridine. Brain Res 1990;521:73–80.

[17] McCarthy KD, de Vellis J. Preparation of separate astroglial and oligodendroglial cell cultures from rat cerebral tissue. J Cell Biol 1980;85:890–902.

[18] Corum LE, Eichinger CD, Hsiao TW, Hlady V. Using microcontact printing of fibrinogen to control surface-induced platelet adhesion and activation. Langmuir 2011;27:8316–22.

[19] Xia Y, Whitesides GM. Soft lithography. Annu Rev Mater Sci 1998;28:153–84.

[20] Victor XV, Nguyen TKN, Ethirajan M, Tran VM, Nguyen KV, Kuberan B. Investigating the elusive mechanism of glycosaminoglycan biosynthesis. J Biol Chem 2009;284:25842–53.

[21] Pixley SKR, Nieto-Sampedro M, Cotman CW. Preferential adhesion of brain astrocytes to laminin and central neurites to astrocytes. J Neurosci Res 1987;18:402–6.

[22] Inman GJ, Nicolás FJ, Callahan JF, Harling JD, Gaster LM, Reith AD, et al. SB-431542 is a potent and specific inhibitor of transforming growth factor- β superfamily type I activin receptor-like kinase (ALK) receptors ALK4, ALK5, and ALK7. Mol Pharmacol 2002;62:65–74.

[23] Friedman A, Kaufer D, Heinemann U. Blood–brain barrier breakdown-inducing astrocytic transformation: novel targets for the prevention of epilepsy. Epilepsy Res 2009;85:142–9.

[24] Ivens S, Kaufer D, Flores LP, Bechmann I, Zumsteg D, Tomkins O, et al. TGF-β receptor-mediated albumin uptake into astrocytes is involved in neocortical epileptogenesis. Brain 2007;130:535–47.

[25] Condic ML, Snow DM, Letourneau PC. Embryonic neurons adapt to the inhibitory proteoglycan aggrecan by increasing integrin expression. J Neurosci 1999;19:10036–43.

[26] Snow DM, Smith JD, Gurwell JA. Binding characteristics of chondroitin sulfate proteoglycans and laminin-1, and correlative neurite outgrowth behaviors in a standard tissue culture choice assay. J Neurobiol 2002;51:285–301.

[27] Tang X, Davies JE, Davies SJA. Changes in distribution, cell associations, and protein expression levels of NG2, neurocan, phosphacan, brevican, versican V2, and tenascin-C during acute to chronic maturation of spinal cord scar tissue. J Neurosci Res 2003;71:427–44.

[28] Lagord C, Berry M, Logan A. Expression of TGFβ2 but not TGFβ1 correlates with the deposition of scar tissue in the lesioned spinal cord. Mol Cell Neurosci 2002;20:69–92.

[29] Bradbury EJ, Moon LDF, Popat RJ, King VR, Bennett GS, Patel PN, et al. Chondroitinase ABC promotes functional recovery after spinal cord injury. Nature 2002;416:636–40.

[30] Alilain WJ, Horn KP, Hu H, Dick TE, Silver J. Functional regeneration of respiratory pathways after spinal cord injury. Nature 2011;475:196–200.

[31] Beck K, Schachtrup C. Vascular damage in the central nervous system: a multifaceted role for vascular-derived TGF-β. Cell Tissue Res 2012;347:187–201.

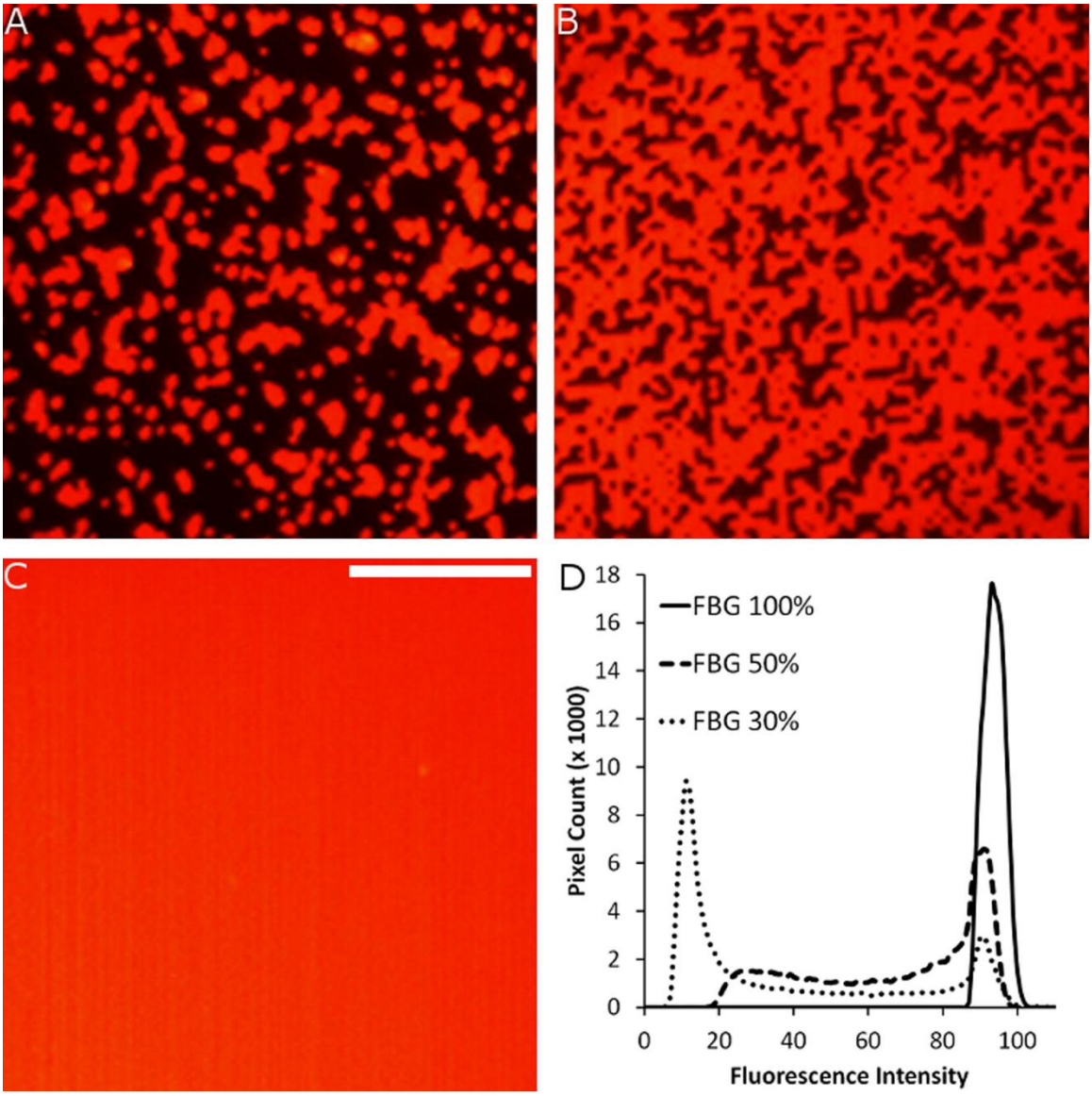

Fig. 2.1. Three substrates created by microcontact printing or adsorption of FBG. (A) 30% fibrinogen coverage with laminin (unlabeled) backfill (FBG30/LN70) and (B) 50% fibrinogen coverage with laminin backfill (FBG50/LN50) surfaces. (C) 100% coverage created by fibrinogen adsorption (FBG100/LN0). Scale bar indicates 50 μm for (A–C). (D) Histograms of the fluorescence intensity from fluorescently labeled FBG images showing differences in FBG deposition on different substrates.

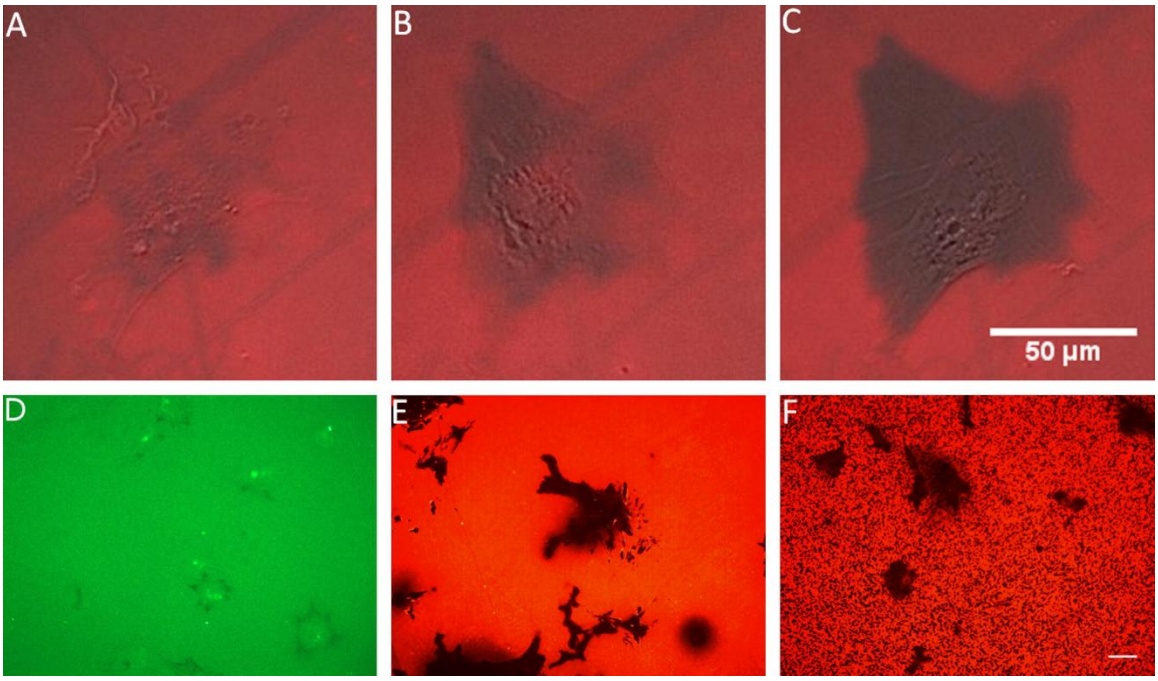

Fig. 2.2. Astrocyte modification of FBG and LN coated substrates. (A–C) FBG removal (DIC + fluorescence) by astrocytes at 4 h (A), 16 h (B) and 23 h (C) post-seeding. (D) Laminin 100% substrate (FBG0/LN100) remains largely unchanged after 48 h of astrocyte culture. (E, F) FBG layers modified by astrocytes after 48 h of culture on FBG100/LN0 (E) and FBG50/LN50 (F) substrates. Scale bars (in C for A–C and in F for D–F): 50 µm.

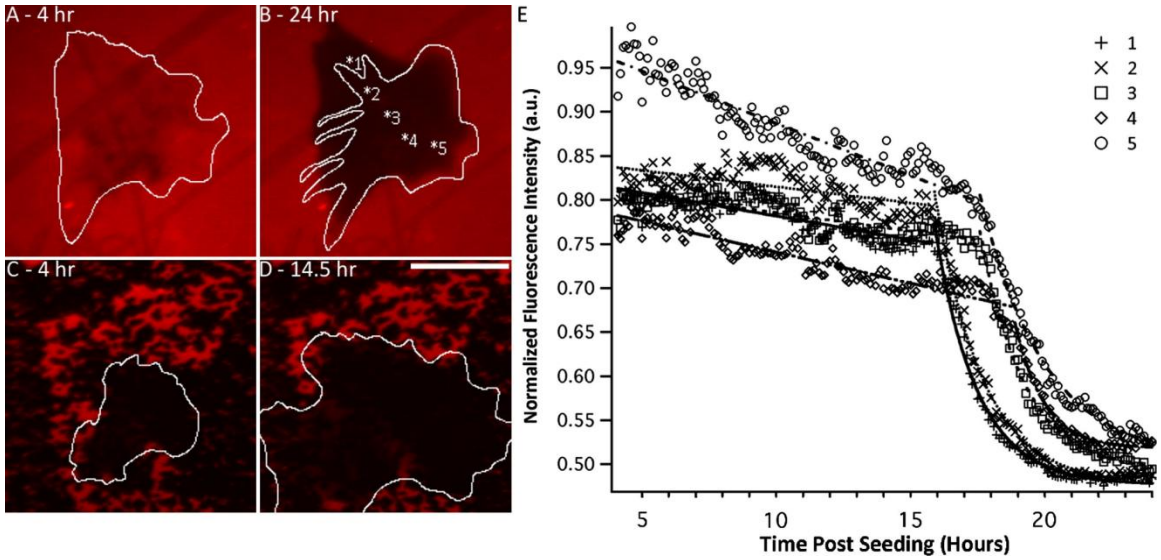

Fig. 2.3. Two-phase FBG removal process. (A) Initial (4 h post seeding) FBG100/LN0 substrate with cell outline. (B) Same region of FBG100/LN0 surface at 24 h post seeding with updated cell outline. Five regions (5 × 5 pixels) used in analysis of removal kinetics are indicated. (C) Initial FBG50/LN50 substrate (LN unlabeled) with outlined cell in early phases of spreading. (D) Same region FBG50/LN50 surface after 14.5 h of culture showing cell outline and removal of underlying FBG layer. Scale bar: 25 μm. (E) Plot of normalized fluorescence intensity as a function of time from five indicated cell locations in (B).

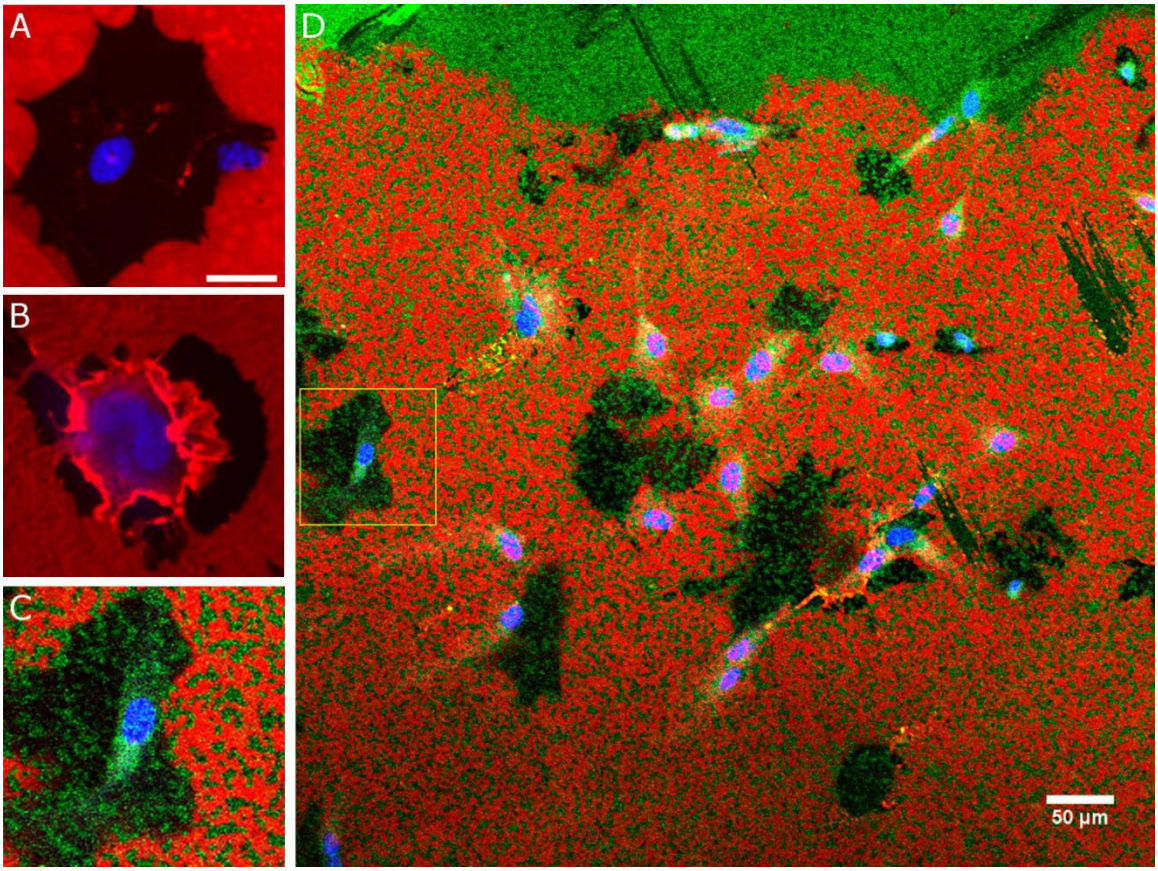

Fig. 2.4. Confocal images of fixed and stained samples showing astrocyte removal of FBG taken 48 h after seeding. (A) Majority of cells removed FBG (red) without any visible intracellular uptake. (B) Smaller fraction of cells showed increased FBG (red) fluorescence in otherwise dark cell footprint regions. (C, D) On a binary protein surface pattern (FBG + albumin) astrocytes did not alter albumin (green) to the degree of removing FBG (red) over 48 h. Cell nuclei were DAPI stained (blue). Yellow square in (D) indicates location of (C). Scale bars: 25 µm for (A–C), 50 µm for (D).

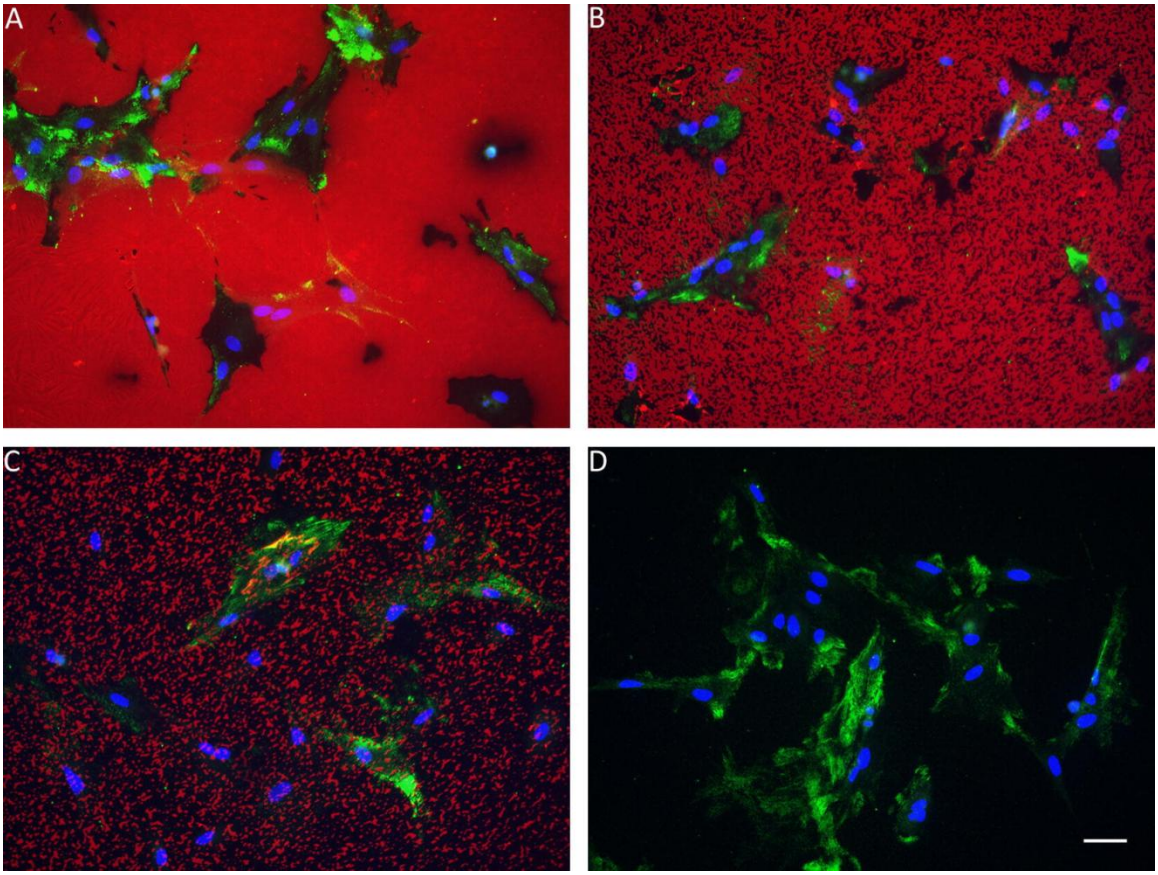

Fig. 2.5. Fluorescence images of fixed and stained samples showing the removal of FBG (red) and expression of CSPG (green) on FBG100/LN0 (A), FBG50/LN50 (B), FBG30/LN70 (C) and on FBG0/LN100 (D) substrates. Cell nuclei were DAPI stained (blue) and laminin was unstained. Scale bar: 50 μm.

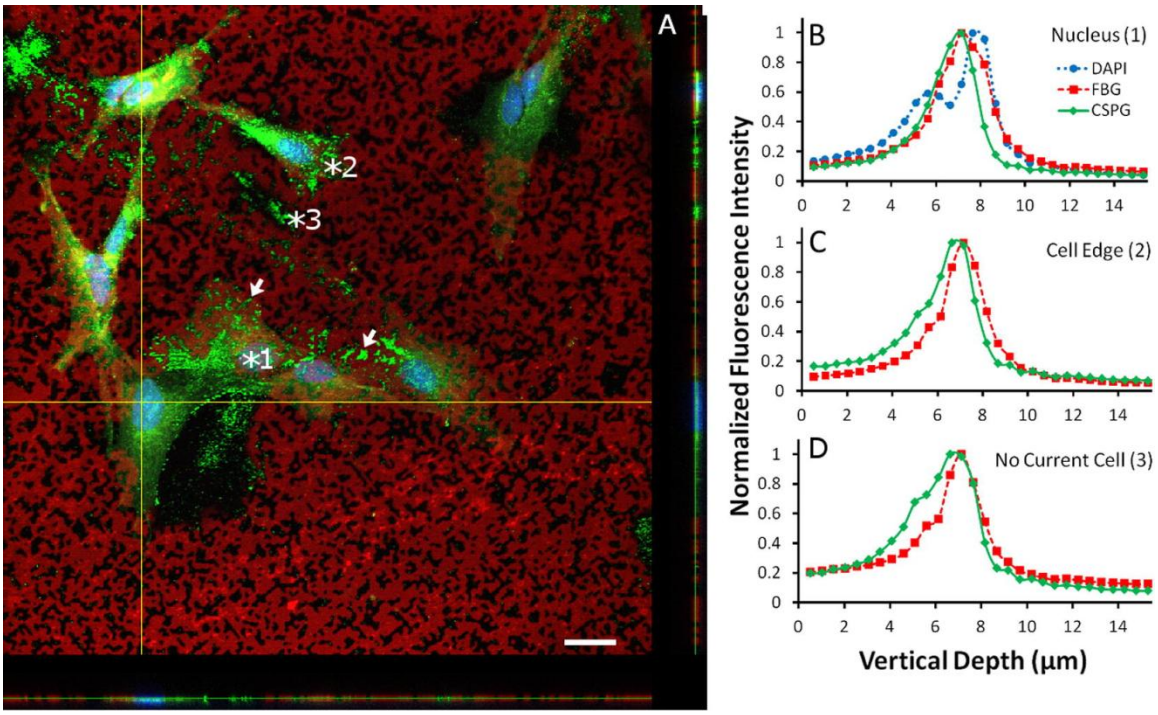

Fig. 2.6. (A) Confocal images stack of a representative fixed and stained sample showing CSPG (green) production on the FBG50/LN50 substrate (FBG in red, nuclei in blue). Yellow lines indicate the planes for z-projections shown beside and below in A. CSPG deposition was high in between the FBG patches prior to FBG removal (arrows). Scale bar: 25 μm. (B and C) Normalized vertical (z) intensity profiles show the peak CSPG intensity coinciding with peak FBG intensity at both the nucleus position (marked ∗1 in A, plot B), the periphery of cell (marked ∗2 in A, plot C), and in the region where the cell was no longer present (marked ∗3 in A, plot D).

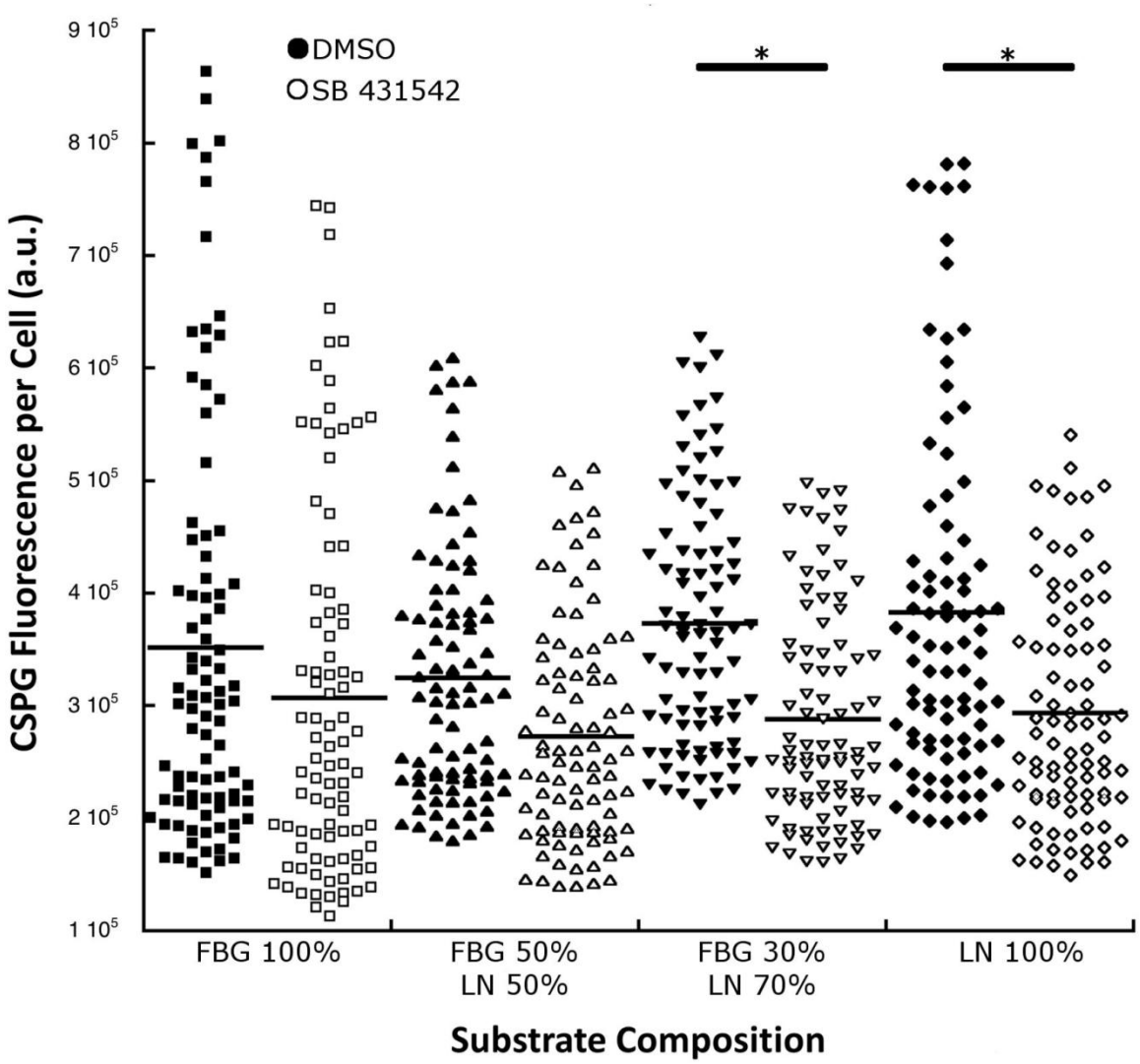

Fig. 2.7. The effect of TGF-β receptor kinase inhibitor SB 431542 on CSPG expression per cell on substrates with different FBG/LN coverage. Solid horizontal lines indicate the mean, and filled or empty points denote absence or presence of inhibitor, respectively. Asterisks denote $P < 0.005$, $n = 90$.

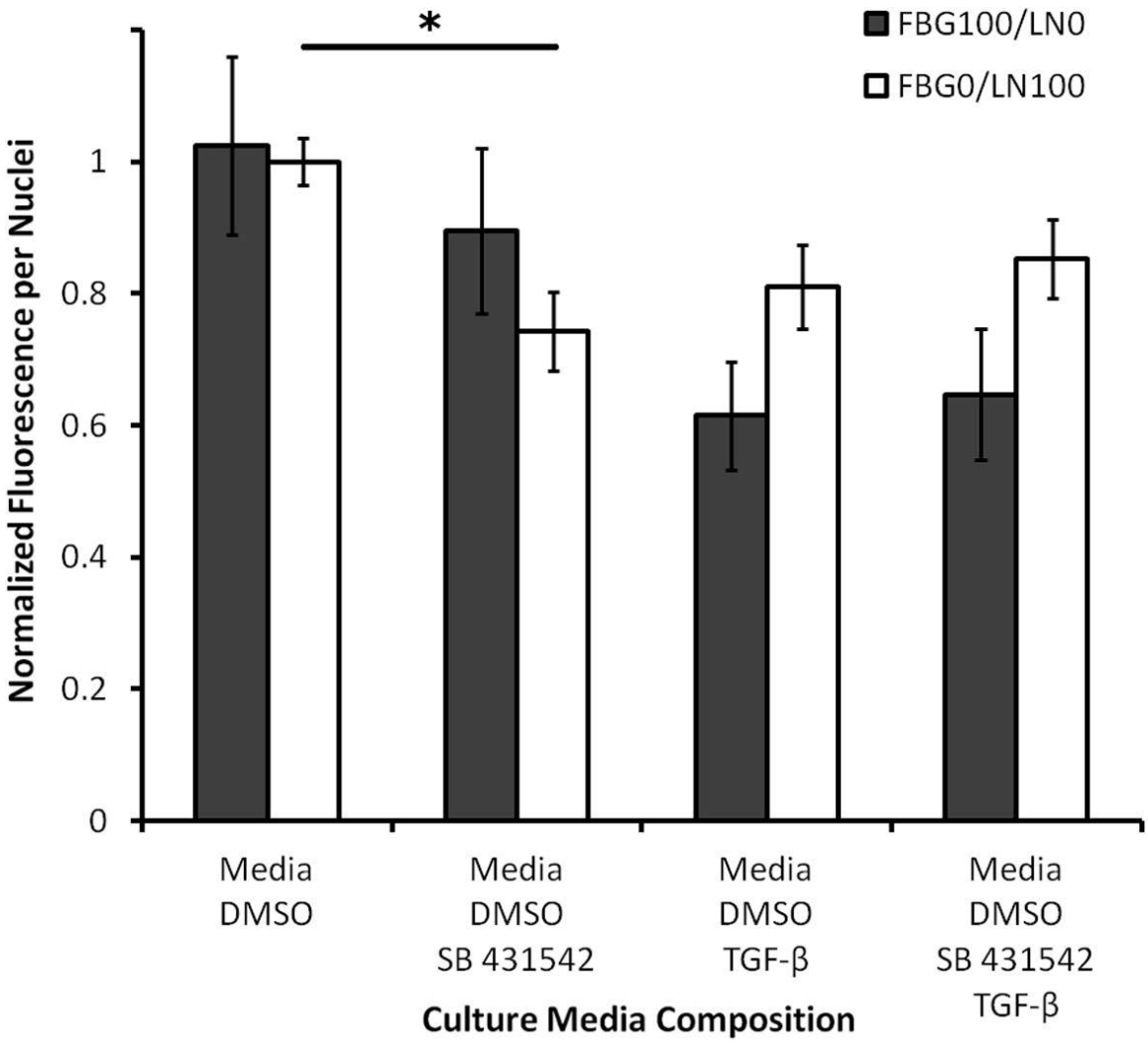

Fig. 2.8. The effect of solution added TGF-β in DMEM/F12/10% FBS media + DMSO on CSPG production. CSPG staining per cell data were normalized to FBG0/LN100 sample. Error bars indicate ±SEM. Asterisk denotes $P < 0.05$, $n = 10$.

CHAPTER 3

ASTROCYTES ALIGNMENT AND REACTIVITY ON COLLAGEN HYDROGELS PATTERNED WITH ECM PROTEINS[*]

3.1. Abstract

To modulate the surface properties of collagen and subsequent cell–surface interactions, a method was developed to transfer protein patterns from glass coverslips to collagen type I hydrogel surfaces. Two proteins and one proteoglycan found in central nervous system extracellular matrix as well as fibrinogen were patterned in stripes onto collagen hydrogel and astrocytes were cultured on these surfaces. The addition of the stripe protein patterns to hydrogels created astrocyte layers in which cells were aligned with underlying patterns and had reduced chondroitin sulfate expression compared to the cells grown on collagen alone. Protein patterns were covalently cross-linked to the collagen and stable over four days in culture with no visible cellular modifications. The present method can be adapted to transfer other types of protein patterns from glass coverslips to collagen hydrogels.

[*] Reprinted from Biomaterials, Vol 39, pp. 124-130, © 2015 with permission from Elsevier.

3.2. Introduction

Glial cells facilitate neuronal guidance in recovering central nervous system (CNS) tissues and, from among them, astrocytes are known to form aligned networks which coincide with regenerating nerve tracts [1]. The poor recovery of neural functionality after CNS injury has been ascribed to the presence of inhibitory molecules as well as the formation of the disorganized tissue known as the glial scar [2], [3] and [4]. In response to CNS tissue injury, astrocytes become reactive and begin to express intermediate filaments as they hypertrophy. While this reactive scarring has beneficial roles, astrocytes also upregulate expression of extracellular matrix (ECM) molecules such as chondroitin sulfate proteoglycan (CSPG) that has been shown to inhibit neuronal regeneration [4]. One approach to improve CNS recovery is to treat the glial scar with chondroitinase, a broad enzyme that digests chondroitin sulfate, thus enzymatically removing the inhibitory components of the scar [5]. An alternative to that approach would be to add a biomaterial to the injury site so that injured neuronal cells could grow directionally and eventually re-establish lost connections [6]. Such a biomaterial should both facilitate re-establishing glial organization and promote neuronal regeneration.

Collagen type I has been used extensively in treating injured CNS with devices ranging from dura replacement sheets to nerve guidance conduits. Collagen has been shown to be bioresorbable and easily incorporated by host tissue. Astrocytes themselves have been shown to deposit collagen in the CNS wound environment [7]. Collagen types I, III, and IV have been found in the glial

scar, though their presence alone is not inhibitory [8], [9], [10] and [11]. Collagen is also a permissive substrate for neuronal outgrowth and regeneration in vivo [12] and [13]. Used as a growth substrate in vitro, collagen has been used to create a scaffolding structure where a quiescent, unreactive astrocyte phenotype is preserved, as opposed to the more reactive, hypertrophic phenotype that occurs in standard 2D astrocyte culture [14]. Collagen has also been used as a scaffold material for cellular therapies including glial precursors [15], Schwann cells [16], and differentiated astrocytes [17].

Rather than implanting a simple biomaterial scaffold to a CNS injury site, the addition of other ECM components to the scaffold has been used to improve CNS recovery as reviewed by Volpato et al. [18]. Collagen has been augmented with various bioactive agents including brain-derived neurotrophic factor (BDNF) [19], neurotrophin-3 [20], fibroblast growth factor (FGF) [21], and chondroitinase [22], which have been cross-linked to collagen gels to improve neuronal outgrowth. Topographical cues, such as the direction of collagen nanofibers, have also been used to align and direct both astrocytes and neurons [23]. Neurons grown at the interface between collagen and ECM components patterned on glass showed that neurons followed associated ECM patterns and largely avoided penetrating deeper into collagen gels [24]. Thus, it seems that both the physical properties of collagen scaffolds and the presence of surface guidance cues are important for determining the CNS cellular response.

Controlling astrocyte alignment and infiltration is a worthy goal for improving CNS regenerative biomaterial potential [21] and [25]. Astrocytes may

serve as a source for guidance cues and growth factors, and, as a large component to the glial scar, their behavior is important for wound healing and neuroprotection [26]. We have shown that even fixed aligned astrocytes will still direct neuronal outgrowth without having to release any active soluble factors [27]. As differentiated astrocytes seeded in collagen constructs have led to functional recovery in vivo [17], the ability of astrocytes to attach to and align on biomaterial constructs may foment subsequent directed neuronal outgrowth and promote regeneration.

The present study aimed at imparting directional guidance cues to collagen gels in a relatively simple way so that astrocytes can attach and align themselves without increasing their reactivity so commonly seen in traditional 2D cultures. The method described here was used to covalently attach patterns of proteins or proteoglycans to collagen hydrogel surfaces. Similar approaches have been proposed for other polymers such as polydimethylsiloxane (PDMS), polyvinyl alcohol, polyacrylamide, and polycaprolactone [28], [29], [30], [31] and [32]. Recently, microcontact printing of proteins to freeze-dried Matrigel™ and gelatin has been demonstrated [33]. However, to the best of our knowledge, the present report is the first application of protein pattern transfer and covalent attachment to the surface of collagen type I hydrogels and requires no additional, specialized equipment beyond standard materials for creating protein patterns. The techniques described here will be conducive to the transfer of multiple proteins deposited in any desired pattern on glass surface by traditional microcontact printing [34], stamp-off [35], sequential stamping, microscope-aided

registration [36], dip-pen nanolithography [37], or inkjet deposition [38], directly to collagen hydrogel surface.

3.3. Materials and Methods

3.3.1. Collagen hydrogel patterning

To visualize patterns transferred to the surface of collagen gels, proteins were labeled with fluorophores. Human plasma fibrinogen (FBG, plasminogen depleted, Calbiochem) and aggrecan (AGG, A1960, Sigma) were fluorescently labeled with Alexa Fluor 594 (A-20004, Invitrogen). Laminin (LN, L2020, Sigma–Aldrich) and fibronectin (FN, F1141, Sigma–Aldrich) were labeled with Alexa Fluor 488 (A-20000, Invitrogen). To separate labeled protein from free dye, labeled protein solutions were eluted in phosphate buffered saline (PBS) through a PD-10 Sephadex column (GE Healthcare). Collected solutions were then filtered through a 0.20 μm syringe filter (Sarstedt), divided into 100 μL aliquots, and stored at −20 °C until use.

To pattern the surface of collagen gels, a two-step process was used. Microcontact printing (μCP) was used first to pattern labeled proteins onto sterilized 18 mm glass coverslips [34] and [39]. The pattern used in this study consisted of 15 μm stripes separated by 25 μm–wide gaps. This pattern was selected as 15 μm stripes previously aligned astrocytes on glass [27], and the added asymmetry was useful to distinguish printed and non-printed regions while maintaining alignment [36]. In the second step, a process was developed for collagen to undergo simultaneous gelling and cross-linking while the protein

patterns were transferred (Fig. 3.1). Bis[sulfosuccinimidyl] suberate (BS3, Thermo Scientific) was prepared immediately before collagen gelling to minimize hydrolysis of its reactive groups. Two mg of BS3 was dissolved in double-distilled, deionized (DDI) water to a concentration of 50 mM. This BS3 solution was placed as a 10 µL droplet on top of the stamped proteins on the coverslip surface and then immediately followed by deposition of 100 µL collagen type I (BD Biosciences) solution at a concentration of 10 mg/mL to the top of the stamped coverslips. NaOH (1 M) was added to bring the gel to neutral pH according to manufacturer specifications. A PDMS sheet (0.005″ thick, Specialty Manufacturing Inc.) was placed on top of the gel to facilitate gel spreading and future handling. Gelling and cross-linking was allowed to proceed for 30 min at 37 °C. The gel constructs were then placed in a humidified incubator to dry for an additional 48 h. The patterned collagen was separated from the stamped coverslip with the aid of physical force (i.e., using a cell scraper). To isolate patterned collagen gel alone, the construct was submerged in water and the hydrogel was lifted off the backing substrate using a fine brush. This procedure was successful with collagen gel concentrations ranging from 5 to 10 mg/mL, with higher concentrations being more amenable to physical manipulation. Removal was facilitated by releasing the entire circumference of the gel by scraping under its edge about a millimeter prior to attempting to separate it entirely from the substrate. By using the separated edges, a peeling motion from one side to the other, while ensuring that the gel was separating evenly, was effective. This also prevented damage to the center of the gel where images

were later acquired. A collagen concentration of 10 mg/mL, which has been shown to have physical properties relevant to CNS tissue [40], was used in this study to eliminate any further variation in gel stiffness.

3.3.2. Cell culture

Primary astrocytes from post-natal day 2 Sprague–Dawley rats were obtained using established protocols [41]. Confluent astrocyte cultures were shaken to remove contaminating cells and frozen. Astrocytes were thawed and cultured for 2 weeks prior to trypsinization and seeding onto collagen gels. Cultures were maintained in a humidified incubator at 37 °C and 5% CO_2. Astrocytes were seeded on collagen gels at a density of approximately 25,000 per cm^2 in SATO- serum-free media [42] and allowed to attach for 5 h. After that time, medium was changed to DMEM/F12 (Caisson Labratories) with 10% fetal bovine serum (FBS, Atlanta Biologicals) for the remaining culture period. Medium was exchanged at 48 h, and the cultures were fixed at 96 h post-seeding.

3.3.3. Immunocytochemistry for CSPG quantification

Because real time phase or DIC microscopy of astrocytes on collagen gels were difficult due to extensive light scattering by the gels, cells on gels were fixed in 4% paraformaldehyde (PFA) for 15 min and rinsed in PBS with 0.1% sodium azide prior to immunocytochemical staining. All procedures were carried out at room temperature. Samples were blocked with 4% goat serum in PBS for one hour and then rinsed thrice in PBS with sodium azide. Primary anti-chondroitin

sulfate (CS-56) antibody (C8035, Sigma) was applied to the astrocytes for one hour in a 1:500 dilution in the block solution. Samples were again rinsed three times in PBS with sodium azide. Secondary goat anti-mouse IgM antibody labeled with Alexa Fluor 488 (A21042, Molecular Probes) or Alexa Fluor 594 (A21044, Molecular Probes) was subsequently applied to the cell samples for 1 h. Following three more PBS rinses, 4′,6-diamidino-2-phenylindole (DAPI, Invitrogen) in a 1:100 dilution was added for 15 min to stain for nuclei. Samples were then rinsed in DDI water and mounted between coverslips (Fisher) with Fluoromount-G (Southern Biotech) for imaging. Astrocytes on plain collagen controls were divided into two batches for use with each type of secondary antibody. Fluorescence images were captured using a Nikon Eclipse E600 epifluorescence microscope with a 20× PlanAPO objective and CCD camera (CoolSNAP, Photometrics).

3.3.4. Quantifying astrocyte CSPG expression

CSPG samples were imaged after staining using identical exposure times in Image Pro Plus (Media Cybernetics) software. A blank image was subtracted from each image and the CSPG fluorescence intensity was quantified using ImageJ (NIH). The CSPG fluorescence was integrated over the entire image and divided by the number of cells per image as identified by DAPI staining. Samples with fewer than five nuclei were not included in analysis. Images were taken of five sample sub-areas where protein patterns and cells were visible and on the

same focal plane. An ANOVA with a Tukey post hoc test ($\alpha = 0.05$) was used to determine the significance of data differences.

3.3.5. Astrocyte alignment analysis

Astrocyte alignment was assessed by measuring the orientation of their nuclei [27] and [36]. To do this, the angle of the major axis of the oval-like astrocyte nuclei were quantified using the measure angle function of Image Pro Plus. Fig. 3.2 shows the measured angles (shown as line segments drawn at the measured angle and superimposed over outlined nuclei). Any nuclei that were on image edges that could not be fully resolved were excluded from analysis. The measured nuclei angles were then converted to an alignment angle with respect to the orientation of the underlying protein pattern. For collagen controls lacking protein patterns, the vertical axis was used as reference. The alignment angles of all nuclei across each given sample type were compiled into a histogram in 10° bins. A zero degree angle indicated nuclei that were completely parallel with the underlying patterns. Histograms were fit with a Gaussian function using Igor Pro (Wavemetrics) to find the mean alignment angle and the full width at half maximum (FWHM) for each nuclei population (FWHM is approximately equal to 2.4 times the standard deviation of the angle distribution).

3.4. Results

3.4.1. Protein patterns transferred to collagen gels and resisted removal by astrocytes

The techniques described here created collagen gels with a covalently immobilized pattern of protein transferred from glass to one of the gels' surfaces. Stripe patterns of aggrecan (AGG), fibrinogen (FBG), fibronectin (FN), and laminin (LN) were all successfully transferred to the surface of collagen type I gels (Fig. 3.3). Fidelity of the pattern on gels required quality protein patterns on glass and careful manual removal of gels to maintain intact gel sheets. As loss of immobilized proteins from the gel surfaces would negate the benefit of patterning these gels, the patterns were imaged prior to and after 96 h of astrocyte culture to determine pattern integrity. No changes in the protein pattern appearance were observed over that time period. Unlike the removal of glass-adsorbed fibrinogen by astrocytes seen previously [43], proteins patterned on collagen were not removed by cells over the given culture time period. We infer that the protocol used created stable, immobilized protein patterns that did not diffuse into the gel or desorb/detach from the collagen surface.

3.4.2. Astrocytes align with underlying protein patterns on collagen

Astrocytes attached and spread onto collagen gel surfaces with and without immobilized protein patterns within the first 5 h of culture. After the addition of 10% serum and subsequent culture for 4 days, astrocytes oriented themselves on the gels. A degree of polarity and alignment was established

locally by the cells even on plain collagen gel controls (Fig. 3.2A) as astrocytes that were close together tended to align with each other in clusters. For samples with immobilized ECM protein patterns, a much stronger alignment was seen (Fig. 3.2B). Only stripes of transferred protein differentiated these surfaces from plain collagen gel controls. A more quantitative measure of the astrocyte alignment is given by the histograms showing the fitted Gaussian function, mean angle, and FWHM values for each sample (Fig. 3.4). On the control collagen gels (Fig. 3.4A), astrocyte alignment was random with angles spread across all possible angles with a FWHM of 176.1°. In contrast, on gels with immobilized ECM protein stripes, the mean angle for astrocyte nuclei was within 8° of the orientation of the underlying pattern for each protein (Fig. 3.4F). The difference between the patterned proteins can be analyzed by the variations in FWHM where the smallest FWHM value indicated better alignment. Nuclei on the FBG pattern showed the narrowest orientation spread (FWHM of 37.6°, equivalent to a standard deviation of ±16°; Fig. 3.4C). FN and LN patterns (Fig. 3.4D,E) were less potent than FBG in aligning cells with FWHMs of 79.6 and 69.9°, respectively. The AGG pattern, which does not strongly align astrocytes on glass [36], was the least effective (Fig. 3.4B; FWHM = 113.8°).

3.4.3. Astrocyte CSPG reactivity is attenuated with the addition of ECM proteins

The overall CSPG expression by astrocytes was significantly lower on the ECM protein patterned gels compared with two sets of controls[1] (Fig. 3.5). The presence of FBG and LN patterns led to a significant reduction (>50%) of CSPG expression. There was no significant CSPG reduction detected for the FN pattern, while on the AGG pattern the CSPG was reduced to about one-third of the mean CSPG expressed per cell for collagen control. As expected, in the case of AGG patterns, there was some staining of underlying AGG stripes with the anti-CS antibody. This fluorescence was included in the integrated CSPG fluorescence so the actual reduction of CSPG expression by astrocytes on AGG patterns could have been greater than shown in Fig. 3.5.

3.5. Discussion

3.5.1. Collagen gels with stripe patterns aid alignment of astrocytes

As previously shown, neurons send outgrowths that follow aligned astrocytes and Schwann cells, as well as biomimetic artificial surfaces [44]. If one can use a biomaterial surface to align astrocytes and other glia, subsequent neuronal growth and layers of glia could then be guided as well. Using the method developed here for decorating collagen surfaces with ECM proteins, it would be possible to transfer any protein pattern prepared on a glass coverslip

[1] For imaging both the ECM protein pattern (see Fig. 3.3) and expressed CSPG, secondary goat anti-mouse IgM antibodies were either labeled with Alexa Fluor 488 or Alexa Fluor 594.

surface to collagen. While others have aligned astrocytes in/on collagen via physical forces [25], the current protocol could be readily adapted to transfer multi-protein patterns, thus increasing the repertoire of the molecular cues for astrocyte alignment and/or neuronal outgrowth.

As there were no added topographical cues on these patterned collagen gels, the alignment was caused by the molecules found on the surface of the gels. These could include the patterned proteins, ECM secreted by the cells, proteins from the culture medium, and collagen itself. The presence of adhered serum proteins could not be ruled out as all samples had the access to 10% serum containing medium. The 10% serum medium was introduced after the initial culture period of 5 h without serum. After this initial attachment period, the composition of the surface proteins might have been altered as both cells and 10% serum were present. Therefore, the actual mechanism as to how the patterned protein stripes functioned to align astrocytes could not be conclusively determined. It is clear, however, that the presence of these protein stripes causes nuclear alignment over plain collagen.

Astrocyte nuclei were seeded randomly across the substrates, and were found to slightly favor the position where the nucleus is partially on the protein stripe pattern and partially off of it after culture. The pattern used in the present study had an unequal distribution of protein vs. collagen-only areas. For any given region, only 37.5% of the area (15/(25 + 15)) was covered with patterned protein stripes. The likelihood of the cell to attach to collagen alone was 62.5%, (25/(15 + 25)), almost twice than that for protein stripes. If a fully spread cell were

50 μm wide and was centered in the middle of a collagen stripe, it could sample both neighboring protein patterns on each of its sides. Conversely, if it finds itself in the middle of the protein stripe, it would only sample collagen on both sides. That may explain why some nuclei were found over the collagen regions between the protein stripes. However, the actual count of the nuclei positions showed no clear preference for collagen-only regions: the majority of nuclei were located over some portion of both collagen and the protein stripe.

We have previously seen that adsorbed FBG was removed from glass surfaces below adhered astrocytes, most likely because of the protein was simply adsorbed to the surface [43]. In the case of immobilized FBG on collagen gel surface, astrocytes did not remove fibrinogen or any of the other three ECM proteins from the surface, indicating that the transfer procedure created stable crosslinks between the protein molecules and the gel surface. Likewise, crosslinks could have also formed between two collagen molecules or two patterned proteins with this technique. Regardless, the ECM proteins patterned here still maintained alignment potency after this process.

The robust nature of transferred protein patterns, coupled with the tendency for guidance information to be carried from cell to cell, indicates that a collagen biomaterial device with appropriately oriented patterns could provide a scaffold for recovering CNS cells that could combat the default tissue disorganization that occurs in CNS injury. The underlying collagen itself could then be remodeled and degraded leaving potentially superior outcomes post injury.

3.5.2. Astrocyte CSPG reactivity decreases with ECM alignment cues

It is well known that in response to CNS injury, astrocytes acquire a reactive phenotype, which includes increased expression of glial fibrillary acidic protein (GFAP) and CSPG [4]. Although some variants of the chondroitin sulfate (CS) chains, such as CS-C, are inhibitory to neuronal outgrowth and others variants (CS-A and CS-E) are not [45], astrocyte expression of CSPG is correlated with their inhibitive properties to neurons. While CSPG are also shed into the surrounding cellular environment by astrocytes [43] and [45], the surface expression on their membranes is important for interfacing with neurons. It is therefore informative to determine if a CNS biomaterial scaffold itself is increasing astrocyte surface expression of CSPG. As compared with the collagen control, three ECM proteins — FBG, AGG, and LN—each able to align astrocytes to some degree, were also able to reduce this CSPG expression. The decrease in CSPG reactivity between unpatterned and patterned gels could have been caused by either the ECM molecule itself or the alignment of astrocytes it caused. Based on the previous reports that the introduction of FBG into the CNS after injury triggers CSPG production [46], and that fact that AGG already contains inhibitory CS chains, it appears that the alignment itself was the dominant contributing factor resulting in the decrease in CSPG expression seen here (Fig. 3.5). It has been shown that the presence of topographical cues that aligned astrocytes also reduced astrocyte reactivity [47]. Similarly, astrocytes grown on aligned electrospun fibers of polycaprolactone had decreased GFAP expression compared to those on random fibers [48]. The findings from the

present study thus indicate that astrocytes and their surface CSPG expression are sensitive to organized, directional cues.

3.6. Conclusions

Creating collagen gels with surfaces patterned with FBG and three ECM proteins was developed and tested on in vitro cultures of astrocytes. Patterns of FBG, AGG, FN, and LN stripes were able to align astrocytes when compared to collagen alone. Additionally, the aligned astrocytes on AGG, FBG, and LN patterns showed reduced overall CSPG expression. Astrocytes survived the entire 96 h culture period, leaving no indication of toxicity of this process. Other cross-linking agents like genipin [21] and disuccinimidyl-disuccinate-polyethyleneglycol (SS-PEG-SS) [49], which have previously been used to link proteins to collagen, should be amenable to the protein pattern lift-off from glass coverslips. The method developed here will also allow transfer of multiple ECM molecules with any desired spatial presentation on collagen and the investigation of cellular responses. In this way, the method may find its application to biomedical devices where surface–cell interactions can be leveraged to improve patient outcomes. Collagen biomaterials with their surfaces decorated with relevant ECM cues may thus augment regeneration of injured CNS tissue.

3.7. Acknowledgments

The authors would like to thank Dr. Elena Budko for astrocyte isolation and the University of Utah Bioengineering Department for its support. This work was partially funded by NIH Grants NS057144 and NS088737.

3.8. References

[1] Davies SJA, Goucher DR, Doller C, Silver J. Robust regeneration of adult sensory axons in degenerating white matter of the adult rat spinal cord. J Neurosci 1999 Jul 15;19(14):5810–22.

[2] Liu BP, Fournier A, GrandPre T, Strittmatter SM. Myelin-associated glycoprotein as a functional ligand for the nogo-66 receptor. Science 2002 Aug 16;297(5584):1190–3.

[3] Chen MS, Huber AB, van der Haar ME, Frank M, Schnell L, Spillmann AA, et al. Nogo-A is a myelin-associated neurite outgrowth inhibitor and an antigen for monoclonal antibody IN-1. Nature 2000 Jan 27;403(6768):434–9.

[4] Silver J, Miller JH. Regeneration beyond the glial scar. Nat Rev Neurosci 2004 Feb;5(2):146–56.

[5] Alilain WJ, Horn KP, Hu H, Dick TE, Silver J. Functional regeneration of respiratory pathways after spinal cord injury. Nature 2011 Jul 14;475(7355):196–200.

[6] Stokols S, Tuszynski MH. Freeze-dried agarose scaffolds with uniaxial channels stimulate and guide linear axonal growth following spinal cord injury. Biomaterials 2006 Jan;27(3):443–51.

[7] Heck N, Garwood J, Schütte K, Fawcett J, Faissner A. Astrocytes in culture express fibrillar collagen. Glia 2003;41(4):382–92.

[8] Weidner N, Grill RJ, Tuszynski MH. Elimination of basal lamina and the collagen “scar” after spinal cord injury fails to augment corticospinal tract regeneration. Exp Neurol 1999 Nov;160(1):40–50.

[9] Joosten EAJ, Dijkstra S, Brook GA, Veldman H, Bär PR. Collagen IV deposits do not prevent regrowing axons from penetrating the lesion site in spinal cord injury. J Neurosci Res 2000;62(5):686–91.

[10] Okada M, Miyamoto O, Shibuya S, Zhang X, Yamamoto T, Itano T. Expression and role of type I collagen in a rat spinal cord contusion injury model. Neurosci Res 2007 Aug;58(4):371–7.

[11] Klapka N, Müller HW. Collagen matrix in spinal cord injury. J Neurotrauma 2006 Apr 21;23(3–4):422–36.

[12] Cholas RH, Hsu H-P, Spector M. The reparative response to cross-linked collagen-based scaffolds in a rat spinal cord gap model. Biomaterials 2012 Mar;33(7):2050–9.

[13] Liu S, Peulve P, Jin O, Boisset N, Tiollier J, Said G, et al. Axonal regrowth through collagen tubes bridging the spinal cord to nerve roots. J Neurosci Res 1997;49(4):425–32.

[14] East E, Golding JP, Phillips JB. A versatile 3D culture model facilitates monitoring of astrocytes undergoing reactive gliosis. J Tissue Eng Regen Med 2009;3(8):634–46.

[15] Ketschek AR, Haas C, Gallo G, Fischer I. The roles of neuronal and glial pre cursors in overcoming chondroitin sulfate proteoglycan inhibition. MicroRNAs—Human Neurobiol Neuropathol 2012 Jun;235(2):627–37.

[16] Goto E, Mukozawa M, Mori H, Hara M. A rolled sheet of collagen gel with cultured schwann cells: model of nerve conduit to enhance neurite growth. J Biosci Bioeng 2010 May;109(5):512–8.

[17] Davies SJA, Shih C-H, Noble M, Mayer-Proschel M, Davies JE, Proschel C. Transplantation of specific human astrocytes promotes functional recovery after spinal cord injury. PLoS One 2011 Mar 2;6(3):e17328.

[18] Volpato FZ, Führmann T, Migliaresi C, Hutmacher DW, Dalton PD. Using extracellular matrix for regenerative medicine in the spinal cord. Biomaterials 2013 Jul;34(21):4945–55.

[19] Houweling D, van Asseldonk JT, Lankhorst A, Hamers FP, Martin D, B€ar P, et al. Local application of collagen containing brain-derived neurotrophic factor decreases the loss of function after spinal cord injury in the adult rat. Neurosci Lett 1998 Jul 31;251(3):193–6.

[20] Houweling DA, Lankhorst AJ, Gispen WH, B€ar PR, Joosten EAJ. Collagen containing neurotrophin-3 (NT-3) attracts regrowing injured corticospinal axons in the adult rat spinal cord and promotes partial functional recovery. Exp Neurol 1998 Sep;153(1):49–59.

[21] Macaya DJ, Hayakawa K, Arai K, Spector M. Astrocyte infiltration into injectable collagen-based hydrogels containing FGF-2 to treat spinal cord injury. Biomaterials 2013 May;34(14):3591–602.

[22] Liu T, Xu J, Chan BP, Chew SY. Sustained release of neurotrophin-3 and chondroitinase ABC from electrospun collagen nanofiber scaffold for spinal cord injury repair. J Biomed Mater Res A 2012;100A(1):236–42.

[23] Liu T, Houle JD, Xu J, Chan BP, Chew SY. Nanofibrous collagen nerve conduits for spinal cord repair. Tissue Eng Part A 2012;18(9–10):1057–66.

[24] Kofron CM, Fong VJ, Hoffman-Kim D. Neurite outgrowth at the interface of 2D and 3D growth environments. J Neural Eng 2009;6(1):016002.

[25] East E, de Oliveira DB, Golding JP, Phillips JB. Alignment of astrocytes increases neuronal growth in three-dimensional collagen gels and is maintained following plastic compression to form a spinal cord repair conduit. Tissue Eng Part A 2010;16(10):3173–84.

[26] Sofroniew MV. Molecular dissection of reactive astrogliosis and glial scar formation. Trends Neurosci 2009 Dec;32(12):638–47.

[27] Meng F, Hlady V, Tresco PA. Inducing alignment in astrocyte tissue constructs by surface ligands patterned on biomaterials. Biomaterials 2012 Feb;33(5):1323–35.

[28] Alford PW, Nesmith AP, Seywerd JN, Grosberg A, Parker KK. Vascular smooth muscle contractility depends on cell shape. Integr Biol 2011;3(11):1063–70.

[29] Yu H, Xiong S, Tay CY, Leong WS, Tan LP. A novel and simple microcontact printing technique for tacky, soft substrates and/or complex surfaces in soft tissue engineering. Acta Biomater 2012 Mar;8(3):1267–72.

[30] Rape AD, Guo W, Wang Y. The regulation of traction force in relation to cell shape and focal adhesions. Biomaterials 2011;32(8):2043–51.

[31] Polio SR, Rothenberg KE, Stamenovic D, Smith ML. A micropatterning and image processing approach to simplify measurement of cellular traction forces. Acta Biomater 2012 Jan;8(1):82–8.

[32] Giannitelli SM, Abbruzzese F, Mozetic P, De Ninno A, Businaro L, Gerardino A, et al. Surface decoration of electrospun scaffolds by microcontact printing. Asia-Pac J Chem Eng 2014;9(3):401–6.

[33] Castano AG, Hortiguela V, Lagunas A, Cortina C, Montserrat N, Samitier J, et al. Protein patterning on hydrogels by direct microcontact printing: application to cardiac differentiation. RSC Adv 2014;4(55):29120–3.

[34] Qin D, Xia Y, Whitesides GM. Soft lithography for micro- and nanoscale patterning. Nat Protoc 2010 Mar;5(3):491–502.

[35] Desai RA, Khan MK, Gopal SB, Chen CS. Subcellular spatial segregation of integrin subtypes by patterned multicomponent surfaces. Integr Biol 2011;3(5):560–7.

[36] Eichinger CD, Hsiao TW, Hlady V. Multiprotein microcontact printing with micrometer resolution. Langmuir 2011 Dec 28;28(4):2238–43.

[37] Piner RD, Zhu J, Xu F, Hong S, Mirkin CA. “Dip-Pen” nanolithography. Science 1999 Jan 29;283(5402):661–3.

[38] Calvert P. Inkjet printing for materials and devices. Chem Mater 2001 Sep 12;13(10):3299–305.

[39] Von Philipsborn AC, Lang S, Bernard A, Loeschinger J, David C, Lehnert D, et al. Microcontact printing of axon guidance molecules for generation of graded patterns. Nat Protoc 2006 Oct;1(3):1322–8.

[40] Elias PZ, Spector M. Viscoelastic characterization of rat cerebral cortex and type I collagen scaffolds for central nervous system tissue engineering. J Mech Behav Biomed Mater 2012 Aug;12(0):63–73.

[41] McCarthy KD, de Vellis J. Preparation of separate astroglial and oligodendroglial cell cultures from rat cerebral tissue. J Cell Biol 1980 Jun 1;85(3):890–902.

[42] Bottenstein JE, Sato GH. Growth of a rat neuroblastoma cell line in serum-free supplemented medium. Proc Natl Acad Sci 1979;76(1):514–7.

[43] Hsiao TW, Swarup VP, Kuberan B, Tresco PA, Hlady V. Astrocytes specifically remove surface-adsorbed fibrinogen and locally express chondroitin sulfate proteoglycans. Acta Biomater 2013 Jul;9(7):7200–8.

[44] Kofron CM, Liu YT, Lopez-Fagundo CY, Mitchel JA, Hoffman-Kim D. Neurite outgrowth at the biomimetic interface. Ann Biomed Eng 2010;38(6):2210–25.

[45] Swarup VP, Hsiao TW, Zhang J, Prestwich GD, Kuberan B, Hlady V. Exploiting differential surface display of chondroitin sulfate variants for directing neuronal outgrowth. J Am Chem Soc 2013 Aug 15;135(36):13488–94.

[46] Schachtrup C, Ryu JK, Helmrick MJ, Vagena E, Galanakis DK, Degen JL, et al. Fibrinogen triggers astrocyte scar formation by promoting the availability of active TGF- b after vascular damage. J Neurosci 2010 Apr 28;30(17):5843–54.

[47] Ereifej ES, Matthew HW, Newaz G, Mukhopadhyay A, Auner G, Salakhutdinov I, et al. Nanopatterning effects on astrocyte reactivity. J Biomed Mater Res A 2013;101A(6):1743–57.

[48] Lau CL, Kovacevic M, Tingleff TS, Forsythe JS, Cate HS, Merlo D, et al. 3D electrospun scaffolds promote a cytotrophic phenotype of cultured primary astrocytes. J Neurochem 2014;130(2):215–26.

[49] Koch S, Yao C, Grieb G, Prevel P, Noah EM, Steffens GCM. Enhancing angio genesis in collagen matrices by covalent incorporation of VEGF. J Mater Sci Mater Med 2006;17(8):735–41.

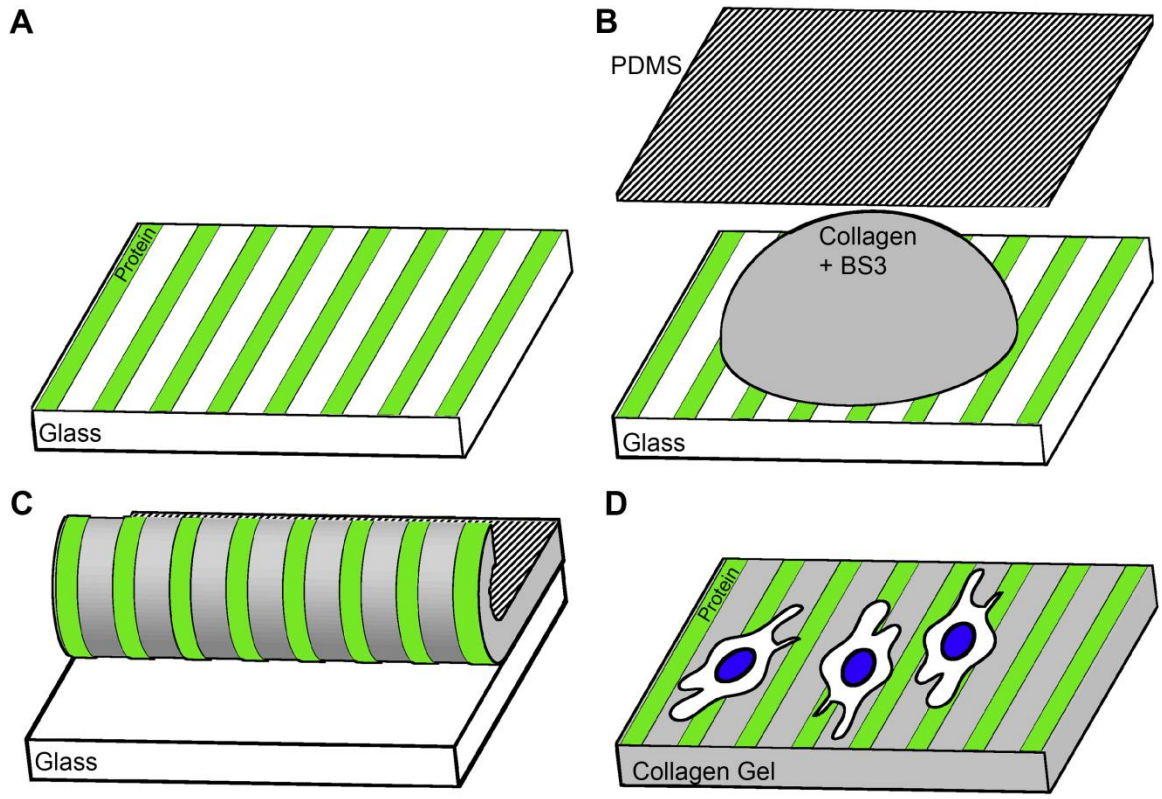

Fig. 3.1. Schematic of process for transferring protein pattern to collagen. A) The desired pattern is first created on a glass surface after which B) BS3 crosslinker solution and collagen are placed on the pattern and spread with a PDMS sheet. C) The gel is allowed to crosslink with the pattern and then peeled from the glass. The PDMS backing can be removed leaving a D) stand-alone collagen gel with a surface with patterned proteins.

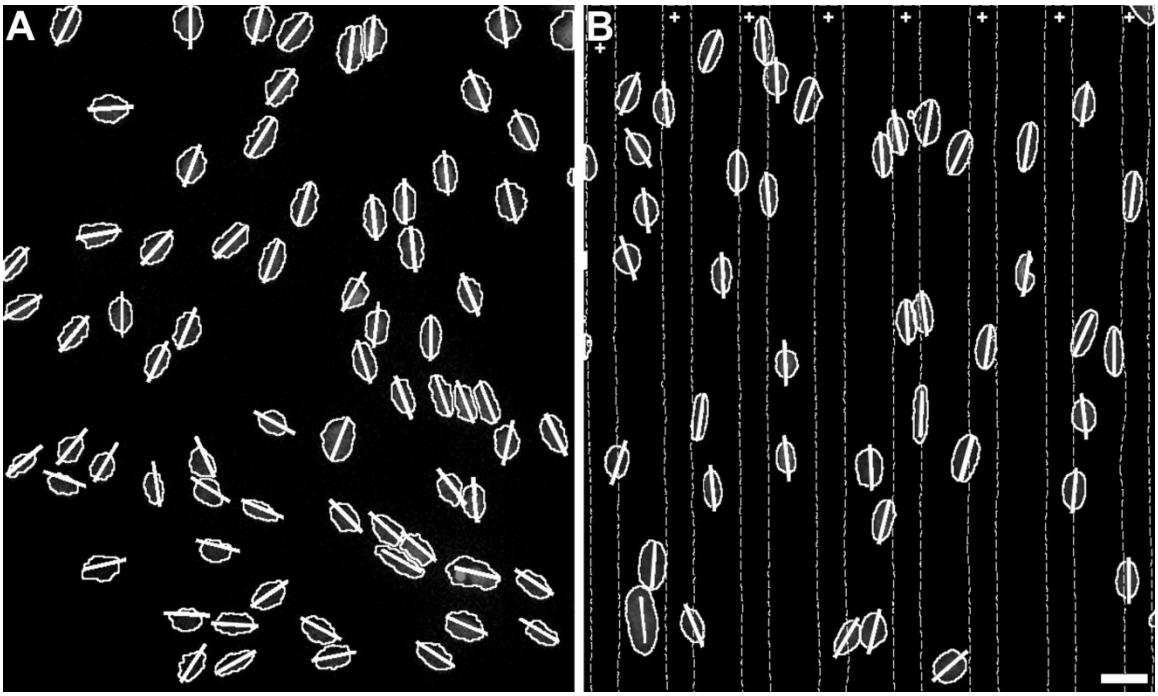

Fig. 3.2. Astrocyte nuclei angle measurements. Representative images of astrocyte nuclei on A) unpatterned collagen control and B) collagen with fibrinogen protein pattern. Areas between dotted lines marked with þ indicate regions with patterned FBG on collagen gel. Short lines drawn for each nucleus indicate the angle measured for the major axis of each nucleus. Scale bar = 25 µm.

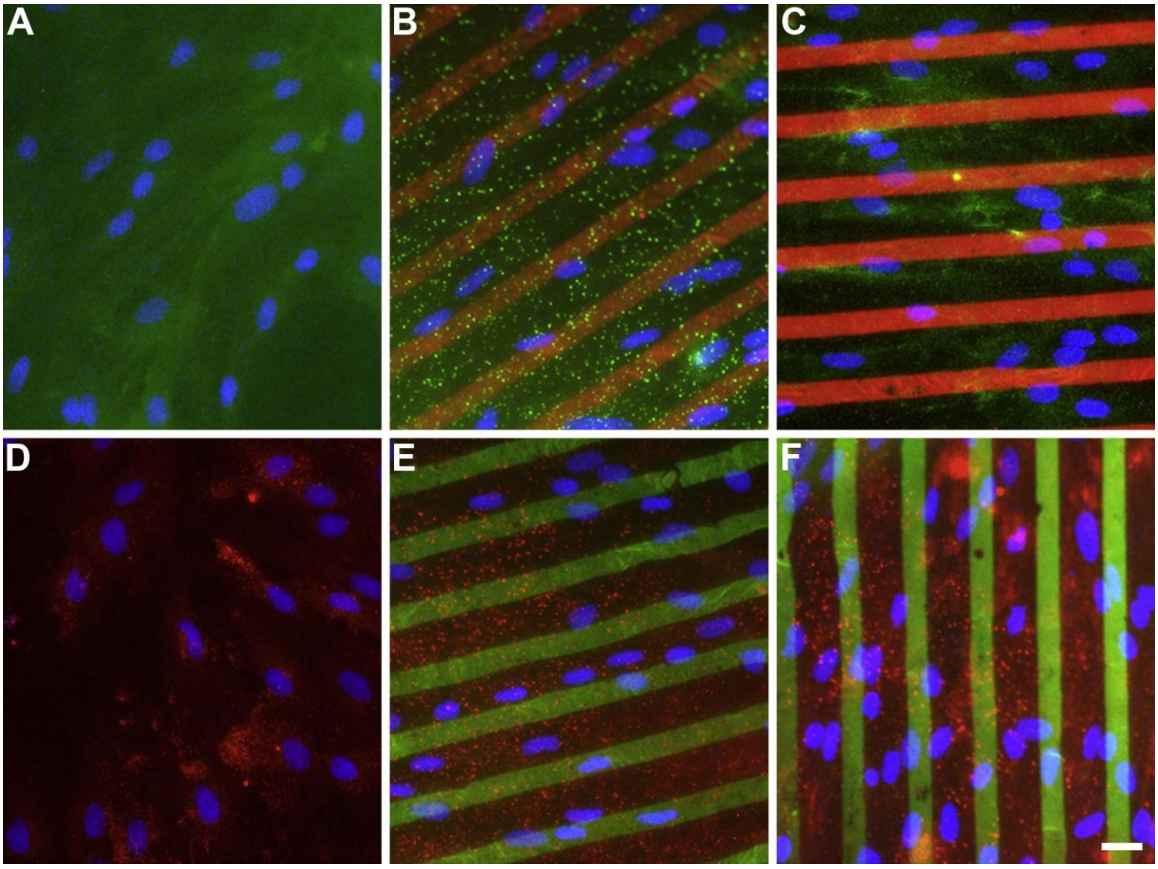

Fig. 3.3. Representative fluorescence images of astrocytes on patterned collagen gels. A,D) unpatterned collagen control; B) aggrecan (red) on collagen; C) fibrinogen (red) on collagen; E) fibronectin (green) on collagen; and F) laminin (green) on collagen gels were created. In panels A–C, CSPG (green) expression was measured using Alexa Fluor 488 labeled secondary antibody. In panels D–F, CSPG (red) was measured using Alexa Fluor 594 labeled secondary antibody. Nuclei (blue) can be seen in each image (A–F). Scale bar = 25 μm. (For interpretation of the references to color in this figure legend, the reader is referred to the web version of this article.)

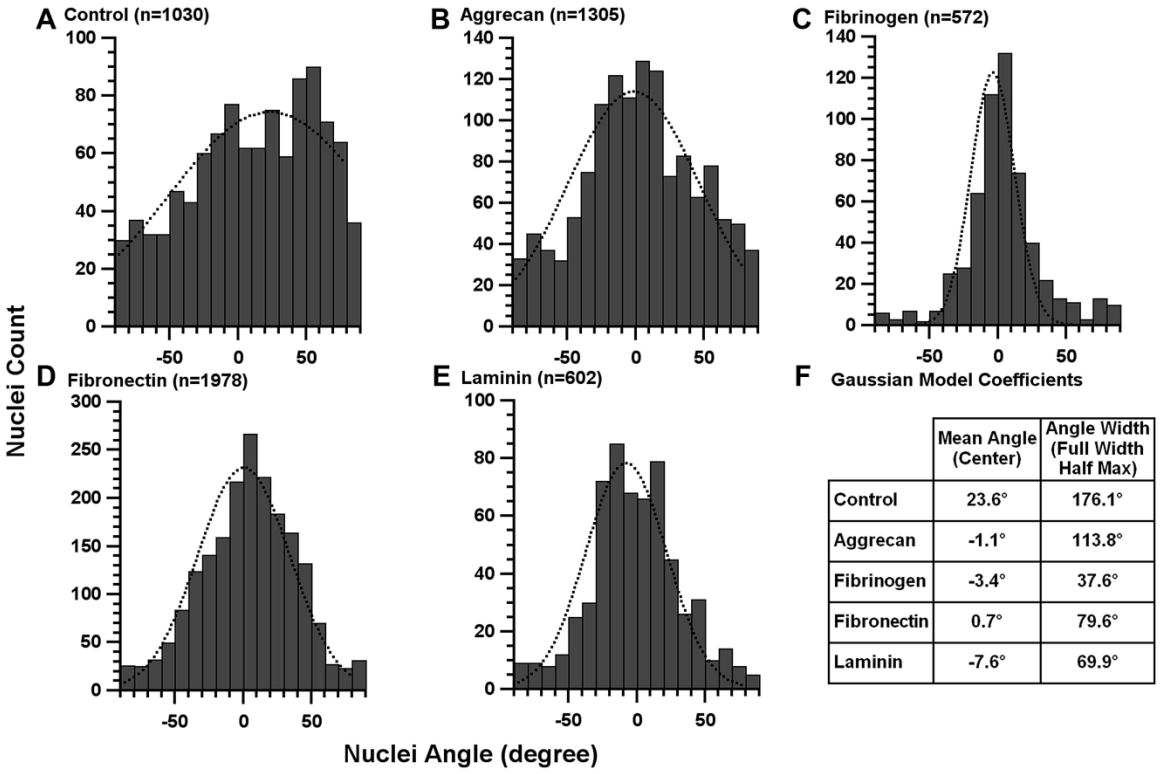

	Mean Angle (Center)	Angle Width (Full Width Half Max)
Control	23.6°	176.1°
Aggrecan	-1.1°	113.8°
Fibrinogen	-3.4°	37.6°
Fibronectin	0.7°	79.6°
Laminin	-7.6°	69.9°

Fig. 3.4. Astrocyte nuclei angle histograms on patterned collagen gels. The angles of observed astrocyte nuclei were compiled into histogram with 10° bins for A) unpatterned collagen control, B) aggrecan stripes, C) fibrinogen stripes, D) fibronectin stripes, and E) laminin stripes. The dotted curves indicate the Gaussian model fit for each data set. These fitted curves were used to calculate the F) mean angle and full-width-half-max (FWHM) for each pattern.

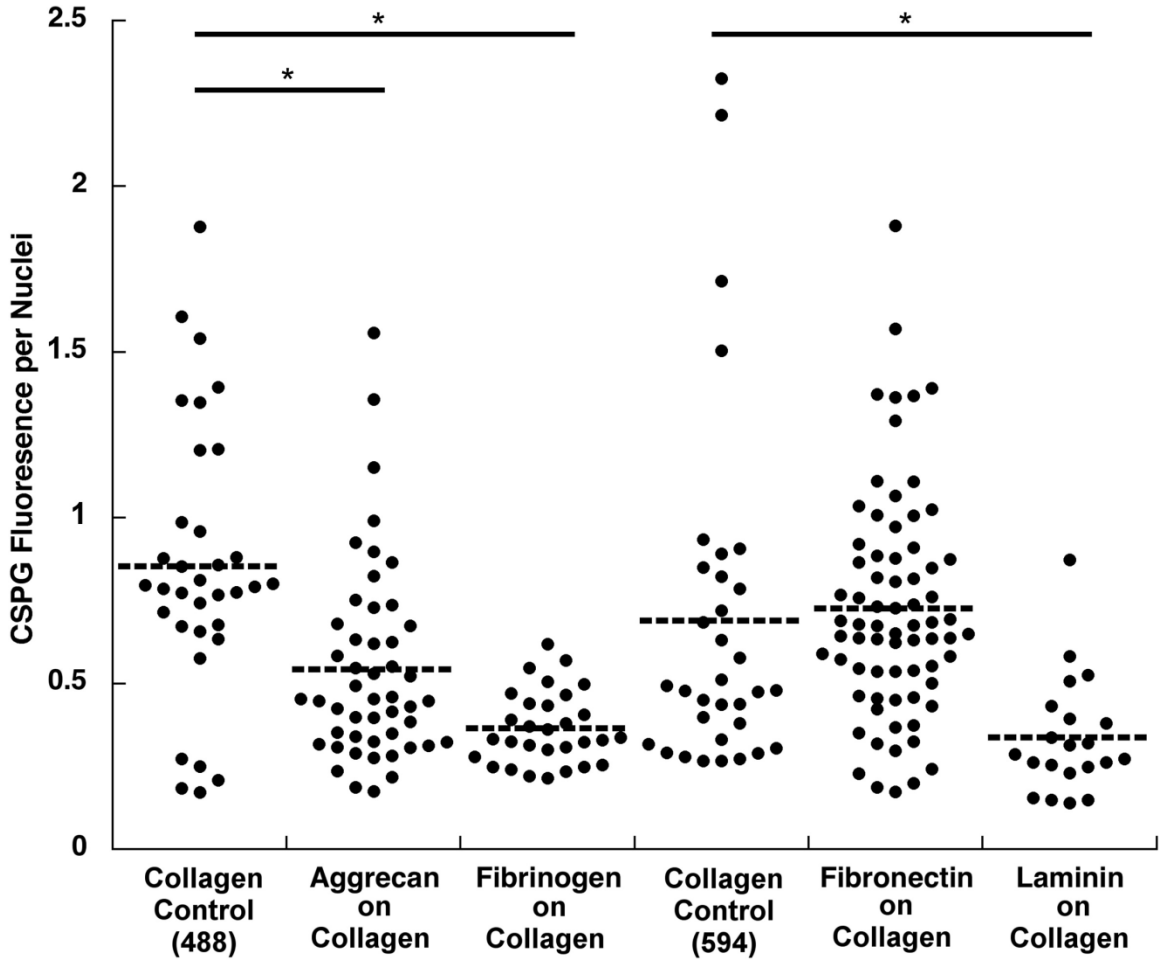

Fig. 3.5. CSPG expression by astrocytes on patterned collagen gels. Each dot represents CSPG fluorescence (in arbitrary units) integrated from a single fluorescence image. To account for the variations in cell numbers in each image, the integrated CSPG fluorescence from each image was divided by the number of cells present. CSPG was either visualized using Alexa Fluor 488 labeled secondary antibody for aggrecan and fibrinogen patterns, or Alexa Fluor 594 labeled secondary antibody for fibronectin and laminin patterns. Unpatterned collagen controls for both fluorophores were used to allow for comparison between proteins. Asterisks denote $p < 0.005$.

CHAPTER 4

ASTROCYTE SPREADING AND MIGRATION ON AGGRECAN-LAMININ DOT GRADIENTS

4.1 Abstract

A surface gradient made of two ECM molecules was developed to understand the migratory and morphological responses of astrocytes to molecular cues typically found in the central nervous system injury environment. The gradient, prepared using microcontact printing, was composed of randomly positioned µm-sized dots of aggrecan (AGG) on a uniform coating of laminin (LN). The aggrecan patches were printed in an increasing number along the 50 µm wide, 1 mm long gradient. Each gradient was surrounded by a uniform region of aggrecan. Astrocytes seeded on gradients were found to attach to exposed LN patches in the gradient. Cellular extensions of the cells were longer than the processes found for cells seeded on uniform control surfaces. Astrocyte extensions were greatest and spanned a distance of 150 µm when they were attached to the mixed AGG+LN patches of the gradient. Astrocytes extended processes in a stellate fashion upon initial attachment and maintain extensions as evidenced by increased area and perimeter when presented with AGG+LN

but not with LN alone. The cells did not migrate large distances after initial attachment, only distances of around 20–35 μm over 24 h, but preferentially shifted from areas of high AGG to high LN concentration regions. These findings indicate that presenting mixed ECM cues caused astrocytes to sample larger areas of the gradient and allowed the cells to preferentially relocate to more permissive regions.

4.2 Introduction

After central nervous system (CNS) injury, resident astrocytes serve important functions to reduce damage by restoring homeostasis, sequestering invading cells, and preserving neuronal cells[1–3]. Astrocytes are also responsible for the neuron inhibitory extracellular matrix (ECM) rich in chondroitin sulfate proteoglycan (CSPG) that is produced following CSN injury[4]. These contrasting characteristics largely arise due to the heterogeneous nature of astrocytes and the varying time course of their roles as the neuroprotective impacts are overshadowed by CSPG production over the course of healing[2,5]. The ability of astrocytes to migrate in the recovering CNS environment and compact lesions has been shown to be beneficial to functional recovery[6].

Several approaches have been undertaken to understand how astrocytes migrate both in vivo and in vitro. Xenogenic astrocyte transplants into mice showed that astrocytes migrated at a rate of 220 μm/day before slowing[7]. Transplanted astrocytes from primary cultures actively entered multiple regions of brain tissue[8,9]. In contrast, there was no marked migration of cortical

astrocytes after stab wounds[10]. This lack of migration has also been observed in real time. After traumatic brain injury (TBI), live tracking of astrocytes showed that there was no bulk recruitment or migration of astrocytes to the wound site, but rather an increase in proliferation of cells adjacent to the injury[11]. However, a subset of astrocytes from the proliferative sub-ventricular zone were shown to migrate to ischemic cortex and have neuroprotective functions[12]. In vitro, scratch wound assays have been commonly used to investigate how astrocytes close gaps in confluent monolayers. Astrocytes at the edge proliferate but individual cells show limited movement[13]. They also upregulate ECM molecule production, especially laminin and CSPG[14,15]. This behavior leads to eventual closing of the defect.

There is conflicting evidence regarding the role of astrocytes at the injury site. Astrocytes differentiated with bone morphogenetic protein that were placed in collagen scaffolds aided functional recovery after spinal cord injury in rats[16]. Conversely, application of collagen fiber-based scaffolds that also improved functional outcomes in canines showed that grafts were not heavily populated with astrocytes while neurons continued to be able to grow[17]. In contrast, polylactic acid (PLA) microfibers were shown to concurrently direct both astrocyte and neuronal growth when used to bridge a spinal transection[18]. While it is unclear if populating scaffolds with astrocytes is important for functional recovery, in vitro studies have been shown that aligned astrocytes increase outgrowth and convey directionality to neurons themselves[19,20]. Alignment of astrocytes and

a subsequent decrease in reactivity can be accomplished using electric fields, topographical features, and molecular cues[20–24].

Rather than a uniform coating of chemoattractant, a potential stimulus for guiding astrocytes onto scaffold surfaces could include a directional gradient containing attractive and/or repulsive molecular cues. Such surface gradients have been valuable in discovering neuronal behavior[25–28], which can be missed in the absence of subtle concentration changes of molecular cues[29]. Laminin has been shown to be supportive of astrocytes adhesion and migration[14], and aggrecan, a proteoglycan with CSPG chains, is often selected as a model inhibitory component. Aggrecan is produced by astrocytes and is known to inhibit Schwann cell migration[30]. Aggrecan has also been shown to have limited alignment effect on astrocytes[31]. In the present study, we utilized time-lapse microscopy to observe astrocytes after being seeded on randomly placed μm-size aggrecan patches printed on a uniform film of laminin. Microcontact printing was used to print these aggrecan patches in an increasing number along the 50 μm wide and 1 mm long area that was surrounded by a uniform field of aggrecan. In this way, each gradient of aggrecan also contained a countergradient of laminin. Random placement of aggrecan patches in gradients resulted in a lack of periodicity found in alternative designs[32–34]. Astrocyte migratory and morphological responses to the aggrecan/laminin and their preference for these two molecular cues were measured over 24 h and quantified.

4.3. Materials and Methods

4.3.1. Cell Culture

Primary P1-3 astrocytes were harvested from Sprague-Dawley rats according to established protocol[35]. Cortical astrocytes were cultured for 1 week, shaken to remove other cell types, and then frozen in liquid nitrogen prior to use. Cells were thawed and cultured for 1–2 weeks in DMEM/F12 media (Gibco) supplemented with 10% fetal bovine serum (FBS, Atlanta Biologicals) prior to treatment with 0.25% trypsin and placement onto gradient patterns. Astrocytes were seeded at low density of 5000-6000 cells per square centimeter in SATO- serum-free[36] medium. Astrocytes were cultured at 5% CO_2 and 37 °C for the duration of the experiments. Only astrocytes that were visibly attached to the surfaces were imaged for subsequent analyses.

4.3.2. Gradient Surface Patterning

Dot gradients were designed using Mathematica (Wolfram) to randomly place pixels as previously described[37]. The gradients were 50 µm wide and 1000 µm long and spaced 100 µm apart by a region of 100% coverage. The design was then translated with L-Edit (Tanner) to create a file for an electromask pattern generator to expose onto a photoresist-coated mask (Telic). Polydimethylsiloxane (PDMS) was then cast on the mask to form stamps. To visualize the stamped protein gradient, aggrecan (AGG, A1960, Sigma) was fluorescently labeled with Alexa Fluor 594 (A-20004, Invitrogen) and eluted through a PD-10 Sephadex column (GE Healthcare) with phosphate buffered

saline (PBS) to remove unreacted fluorophore. The AGG solution was diluted to a concentration of 0.3 mg/mL in PBS and stored at 4 °C until use. Glass-bottomed petri dishes (Fluorodish) were coated by adsorption with a 0.3 mg/mL laminin (LN, L2020, Sigma-Aldrich) solution at 4 °C overnight and then rinsed with double-distilled, deionized water (DDI) and dried under nitrogen prior to microcontact printing. Gradient stamps were adsorbed with labeled AGG solution for 1–2 h at room temperature and then rinsed thrice with DDI and dried with nitrogen. Stamps were manually placed into conformal contact with the glass dish bottoms, and remained in contact for 5–10 min prior to stamp removal. Gradient transfer was confirmed by imaging the fluorescent AGG.

4.3.3. Time-Lapse Microscopy

A fully-automated Olympus IX81 inverted microscope with a 20x objective was used to image astrocytes in glass-bottomed dishes. A custom-machined aluminum holder was used to securely keep dishes in the temperature-controlled stage chamber. Uncovered dishes filled with DDI water were included in the chamber to maintain humidity. Metamorph imaging software (Molecular Devices) was used to control the computerized stage, filters, and CCD camera to automatically take images every 5 min for chosen locations. The built-in autofocus function of the software was used every 5 images over the imaging period. The captured digital images were mapped to 0.65 µm per pixel. For substrates with aggrecan/laminin gradients, cells were allowed to attach for 4 h post-seeding and then were imaged for 20 h. A substrate with a uniform laminin

coating was used as a control. On this substrate, the cells were imaged within 30 min post-seeding for 24 h. Regions with cells that left the field of view, underwent apoptosis or were obscured by debris or intercellular contact were neglected. All images had background correction using a fitted 2D cubic polynomial prior to analysis.

4.3.4. Astrocyte Morphology Quantification

Astrocyte outlines were measured for each cell with the aid of the ESnake plugin (EPFL) [38] for ImageJ (NIH). The ESnake setting for control points ranged from 20-50 based on cell size and morphology complexity. The Gaussian blur setting was adjusted from 2–8 depending on image contrast. Cell images taken every 30 min were analyzed. Cell outlines were measured using ImageJ to quantify perimeter, area, centroid, circularity (4π*area/perimeter^2), and maximum span or so-called Feret diameter. The cell centroid was subsequently used to calculate speed of migration and overall cell displacement. To analyze the changes in astrocyte migratory and morphological behaviors, measurements from the first (4 h post-seeding) and last (24 h post-seeding) observations were compared and reported as initial and final parameters, respectively.

Astrocytes were divided into three categories based on the composition of the underlying substrate. For controls, the cells were cultured on uniform LN (n=15) or AGG (n=6) substrates. Astrocytes that attached with some portion of their cell body on the gradient area over the culture period were identified as gradient cells (n=8). Cells that landed on the extreme end of the gradient where

there were no printed patches were presented with a binary surface of a full 50 μm wide stripe of laminin flanked by full aggrecan regions. Such cells were classified as binary footprint cells (n=6). The size of the binary regions varied slightly with each sample, but covered around the first 100 μm of the stamped pattern. Data were tested for statistical significance using an ANOVA with a Tukey-HSD post-hoc test (α=0.05).

4.3.5. Assessment of Protein Preference

To determine how astrocytes migrate and shift their locations with respect to the underlying AGG/LN pattern, the fluorescence intensities of the areas underneath the cells with printed AGG (Alexa Fluor 594 labeled) and unlabeled LN patterns were compiled into histograms. Histograms that showed two distinct fluorescence intensity peaks; one for AGG, and the other for unlabeled LN, over the course of culture were used for analysis (n=7). The heights of the two histogram peaks were measured at 5 h intervals to track changes in substrate composition below individual astrocytes over time.

4.4. Results

4.4.1. Dot gradient templates successfully transferred AGG/LN gradients to glass substrates

AGG/LN dot gradients were successfully transferred to glass using microcontact printing methods. Observation of the AGG/LN dot gradients after their transfer to glass substrates revealed that small features surrounded by high

density of the other macromolecule were often lost compared to the design template (Fig. 4.1A,B). This made the printed gradient steeper than originally designed and also resulted in areas near each end of the gradient with uniform surface coverage of LN or AGG. For morphological analyses, astrocytes on the uniform AGG end or bounding regions that never encountered LN were grouped with cells cultured on uniform AGG coatings. Cells which encountered the µm-sized patches along the gradient were classified as cells on the gradient. The remaining category for astrocytes included cells that interfaced with the uniform LN end of the gradient but also adhered to the AGG area surrounding the gradient (so-called binary cells) (Fig. 4.1C–E).

4.4.2. Astrocytes exhibit stellate morphology during early attachment on LN

During initial attachment within 30 min of seeding on control surfaces with uniform LN coatings, astrocytes first extended long processes followed by retraction and spreading of the cell body (Fig. 4.2). Due to the latency required to determine astrocyte locations on gradient patterns, this early spreading behavior could not be observed on gradients. On uniform AGG substrates, however, cells maintained more active processes over the entire culture time (Fig. 4.3).

4.4.3. AGG/LN dot gradients cause astrocytes to increase process extension length

Astrocytes on uniform LN were more evenly amoeboid than cells on the other types of substrates and attained the smallest average perimeters while having similar cell areas. Average perimeters on LN remained unchanged between initial and final observations. Similarly, astrocyte footprint areas on LN surfaces were little changed (Fig. 4.4A,B). Astrocytes had similar sizes on uniform AGG vs. on gradient patterns both at initial and final observations, but cells on these two substrates doubled in size over the course of the experiment.

The presence of μm-sized patches of LN in the AGG gradients caused the astrocytes to extend processes such that the perimeter of these cells was higher than on any other surface type at both the initial and final time points. In addition, the cells on AGG/LN gradients also had a significant 25% increase in average perimeter over the time of the study while maintaining a significantly less circular morphology compared to cells on control LN substrates (Fig. 4.4C). Astrocytes on AGG and binary regions had similar perimeters that were smaller than those for gradients but were approximately 30% larger than those on uniform LN controls at the final time point. Astrocytes on substrates other than LN were less amoeboid in general. Astrocytes processes appeared to attach to μm-sized patches of LN and some astrocytes at the binary footprint location extended a process along the 5 μm wide gap of LN between gradient patterns.

Astrocyte spreading resulted with an average span of around 65 μm after initial attachment on all substrates (Fig. 4.4D). However, over the next 20 h,

astrocyte spans on uniform LN controls remained largely unchanged, while astrocytes on uniform AGG had a significant increase in span over that time. Astrocytes attached on gradient areas and binary footprint locations had an even larger increase in maximum span to an average around 150 μm, but were not significantly different from each other. Both pattern types (gradient and binary) caused astrocytes to have a span nearly double that of cells on uniform LN substrates. The span for an individual cell ranged from 40 μm at the smallest and 220 μm at the largest across all samples.

4.4.4. Astrocyte migration speed largely unchanged on AGG/LN substrates

Astrocytes migrated at an average speed around 10 μm/hr on all substrate types (Fig. 4.4E). There were no discernible differences between astrocytes migration speeds at initial and final observations. Amongst all observations, astrocyte speed ranged from less than 1 to up to 120 μm/hr. There was also no significant difference in overall displacement over time of cell culture between different substrates, with cells being located on average 20–35 μm away from their initial locations (Fig. 4.4F). Distances covered by individual astrocytes ranged from 1 to over 65 μm.

4.4.5. Astrocytes prefer LN over AGG substrates

When the fluorescence intensity below each cell was presented in a form of a histogram (Fig. 4.5A, insert), the magnitude of the AGG peaks was found to decrease over culture time, while the LN peak magnitudes showed an opposite

trend (Fig. 4.5A). These changes in the substrate composition below the attached cells illustrate how the cells that encountered both AGG and LN at some point preferentially moved their cell bodies onto LN areas by the end of the culture period (Fig. 4.5B). This behavior consisted of an initial preference of cellular extensions toward LN followed by an eventual shift of the cell body. Astrocytes which initially encountered no LN patches extended process in all directions until LN was contacted and then preferential extension and shifting occurred toward LN at later time points.

4.5. Discussion

4.5.1. Astrocytes extend processes not seen on uniform, adhesive culture substrates

While alignment of astrocytes on substrates patterned with ECM molecules has been well documented[20,37], much less is known about how astrocytes interact with substrates containing composite permissive and inhibitory ECM molecular cues. One rationale for deciphering responses of astrocytes to such complex environments is to find whether there is a causal relationship between astrocyte morphology and migration and presented molecular cues. Although astrocyte morphology cannot be used a direct indicator of their reactivity, especially at the CNS injury site[5], it is interesting to note that astrocytes on standard culture substrates, such as tissue-culture polystyrene, polylysine or laminin, exhibit a more amoeboid morphology than what is found in the CNS. The observation of the initial spreading of astrocytes in a stellate

fashion here indicates that the presence of the uniformly adhesive substrate causes astrocytes to change shape over the course of several h (Fig. 4.2). Astrocytes presented with the μm-sized patches of AGG and LN in this study showed the greatest amount of process extension, as evidenced by their large perimeters (Fig. 4.4). Although altering morphology of astrocytes from amoeboid to stellate on topographically organized substrates has been show to decrease several markers for reactivity[22,23], it remains uncertain if the use of discretely patterned substrates would also influence astrocyte culture reactivity. An assessment of GFAP or CSPG expression of the more stellate astrocyte cultures observed in the present study could provide further insight for the relationship between morphology and reactivity. If patterns are effective at reducing astrocyte reactivity, they may be incorporated with other approaches that provide less reactive and more quiescent astrocyte cultures, such as with 3D gels and various alternative ECM substrates[39,40].

4.5.2. Astrocytes are capable of sampling between large distances

The present measurements indicate that astrocytes were able to sample immobilized ECM molecules separated by as many as 150 μm. The greatest extensions for these cells were triggered by the presence of mixed molecular cues within the AGG/LN gradient. When presented with mixed substrate choices for attachment, the astrocyte may be extending processes farther as a means to “find” a more suitable ECM component for its final location. In the case of a less preferable substrate like AGG, the spans and perimeters of astrocytes were

higher than for LN, suggesting an attempt to find more permissive areas (Figs. 4.3, 4.4). It is also possible that this difference in behavior is due to a subset of cells that were more prone to adhesion onto AGG and were also more likely to extend processes and avoid ameboid spreading. However, astrocytes on LN also initially extended process as aforementioned, and astrocytes that encountered both AGG and LN appeared to maintain spreading behavior on LN and not on AGG (Fig. 4.1E). Additionally, previous evidence indicates overall astrocyte adhesion is not influenced by the presence of adhesion peptides inspired by LN or FN compared to plain glass[41], and that substrate stiffness is a larger contributor to astrocyte attachment than LN availability[42]. Therefore multiple, mixed cues within the cellular span may augment astrocyte extension and sampling of substrate-bound cues compared to uniformly coated substrates (Fig. 4.4).

Previous studies of the effect that varying stripe widths and spacings have on confluent layers of astrocytes determined that the best astrocyte alignment occurred with 50 μm stripes of laminin, with 17 μm spacing between them[43]. We previously have effectively applied 15 μm stripes as well[20]. Both of these values are well within the range of astrocyte span found here. Similar values ranging from 100 to 150 μm for longest astrocyte length have been reported for cultures on polylysine and silk fibroin fibers[44]. Astrocytes grown on fibronectin-coated polylactic acid fibers for 4 days were measured to extend processes around 50 μm on random fibers and around 200 μm on aligned fibers[45], indicating that restricting the available attachment points to the microfibers may

extend astrocyte growth even farther than patterns. Therefore, by providing contrasting locations for cellular attachment, astrocytes will extend processes farther. This response could be leveraged to increase astrocyte extension onto and sampling of a material by a modifying its surface to contain both permissive and inhibitory molecules.

4.5.3. Astrocytes shift cell bodies onto LN areas, but displacement and speed remain low

Astrocytes prefer to be attached to LN areas over regions of AGG (Fig. 4.5). In the context of glial scar formation, the upregulation of CSPG expression which is present at the site of CNS injury may impede astrocyte infiltration into the site. CSPG inhibits supportive PNS Schwann cell migration[30]. Substrates with regions rich in LN would promote astrocytes to preferentially attach. This effect, however, would be highly localized. Even though astrocytes were capable of moving large distances during the experiment, most cells vacillated around a given position where they had initially adhered. The speed of individual cells measured here (Fig. 4.4E) corresponded with the speed of 9 μm/hr for populations of astrocytes migrating through cortex in vivo and to speeds of mostly 10-20 μm/hr for layers of astrocytes closing a scratch wound in vitro[7,13]. As previously observed, astrocyte migration to the wound site is not as important as proliferation of the cells bordering the injury for neuroprotective roles[3]. The results from the present study suggest that the populating of implant surfaces with astrocytes will likely be analogous to formation of the glial scar, reliant on

astrocyte proliferation at the injury site, as opposed to recruitment of distant cells. However, the addition of LN patterns to such scaffolds could allow more astrocytes to remain attached to the scaffold and avoid their potential migration away from injury-induced aggrecan.

4.6. Conclusions

Random dot gradients were created to investigate how astrocytes sample and migrate on surface protein patterns containing mixed adhesion cues. Astrocytes extend processes in a stellate fashion upon initial attachment and maintain extensions as evidenced by increased area and perimeter when presented with AGG but not with LN alone. Astrocytes do not migrate large distances after initial attachment, though they will shift position towards higher LN concentrations versus AGG. Cellular extensions were greater when astrocytes interfaced with discrete micrometer-scale patches of LN amongst AGG spanning a distance of 150 μm. These findings indicate that presenting mixed cues on surfaces cause astrocytes to interact with larger areas of the surface, which allows astrocytes to preferentially relocate.

4.7. Acknowledgements

This work was supported by NIH Grant R01 NS057144. The authors would like to thank Brian Baker for assistance in creating stamp templates. We also thank Dr. M. Condic for valuable discussion and suggestions.

4.8. References

[1] Faulkner JR, Herrmann JE, Woo MJ, Tansey KE, Doan NB, Sofroniew MV. Reactive astrocytes protect tissue and preserve function after spinal cord injury. J Neurosci 2004;24:2143–55.

[2] Rolls A, Shechter R, Schwartz M. The bright side of the glial scar in CNS repair. Nat Rev Neurosci 2009;10:235–41. doi:10.1038/nrn2591.

[3] Wanner IB, Anderson MA, Song B, Levine J, Fernandez A, Gray-Thompson Z, et al. Glial scar borders are formed by newly proliferated, elongated astrocytes that interact to corral inflammatory and fibrotic cells via STAT3-dependent mechanisms after spinal cord injury. J Neurosci 2013;33:12870–86.

[4] Silver J, Miller JH. Regeneration beyond the glial scar. Nat Rev Neurosci 2004;5:146–56. doi:10.1038/nrn1326.

[5] Anderson MA, Ao Y, Sofroniew MV. Heterogeneity of reactive astrocytes. Astrocytes Inj Brain Gliosis Adapt Mal 2014;565:23–9. doi:10.1016/j.neulet.2013.12.030.

[6] Renault-Mihara F, Okada S, Shibata S, Nakamura M, Toyama Y, Okano H. Spinal cord injury: Emerging beneficial role of reactive astrocytes' migration. Int J Biochem Cell Biol 2008;40:1649–53. doi:10.1016/j.biocel.2008.03.009.

[7] Zhou HF, Lee LH-C, Lund RD. Timing and patterns of astrocyte migration from xenogeneic transplants of the cortex and corpus callosum. J Comp Neurol 1990;292:320–30. doi:10.1002/cne.902920213.

[8] Andersson C, Tytell M, Brunso-Bechtold J. Transplantation of cultured type 1 astrocyte cell suspensions into young, adult and aged rat cortex: Cell migration and survival. Int J Dev Neurosci 1993;11:555–68. doi:10.1016/0736-5748(93)90045-F.

[9] Hatton JD, Garcia R, Sangu H. Migration of grafted rat astrocytes: Dependence on source/target organ. Glia 1992;5:251–8. doi:10.1002/glia.440050403.

[10] Hatton JD, Finkelstein JP, Sang U H. Native astrocytes do not migrate de novo or after local trauma. Glia 1993;9:18–24. doi:10.1002/glia.440090104.

[11] Bardehle S, Kruger M, Buggenthin F, Schwausch J, Ninkovic J, Clevers H, et al. Live imaging of astrocyte responses to acute injury reveals selective juxtavascular proliferation. Nat Neurosci 2013;16:580–6.

[12] Benner EJ, Luciano D, Jo R, Abdi K, Paez-Gonzalez P, Sheng H, et al. Protective astrogenesis from the SVZ niche after injury is controlled by Notch modulator Thbs4. Nature 2013;497:369–73.

[13] Környei Z, Czirók A, Vicsek T, Madarász E. Proliferative and migratory responses of astrocytes to in vitro injury. J Neurosci Res 2000;61:421–9. doi:10.1002/1097-4547(20000815)61:4<421::AID-JNR8>3.0.CO;2-4.

[14] Peng H, Shah W, Holland P, Carbonetto S. Integrins and dystroglycan regulate astrocyte wound healing: The integrin β1 subunit is necessary for process extension and orienting the microtubular network. Dev Neurobiol 2008;68:559–74. doi:10.1002/dneu.20593.

[15] Faber-Elman A, Solomon A, Abraham JA, Marikovsky M, Schwartz M. Involvement of wound-associated factors in rat brain astrocyte migratory response to axonal injury: in vitro simulation. J Clin Invest 1996;97:162.

[16] Davies SJA, Shih C-H, Noble M, Mayer-Proschel M, Davies JE, Proschel C. Transplantation of Specific Human Astrocytes Promotes Functional Recovery after Spinal Cord Injury. PLoS ONE 2011;6:e17328. doi:10.1371/journal.pone.0017328.

[17] Han S, Wang B, Jin W, Xiao Z, Chen B, Xiao H, et al. The collagen scaffold with collagen binding BDNF enhances functional recovery by facilitating peripheral nerve infiltrating and ingrowth in canine complete spinal cord transection. Spinal Cord 2014;52:867–73.

[18] Hurtado A, Cregg JM, Wang HB, Wendell DF, Oudega M, Gilbert RJ, et al. Robust CNS regeneration after complete spinal cord transection using aligned poly-l-lactic acid microfibers. Biomaterials 2011;32:6068–79. doi:10.1016/j.biomaterials.2011.05.006.

[19] East E, de Oliveira DB, Golding JP, Phillips JB. Alignment of astrocytes increases neuronal growth in three-dimensional collagen gels and is maintained following plastic compression to form a spinal cord repair conduit. Tissue Eng Part A 2010;16:3173–84.

[20] Meng F, Hlady V, Tresco PA. Inducing alignment in astrocyte tissue constructs by surface ligands patterned on biomaterials. Biomaterials 2012;33:1323–35. doi:10.1016/j.biomaterials.2011.10.034.

[21] Alexander JK, Fuss B, Colello RJ. Electric field-induced astrocyte alignment directs neurite outgrowth. Neuron Glia Biol 2006;2:93–103. doi:10.1017/S1740925X0600010X.

[22] Liu T, Houle JD, Xu J, Chan BP, Chew SY. Nanofibrous collagen nerve conduits for spinal cord repair. Tissue Eng Part A 2012;18:1057–66.

[23] Lau CL, Kovacevic M, Tingleff TS, Forsythe JS, Cate HS, Merlo D, et al. 3D Electrospun scaffolds promote a cytotrophic phenotype of cultured primary astrocytes. J Neurochem 2014;130:215–26. doi:10.1111/jnc.12702.

[24] Hsiao TW, Tresco PA, Hlady V. Astrocytes alignment and reactivity on collagen hydrogels patterned with ECM proteins. Biomaterials 2015;39:124–30. doi:10.1016/j.biomaterials.2014.10.062.

[25] Mai J, Fok L, Gao H, Zhang X, Poo M. Axon Initiation and Growth Cone Turning on Bound Protein Gradients. J Neurosci 2009;29:7450–8. doi:10.1523/JNEUROSCI.1121-09.2009.

[26] Tom VJ, Steinmetz MP, Miller JH, Doller CM, Silver J. Studies on the development and behavior of the dystrophic growth cone, the hallmark of regeneration failure, in an in vitro model of the glial scar and after spinal cord injury. J Neurosci 2004;24:6531–9.

[27] Von Philipsborn AC, Lang S, Loeschinger J, Bernard A, David C, Lehnert D, et al. Growth cone navigation in substrate-bound ephrin gradients. Development 2006;133:2487–95. doi:10.1242/dev.02412.

[28] Fricke R, Zentis PD, Rajappa LT, Hofmann B, Banzet M, Offenhäusser A, et al. Axon guidance of rat cortical neurons by microcontact printed gradients. Biomaterials 2011;32:2070–6. doi:10.1016/j.biomaterials.2010.11.036.

[29] Kuboyama T, Luo X, Park K, Blackmore MG, Tojima T, Tohda C, et al. Paxillin phosphorylation counteracts proteoglycan-mediated inhibition of axon regeneration. Exp Neurol 2013;248:157–69. doi:10.1016/j.expneurol.2013.06.011.

[30] Afshari FT, Kwok JC, White L, Fawcett JW. Schwann cell migration is integrin-dependent and inhibited by astrocyte-produced aggrecan. Glia 2010;58:857–69. doi:10.1002/glia.20970.

[31] Eichinger CD, Hsiao TW, Hlady V. Multiprotein Microcontact Printing with Micrometer Resolution. Langmuir 2011;28:2238–43. doi:10.1021/la2039202.

[32] Von Philipsborn AC, Lang S, Bernard A, Loeschinger J, David C, Lehnert D, et al. Microcontact printing of axon guidance molecules for generation of graded patterns. Nat Protoc 2006;1:1322–8. doi:10.1038/nprot.2006.251.

[33] Hodgkinson GN, Tresco PA, Hlady V. The influence of sub-micron inhibitory clusters on growth cone substratum attachments and CD44 expression. Biomaterials 2008;29:4227–35.

[34] Hodgkinson GN, Tresco PA, Hlady V. The role of well-defined patterned substrata on the regeneration of DRG neuron pathfinding and integrin expression dynamics using chondroitin sulfate proteoglycans. Biomaterials 2012;33:4288–97. doi:10.1016/j.biomaterials.2012.02.046.

[35] McCarthy KD, de Vellis J. Preparation of separate astroglial and oligodendroglial cell cultures from rat cerebral tissue. J Cell Biol 1980;85:890–902. doi:10.1083/jcb.85.3.890.

[36] Bottenstein JE, Sato GH. Growth of a rat neuroblastoma cell line in serum-free supplemented medium. Proc Natl Acad Sci 1979;76:514–7.

[37] Hsiao T, Swarup V, Eichinger C, Hlady V. Cell Substrate Patterning with Glycosaminoglycans to Study Their Biological Roles in the Central Nervous System. In: Balagurunathan K, Nakato H, Desai UR, editors. Glycosaminoglycans, vol. 1229, Springer New York; 2015, p. 457–67.

[38] Delgado-Gonzalo R, Unser M. Spline-based framework for interactive segmentation in biomedical imaging. IRBM 2013;34:235–43. doi:10.1016/j.irbm.2013.04.002.

[39] Placone AL, McGuiggan PM, Bergles DE, Guerrero-Cazares H, Quiñones-Hinojosa A, Searson PC. Human astrocytes develop physiological morphology and remain quiescent in a novel 3D matrix. Biomaterials 2015;42:134–43. doi:10.1016/j.biomaterials.2014.11.046.

[40] Levy AF, Zayats M, Guerrero-Cazares H, Quiñones-Hinojosa A, Searson PC. Influence of Basement Membrane Proteins and Endothelial Cell-Derived Factors on the Morphology of Human Fetal-Derived Astrocytes in 2D. PloS One 2014;9:e92165.

[41] Kam L, Shain W, Turner JN, Bizios R. Selective adhesion of astrocytes to surfaces modified with immobilized peptides. Biomaterials 2002;23:511–5. doi:10.1016/S0142-9612(01)00133-8.

[42] Georges PC, Miller WJ, Meaney DF, Sawyer ES, Janmey PA. Matrices with Compliance Comparable to that of Brain Tissue Select Neuronal over Glial Growth in Mixed Cortical Cultures. Biophys J 2006;90:3012–8. doi:10.1529/biophysj.105.073114.

[43] Kofron C, Hoffman-Kim D. Optimization by Response Surface Methodology of Confluent and Aligned Cellular Monolayers for Nerve Guidance. Cell Mol Bioeng 2009;2:554–72. doi:10.1007/s12195-009-0087-1.

[44] Qu J, Wang D, Wang H, Dong Y, Zhang F, Zuo B, et al. Electrospun silk fibroin nanofibers in different diameters support neurite outgrowth and promote astrocyte migration. J Biomed Mater Res A 2013;101A:2667–78. doi:10.1002/jbm.a.34551.

[45] Zuidema JM, Hyzinski-García MC, Van Vlasselaer K, Zaccor NW, Plopper GE, Mongin AA, et al. Enhanced GLT-1 mediated glutamate uptake and migration of primary astrocytes directed by fibronectin-coated electrospun poly-l-lactic acid fibers. Biomaterials 2014;35:1439–49. doi:10.1016/j.biomaterials.2013.10.079.

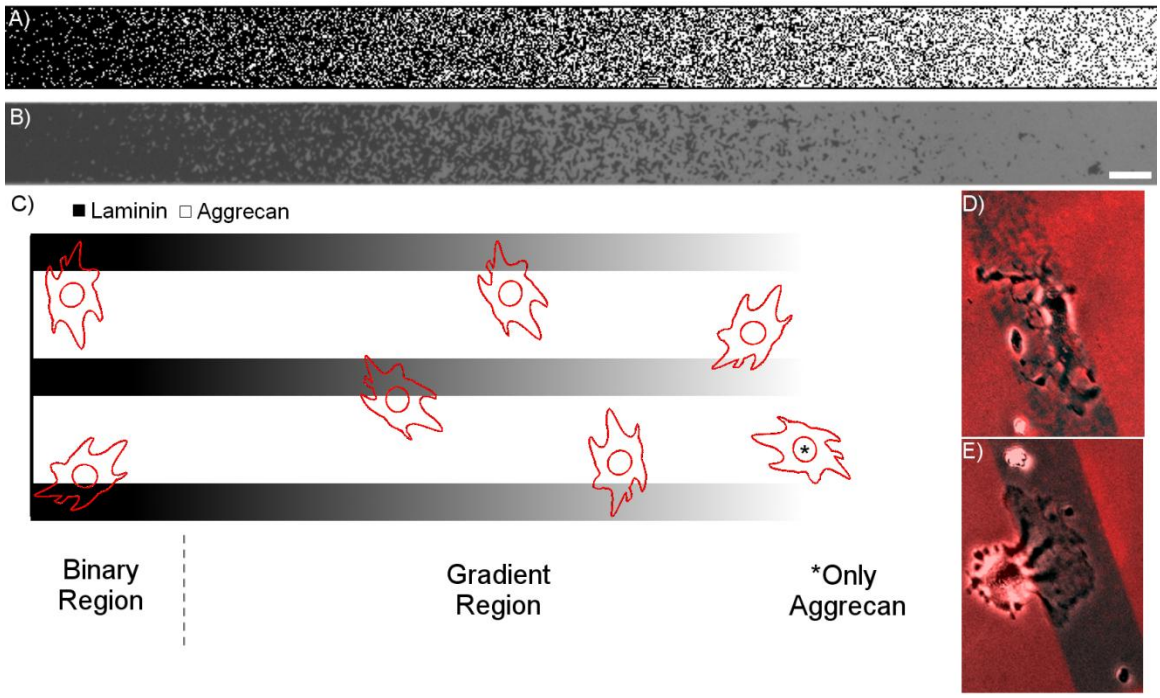

Figure 4.1. Dot gradient pattern transfer and definitions of different regions. A) Computer-generated dot gradient template and subsequently fabricated polymeric stamp led to B) transferred fluorescent pattern onto glass. Scale bar = 25 µm. C) Schematic of astrocyte characterization based on interaction with gradient patterns. Astrocytes in binary footprint regions did not encounter µm-sized patterns. Cells which encountered only aggrecan were grouped in analysis with astrocytes cultured on uniform aggrecan controls. Representative images of astrocytes interacting with AGG/LN gradient and binary footprint regions are shown in panels D and E, respectively.

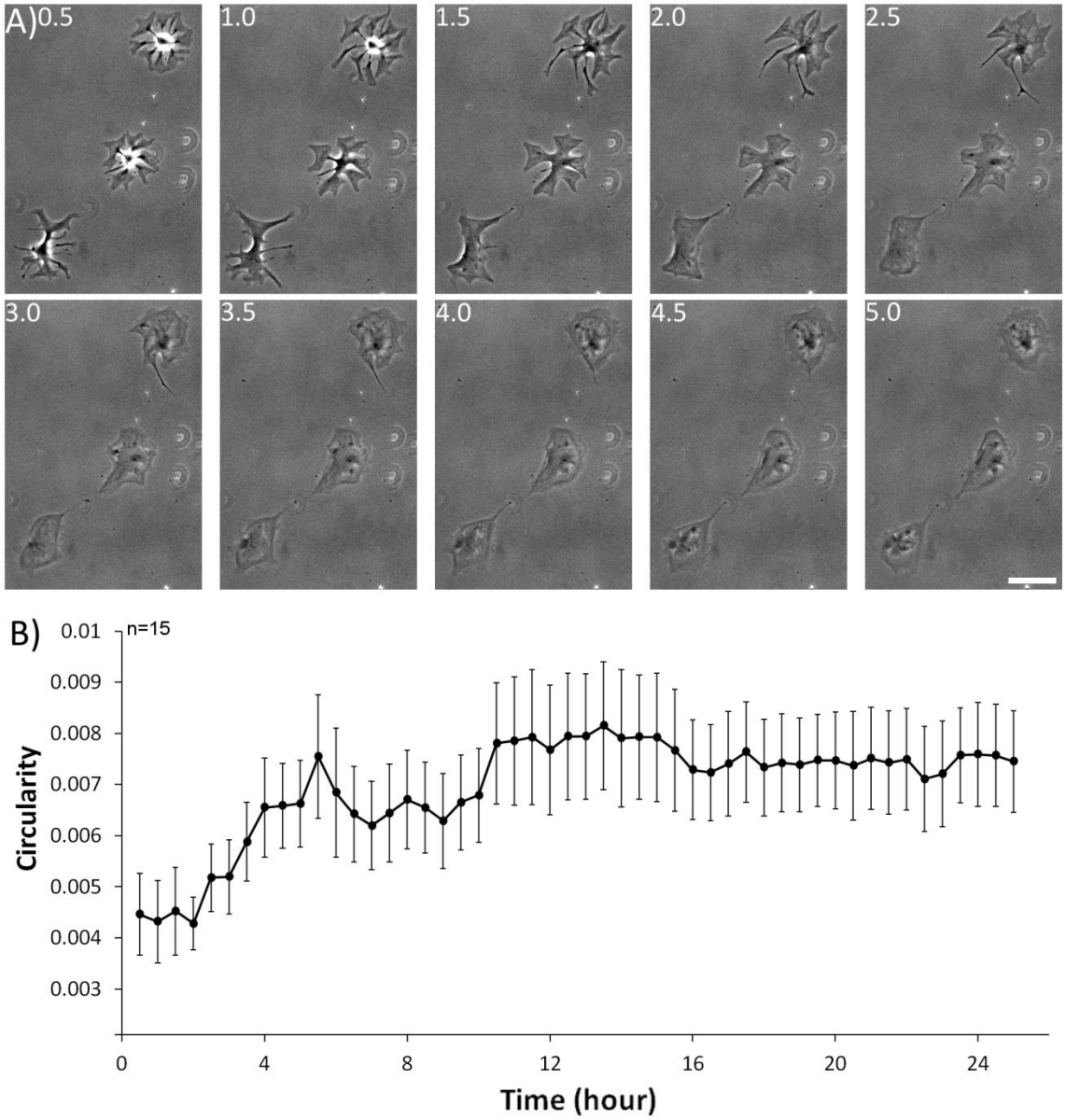

Figure 4.2. Initial stellate spreading of astrocytes on uniform LN–coated substrate is observed prior to final amoeboid morphology. A) Representative image of three astrocytes during the initial 5 h attachment period. Scale bar = 50 µm. B) Circularity of astrocytes on control LN substrates measured over time indicated that a period of 5 h was required to achieve stable, round morphology. Error bars indicate ± SEM.

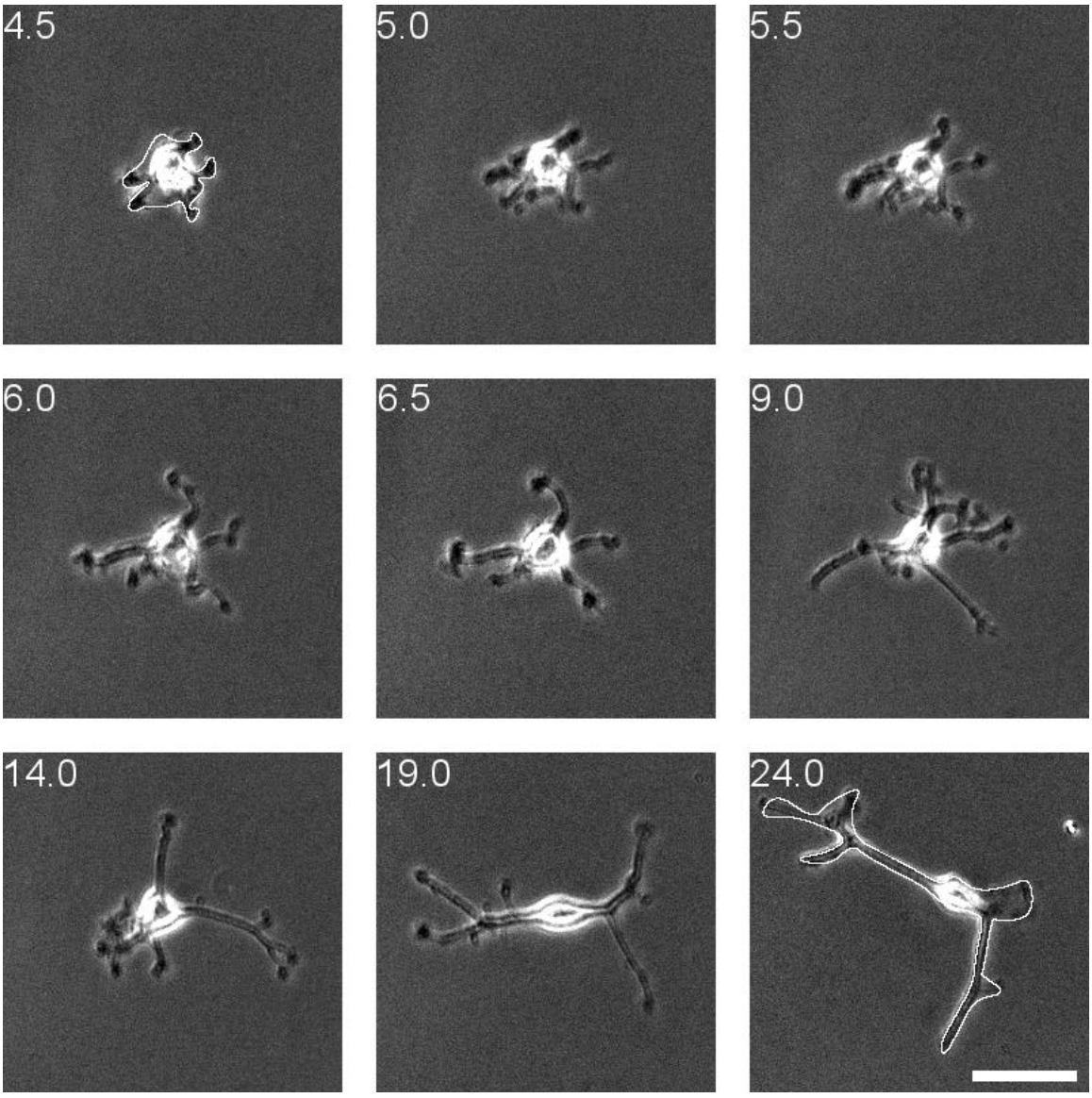

Figure 4.3. Astrocyte spreading on aggrecan surface. The progression of an astrocyte spreading on aggrecan in 0.5 h intervals. Measured outlines are shown for the 4.5 and 24.0 h timepoints only. Scale bar = 50 μm.

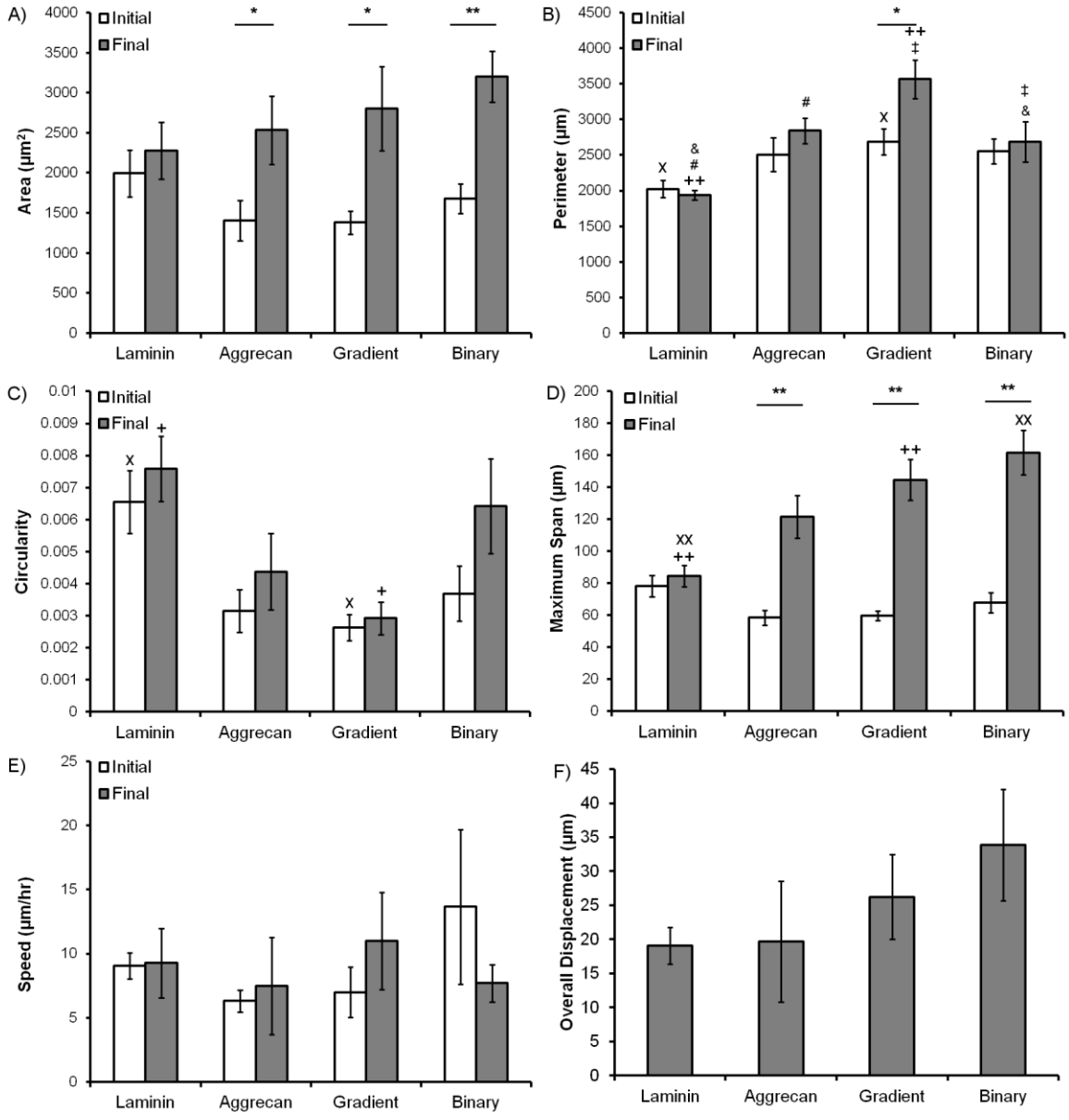

Figure 4.4. Average astrocyte morphology parameters on various substrates. A) Area, B) perimeter, and C) circularity of cells at initial and final observations. D) Maximum span, E) speed, and F) overall displacement from initial attachment location for astrocytes on the given pattern regions and uniform surfaces. Statistically significant differences over time are indicated (* = $p<0.05$; ** = $p<0.005$) and significant differences between substrates are indicated by matching symbols (x, +, ‡, & = $p<0.05$; xx, ++ = $p<0.005$). Error bars indicate ± SEM.

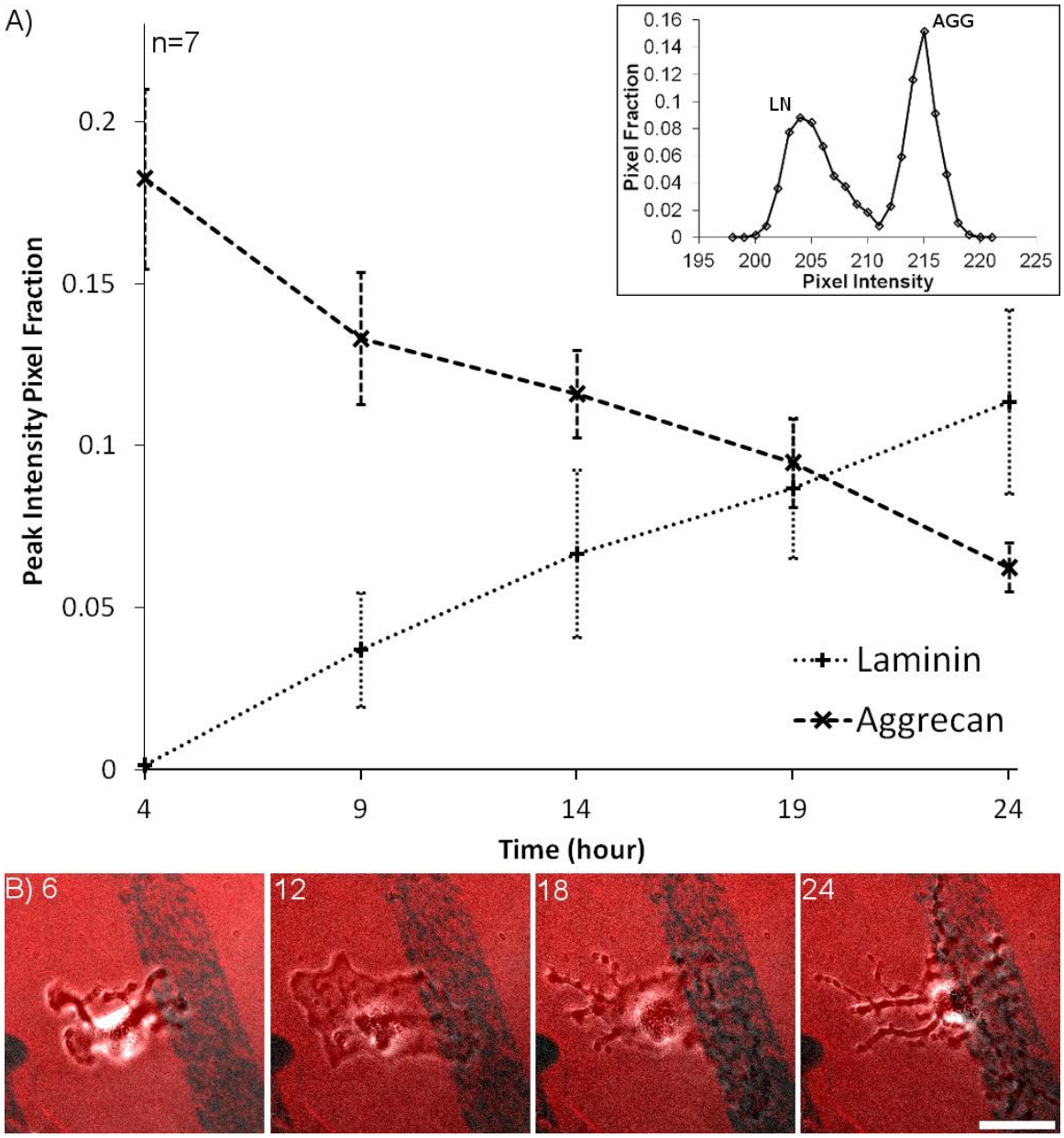

Figure 4.5. A) Astrocyte adhesion footprint shows preference for LN over time. Representative histogram (inset) shows two peaks corresponding to LN and AGG covered by an astrocyte footprint at the 14 h time point. The fraction of pixels of the imaged cell at peak florescent intensities for LN and AGG tracked in 5 h intervals over time. Error bars indicate ± SEM. B) Astrocyte shifting to gradient pattern 6, 12, 18 and 24 h post seeding. Scale bar = 50 µm.

CHAPTER 5

SUMMARY, DISCUSSION, AND FUTURE DIRECTIONS

5.1. Summary and Discussion

Spinal cord injury remains a challenging clinical problem with bleak prospects for recovery. Towards combating this problem, nerve guidance devices have been extensively developed for research use. Such devices can provide sustained guidance and support of neurons as they attempt to regrow during the chronic phases of recovery (after acute and secondary inflammation have passed). Because reactive astrocytes will be present and interface with these devices after implantation, I investigated how surface protein patterns influence astrocyte expression of CSPG and morphology. From this work, my findings contribute further understanding of astrocyte behavior on substrates with protein patterns and provide a novel method for imparting directional information to NGC material surfaces.

In Chapter 2, I employed microcontact printing of various densities of FBG to understand how astrocytes respond to adsorbed FBG on surfaces. The impetus for this study arose from two key factors: all implants are coated with FBG after contacting blood and soluble FBG triggers production of neuron

inhibitory CSPGs by astrocytes. Astrocytes specifically removed only FBG over a period of around 1.5 h after an initial attachment period of 4 h and did so while leaving other proteins behind. CSPG expression was also established as a quantitative tool for comparing astrocyte reactivity in this study. While much of produced CSPG is shed from cell surfaces, cell-associated CSPG was reduced when astrocytes were treated with a small molecule inhibitor of TGF-β type I activin receptor-like kinase receptors. No dose dependence based on FBG exposure was found; however, CSPG expression was demonstrated to occur at the FBG presenting interface. The lack of dose dependence may arise due to astrocytes already being in a reactive state in culture conditions, perhaps as a result of being on rigid substrates or the presence of albumin and other serum molecules. Changes in surface density of FBG may be too subtle compared to these other activation signals. Comparing adsorbed FBG to surface-linked FBG in future work would be interesting to test if the availability of FBG for uptake versus FBG-membrane binding events causes a change in CSPG production. The present results demonstrated that FBG was removed, but there was no obvious evidence of uptake within the astrocytes themselves. With respect to NGC design, these results indicates that, if astrocytes in vivo behave like these in vitro cells, the presence of FBG on the surface will not cause an overall increase in CSPG production by astrocytes, and the FBG stimulus will be removed within a period of h after recognition by astrocytes. This suggests that prevention of FBG binding may not be a determining design concern for reducing astrocyte reactivity. Concurrent treatment of TGF-signal inhibiting molecules would be

more effective at diminishing CSPG production. These studies also indicate that surface patterns of adsorbed proteins may be subjected to removal by astrocytes. Therefore, any device designed to maintain effective, continuing surface patterns must mitigate the removal by astrocytes.

Directional alignment of astrocytes has been effective at increasing neuronal outgrowth in vitro. Several aligning methods have been translated to NGC materials and devices. Directional surface protein patterns had yet to be tested on NGC materials, so I developed a method for transferring them to collagen gels. The technique relies on BS3, a bifunctional crosslinker, to facilitate binding of proteins to the surface of collagen. By peeling already printed patterns off of glass, the difficulties of directly printing a gel were circumvented. The objective for Chapter 3 was to verify if such patterns on collagen made any changes to astrocyte CSPG expression. Stripe patterns of AGG, FBG, FN and LN were tested. Astrocytes attached to all surfaces, and aligned to some degree on the patterns. Cells on FBG were the most aligned, followed by LN and FN. However, astrocytes on AGG had the least alignment, but they were still more aligned than cells on plain collagen. It is possible that the alignment efficacy was not only a result of the patterned stripes, but rather in response to altered binding of serum available or cell-secreted molecules. Likewise, astrocytes could prefer collagen and the effect of the patterns would be to delineate regions of available collagen. Such effects would also create directional patterns for astrocytes to align to, albeit made of different molecules than what was applied. The fact that astrocytes also align on striped glass with the same printed molecules suggests

that the stripes themselves are providing directional cues, and not the masking of available collagen. Likewise the limited alignment in AGG-striped collagen samples indicates that the periodic masking of collagen is less effective in causing astrocyte alignment. Astrocytes aligned on FBG and LN expressed half as much CSPG as cells on collagen alone. In all cases, the transferred patterns resisted modification and removal by astrocytes over the course of 4 days in culture. These results indicate that while directionality corresponds with reduced CSPG production in some cases, this relationship is not straightforward in all cases. Surprisingly, astrocytes on AGG also had around a one-third decrease in CSPG production, although cellular alignment was less pronounced, and FN stripes did not impact CSPG expression although cells were aligned by FN. To improve on this work, it would be interesting to pattern the same ECM compounds in either random dots or a grid-like pattern on collagen to observe how removing directionality impacts CSPG expression. I would hypothesize that alignment would be reduced and that CSPG production would not be decreased except for patterns with AGG that, as previously mentioned, reduced CSPG without extreme alignment. The gels tested here were of relatively high concentration of collagen and are likely even stiffer after crosslinker application. In the future, more dilute and less rigid gels may need to be patterned using alternative approaches such as freeze-drying and rehydrating. Another potential tool would be to pattern temperature-responsive polymer surfaces while in a hydrophilic state and then drive the surface to become more hydrophobic with temperature to facilitate softer hydrogel release.

In Chapter 4, my goal was to gain insight on astrocyte morphology and migration as they attached to patterned surfaces. Because previous astrocyte alignment studies relied on artificially chosen patterns, it would be helpful to obtain measurements of astrocytes as they interacted with surfaces to inform future pattern designs. Similarly, most previous studies relied on observation of astrocyte orientation after they had established confluent monolayers, as in Chapter 3. By imaging quickly after seeding, individual cell movements can be more readily resolved and the influence of intercellular contacts can be limited. In addition to uniform surfaces of AGG and LN, astrocytes were also seeded onto random dot gradients of AGG/LN to assess substrate preference and were observed in real time using time-lapse microscopy. An unanticipated finding was the early stellate spreading of astrocytes on uniform LN, which parallels morphology in the CNS but is in stark contrast with the classic amoeboid astrocyte appearance in long-term astrocyte cultures. This behavior is not easily captured without this early attachment imaging. Astrocytes appear primed to make multiple, separate surface attachments, but this behavior is lost in the presence of uniformly adhesive signals. On uniform aggrecan printed on adsorbed laminin, astrocytes maintained more spindly morphologies. This is perhaps from selective attachment to LN molecules that might be available through the AGG layer or from limited adhesion to AGG itself. Astrocytes on dot gradients of mixed AGG/LN cues maintained a greater level of process extension and had the largest spans (around 150 μm). This appears to be due to astrocytes binding to available LN from amongst the AGG as evidenced by the ends of

cellular processes residing on LN patches. Astrocytes on all surfaces moved at a rate around 10 μm/h, but they tended to migrate locally around initial adhesion locations as overall displacement was of about 30 μm over the course of 20 h. I anticipated most cells on uniform surfaces would have little motivation to migrate, but astrocytes with a directional gradient did not travel far either. This may be due to astrocytes already finding a sufficient level of LN for attachment, thus negating the need to find more. Inverted gradients of LN stamped on AGG were created as well but not quantified. Qualitative observations showed that astrocytes remained on the flanking regions of full LN and avoided attachment to the mixed AGG/LN gradient region. This further indicates that once astrocytes have encountered LN, they will prefer those locations over any containing AGG. It is also possible that the limited migration is a function of cell density, but this seems unlikely as scratched astrocyte layers with contact-mediated signaling also close cell layer gaps with leading edges moving at similar rates. Future time-lapse studies on stripes of varying widths and spacings would provide helpful size references for stripe designs. Establishing pattern features that maximized the rate of alignment or shifting to adhesion molecules could provide a more rapid response from device interfacing cells. Although from gradient patterns, the present measurements provide feature dimensions that estimate maximum cellular reach and insight that mixed cues trigger increased cellular investigation of surface patterns.

The results from these chapters together indicate that, while not all patterns will alter astrocyte behavior, the placement of ECM molecules can

impact astrocyte CSPG reactivity. In designing guidance devices, there are multiple stimuli strategies to alter astrocyte response, including soluble and topographical approaches. Within the scope of the in vitro systems used, surface patterned stripes of LN and FBG which align astrocyte layers are effective at reducing their expression of neuron inhibitory CSPG, and such patterns can be patterned to collagen hydrogels. While FBG leakage into the CNS may trigger astrcoyte reactivity, its presence on surfaces is not the determining factor for CSPG production in cultured sparse astrocytes as they are concurrently presented with rigid surfaces and serum proteins. To enhance astrocyte exploration of surface patterns, mixed adhesive cues may be more effective at triggering individual cellular extensions. Unfortunately, the present work provides no clear cellular mechanisms for the observed behavior. It does, however, provide promising perspectives towards reducing astrocyte CSPG reactivity and adds an engineering tool for translating the advances in surface patterning technologies to NGC materials. As astrocytes in the glial scar play a determinant role in neuronal inhibition at wound sites, attenuating their negative impacts may bring new treatment options for those suffering from debilitating CNS injuries.

5.2. Future Directions

5.2.1. Macrophage response to patterned materials

Macrophages and microglia play key roles in causing inflammation leading to secondary injury after SCI. These cells also demonstrate neuroprotective behaviors. In an effort to reconcile these contrasting functions, researchers have

pointed to activation pathways as an important factor in altering macrophage behavior[1]. The M1, classically activated, and M2, alternatively activated, classifications have corresponded with damaging and protective influences, respectively. By predisposing macrophages at the wound site to express more beneficial roles, secondary tissue loss may be diminished which may lead to improved outcomes for SCI. Since the patterned materials developed in Chapter 3 reduced the CSPG expression in astrocytes, it would be interesting to see if these patterns could also reduce macrophage and microglia reactivity, either alone or in concert with astrocytes. Similar to astrocyte studies, it has been demonstrated that macrophage reactivity can be modulated with topographical signals provided by PLA micro- and nanofibers. When compared to being cultured on PLA films, macrophages on fibers produced lower amounts of proinflammatory cytokines and had fewer occurrences of foreign body giant cells. There was no dependence on alignment for these fibers, but narrower diameter fibers led to greater reductions in macrophage reactivity[2]. Nanofibers made with PCL, both aligned and random, were tested with human monocytes in vitro and implanted subcutaneously in rats. Initial monocyte attachment was reduced on aligned fibers compared with random and plain PCL film controls. Both nanofiber constructs led to thinner fibrous capsules in vivo compared to PCL films after 4 weeks, with random fibers having the thinnest capsules[3]. While not indicative of macrophage activation pathways, fewer macrophages could lead to less overall chemokine production at the material interface.

Less is known concerning macrophages and surface protein patterns. One study reported that macrophage migration speed increased with increasing FN surface concentrations, but no measurement of inflammatory markers was explored[4]. The stripe patterns used in this work are on the appropriate size scale, as microglia have been measured to span around 30–40 um on average depending on their level of reactivity[5]. It would be interesting to investigate if restriction of macrophage morphology via surface patterns leads to diminished attachment or reactivity. I would anticipate that macrophages and microglia cultured on ECM-striped collagen gels would express lower levels of reactivity. This is based on the observations that macrophages on fibers which showed less reactivity are also restricted by their physical environment. Likewise, as there was an effect of pattern alignment on astrocyte reactivity, similar behavior may exist in macrophages, although we lack a fundamental understanding of what mechanisms are causing these behavioral changes

Even if directional surface patterns do not cause direct reduction of macrophage and microglia reactivity, the demonstrated influence of such patterns on astrocytes could lead to diminished macrophage activity in cocultures and potentially in vivo. The reduction in astrocyte CSPG expression could also contribute to lower levels of macrophage inflammation. It has been shown that removing CSPG with systemic ChABC treatments decreases M1 macrophage prevalence as evidenced by CD68 expression and increases in the M2 marker CD206 after SCI. Importantly, IBA-1 staining indicated that overall macrophage numbers were similar with systemic treatment. These changes led to decreased

neuronal death and improved functional recovery[6]. In contrast, there is also evidence that CSPG from astrocytes in the early stages of injury helps microglia reduce production of inflammatory TNF-α and NO species[7]. As astrocyte CSPG is decreased with directional protein patterns, these cells may subsequently elicit a less inflammatory phenotype from associated macrophages. While coculture with astrocytes already creates less reactive microglia compared to microglia in monoculture[8], I would predict that microglia and macrophages cocultured with astrocytes aligned by surface patterns would have even further reductions in inflammatory markers.

5.2.2. In vivo testing of patterned devices

The patterned collagen developed in this work could be rolled or formed into a basic tube (Fig. 5.1). In vivo testing in a hemisection or transection model would be interesting to identify potential benefits of the patterns over plain collagen. However, such incremental improvements are not the ultimate goal of SCI research as partial progress still leaves patients with the debilitating symptoms of paralysis, spasticity, autonomic dysfunction and/or pain. Therefore, the combinational synergy of multiple guidance approaches would likely lead to greater improvements. A schematic of some potential synergistic approaches to reduce CSPG reactivity and improve alignment is diagramed in Fig. 5.2. A key benefit to the presently developed method is that it is compatible with many sheet-forming processes. Pattern peel-off is not compatible with multilumen constructs or extruded materials, and it is incongruent with injectable materials or

in situ gelling. However, any process where a polymer sheet or film can withstand physical manipulation to be peeled should be able to lift off a protein pattern. Depending on its application, alternative bifuntional cross linkers, such as genipin, could be substituted to bind the correct reactive groups. Likewise, placing protein patterns onto a flexible polymer such as PDMS [9,10] could facilitate sheet removal steps. Patterning of random PCL nanofibers with polylysine has been demonstrated using microcontact printing[11], and could be applied to CNS studies. Rather than utilizing a uniform coating of fibers with some protein, as was previously done[12], aligned fibers could be printed with corresponding directional stripes. This duality of guidance information could augment the directional response. As suggested by the findings in Chapter 4, the presence of multiple aligned signals may improve cellular response. I would expect that aligned fiber materials subsequently patterned with direction ECM stripes would increase both directional neuronal outgrowth and astrocyte alignment when compared to only aligned fibers or patterns alone.

To infer the impact of each signal type, directional patterns could be placed perpendicular to topographical cues provided by fibers. Such conflicting designs are also informative in providing hierarchal information concerning directional stimuli. For example, when testing PLA fibers and electrical fields, DRGs were found to extend the longest outgrowth when they were concurrently placed on fibers and influenced by a field in the same direction. Interestingly, increased outgrowth was also observed on fibers perpendicular to the electric field. Very little outgrowth, however, was aligned with the field in contradiction to

the fibers. Based on these observations, topographical cues dominate electrical stimulus for guiding neurons[13]. Therefore, the efficacy of directional stimuli should be investigated to provide clues as to what factors are most important for directional cellular growth. I think that the directionality of fibers would likely override conflicting stripe patterns, but that cells presented with such contradicting cues will grow more slowly than those with parallel directions. Additionally, with the methods developed here, similar in vitro tests should be performed to more fully understand how surface placement of popular NGC molecules, such as NGF and BDNF, may work in tandem with bulk release of the same factors from gels. I hypothesize that directional patterns of neurotrophic factors would improve guided neuronal outgrowth compared to uniformly coated surfaces or gels solely reliant on bulk release.

As mentioned earlier, invasive procedures to implant devices are not always ideal for the common contusion injuries found in human SCI, especially when some existing tissue has been spared. For those with complete transections, however, the addition of guiding structures may be beneficial. A recent human patient experienced partial sensory and motor recovery when autologous olfactory ensheathing cells were implanted into his SCI and were accompanied by autologous nerve grafts to provide directional support[14]. This is an encouraging result. No doubt the transplanted cells played an important role, but the question remains whether support structures are also vital for functional recovery. Work is also needed to understand which human patients with SCIs would benefit more from implanted NGCs than other treatments.

However, not all devices for restoring function after SCI require directional information at the tissue-device interface, such as stimulating electrodes. The demonstrated reduction in astrocyte CSPG produced by patterns could be beneficial in those and similar situations. The addition of astrogliosis-reducing patterns or coatings could lead to less inhibition of neural populations for better recording and stimulation. Existing electrode coatings include parylene-C which reduces macrophage attachment[15], and sodium alginate hydrogel which reduced macrophage and astrocyte reactivity around electrodes by acting as a cytokine sink[16]. I would expect that adding directional patterns to such gels or using collagen in a similar application would serve to reduce the activity of cells that contact the surface and maintain the diffusion sink function of the gel.

Lastly, the developed patterned collagen from this work may also find application for individuals with PNS injuries where NGCs made of type I collagen have already been approved for use by the FDA[17]. I would anticipate that the addition of directional guidance molecules to collagen NGC surfaces would provide more rapid and efficient alignment of PNS Schwann cells which would also positively impact neuronal regrowth.

5.2.3. Biomimetic surface patterns

To date, most guiding patterns have been grooves, stripes or fibers. These artificial designs have proven effective at guiding neurons and astrocytes. In native tissue, however, the cellular environment is less binary. One simple experiment to increase pattern complexity and test synergistic effects would be to

stamp multiple proteins onto glass and then transfer them to collagen. For example, the most potent reducers of CSPG expression in Chapter 3, FBG and LN, could be patterned in alternating stripes to see how it impacts alignment and whether CSPG expression was further reduced. It would also be interesting to investigate more intricate patterns to see if there are improvements on neuronal and astrocytic growth. Kofron et al. created cell-inspired topographical patterns that mimicked Schwann cells and astrocytes in PDMS. They also cast PDMS directly onto cell layers to replicate their topography and found that such surfaces were effective at guiding neuronal outgrowth[18]. Unfortunately, there were no direct comparisons with grooves to infer whether biomimetic or artificial patterns are more potent.

A similar approach may be considered for the molecular cues presented by astrocytes. Work with fixed astrocytes showed that they are capable of reducing microglia activation without active release of soluble factors, albeit to a lesser extent than their live counterparts[8]. Similarly, fixed layers of aligned astrocytes maintain surface ligands that facilitate neurite growth and extension. Astrocytes were also shown to propagate alignment signals from layer to layer of seeded cells, thus indicating that an astrocyte aligning patterned surface may subsequently align both astrocytes and neurons as tissue regrows[19]. Based on this theory, I have developed some astrocyte mimetic patterns that were inspired by astrocyte expression of CSPG and FN (Fig. 5.3 A, B). Surfaces patterned with mixed molecules could provide potential synergy as mentioned above, and an alternative to periodic patterns could be random dots of cell-inspired densities

that would help clarify the roles of molecule concentrations (Fig. 5.3C). These FN and AGG patterns qualitatively appear less effective at guiding neurons (Fig 5.3D); however, I expect they would prove more effective at orienting astrocytes. Such patterns are on the size scale of astrocyte extensions and astrocytes are less likely to migrate large distances but rather shift to more preferable pattern locations. Comparison of these patterns against both random dots and alternating stripes could reveal what types of patterns are most effective at aligning astrocytes and reducing reactivity. I anticipate that alignment would be best on stripes, but that reactivity would be further decreased on mimetic patterns. The random dots would likely lead to no alignment, so any decreases in CSPG reactivity could be attributed to the synergy of the patterned molecules. Such an approach would also be improved by a more exhaustive survey of adhesion molecules expressed on astrocyte membranes. These could be individually tested in artificial stripe assays to determine those with maximum neuronal or astrocytic guidance which would then be mapped for translation to stamps for patterning.

5.3. References

[1] David S, Kroner A. Repertoire of microglial and macrophage responses after spinal cord injury. Nat Rev Neurosci 2011;12:388–99. doi:10.1038/nrn3053.

[2] Saino E, Focarete ML, Gualandi C, Emanuele E, Cornaglia AI, Imbriani M, et al. Effect of Electrospun Fiber Diameter and Alignment on Macrophage Activation and Secretion of Proinflammatory Cytokines and Chemokines. Biomacromolecules 2011;12:1900–11. doi:10.1021/bm200248h.

[3] Cao H, Mchugh K, Chew SY, Anderson JM. The topographical effect of electrospun nanofibrous scaffolds on the in vivo and in vitro foreign body reaction. J Biomed Mater Res A 2010;93A:1151–9. doi:10.1002/jbm.a.32609.

[4] Hind LE, Mackay JL, Cox D, Hammer DA. Two-dimensional motility of a macrophage cell line on microcontact-printed fibronectin. Cytoskeleton 2014;71:542–54. doi:10.1002/cm.21191.

[5] Kurpius D, Wilson N, Fuller L, Hoffman A, Dailey ME. Early activation, motility, and homing of neonatal microglia to injured neurons does not require protein synthesis. Glia 2006;54:58–70. doi:10.1002/glia.20355.

[6] Bartus K, James ND, Didangelos A, Bosch KD, Verhaagen J, Yáñez-Muñoz RJ, et al. Large-Scale Chondroitin Sulfate Proteoglycan Digestion with Chondroitinase Gene Therapy Leads to Reduced Pathology and Modulates Macrophage Phenotype following Spinal Cord Contusion Injury. J Neurosci 2014;34:4822–36.

[7] Rolls A, Shechter R, London A, Segev Y, Jacob-Hirsch J, Amariglio N, et al. Two faces of chondroitin sulfate proteoglycan in spinal cord repair: a role in microglia/macrophage activation. PLoS Med 2008;5:e171.

[8] Alford PW, Nesmith AP, Seywerd JN, Grosberg A, Parker KK. Vascular smooth muscle contractility depends on cell shape. Integr Biol 2011;3:1063–70. doi:10.1039/C1IB00061F.

[9] Yu H, Xiong S, Tay CY, Leong WS, Tan LP. A novel and simple microcontact printing technique for tacky, soft substrates and/or complex surfaces in soft tissue engineering. Acta Biomater 2012;8:1267–72. doi:10.1016/j.actbio.2011.09.006.

[10] Giannitelli SM, Abbruzzese F, Mozetic P, De Ninno A, Businaro L, Gerardino A, et al. Surface decoration of electrospun scaffolds by microcontact printing. Asia-Pac J Chem Eng 2014:n/a – n/a. doi:10.1002/apj.1809.

[11] Zuidema JM, Hyzinski-García MC, Van Vlasselaer K, Zaccor NW, Plopper GE, Mongin AA, et al. Enhanced GLT-1 mediated glutamate uptake and migration of primary astrocytes directed by fibronectin-coated electrospun poly-l-lactic acid fibers. Biomaterials 2014;35:1439–49. doi:10.1016/j.biomaterials.2013.10.079.

[12] Koppes AN, Zaccor NW, Rivet CJ, Williams LA, Piselli JM, Gilbert RJ, et al. Neurite outgrowth on electrospun PLLA fibers is enhanced by exogenous electrical stimulation. J Neural Eng 2014;11:046002.

[13] Winslow BD, Tresco PA. Quantitative analysis of the tissue response to chronically implanted microwire electrodes in rat cortex. Biomaterials 2010;31:1558–67. doi:doi: 10.1016/j.biomaterials.2009.11.049.

[14] Skousen JL, Bridge MJ, Tresco PA. A strategy to passively reduce neuroinflammation surrounding devices implanted chronically in brain tissue by manipulating device surface permeability. Biomaterials 2015;36:33–43. doi:10.1016/j.biomaterials.2014.08.039.

[15] Tabakow P, Raisman G, Fortuna W, Czyz M, Huber J, Li D, et al. Functional regeneration of supraspinal connections in a patient with transected spinal cord following transplantation of bulbar olfactory ensheathing cells with peripheral nerve bridging 2014.

[16] Straley K, Foo C, Heilshorn S. Biomaterial design strategies for the treatment of spinal cord injuries. J Neurotrauma 2010;27:1–19.

[17] Kofron CM, Liu YT, López-Fagundo CY, Mitchel JA, Hoffman-Kim D. Neurite outgrowth at the biomimetic interface. Ann Biomed Eng 2010;38:2210–25.

[18] Tanaka J, Maeda N. Microglial ramification requires nondiffusible factors derived from astrocytes. Exp Neurol 1996;137:367–75.

[19] Meng F, Hlady V, Tresco PA. Inducing alignment in astrocyte tissue constructs by surface ligands patterned on biomaterials. Biomaterials 2012;33:1323–35. doi:10.1016/j.biomaterials.2011.10.034.

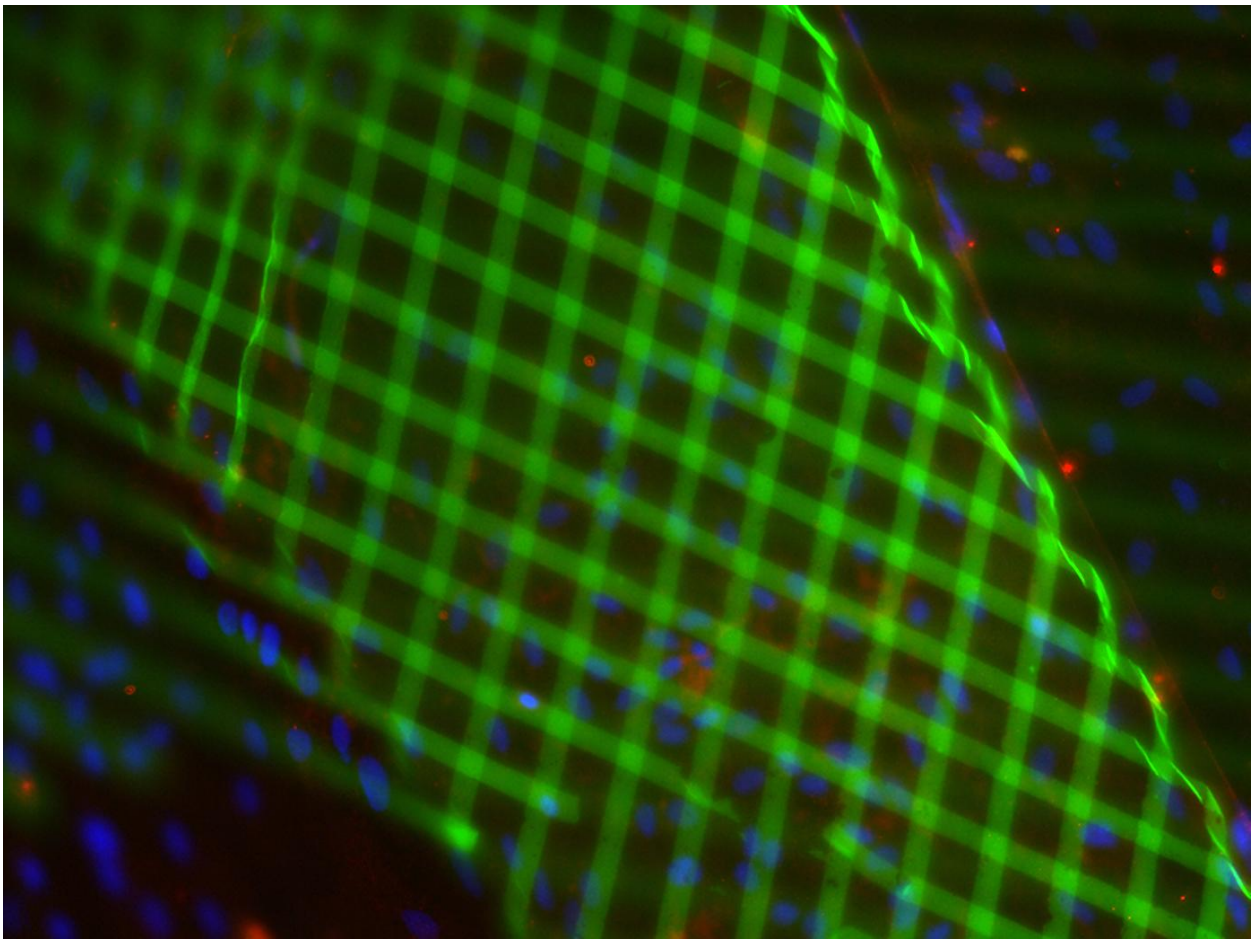

Figure 5.1. Stripe-patterned collagen rolled into a tube. Laminin stripes (15 µm wide, green) are transferred to collagen gel, which is amenable to physical manipulation. Astrocyte nuclei (blue) and CSPG (red) are visible around and on the outside of the tube.

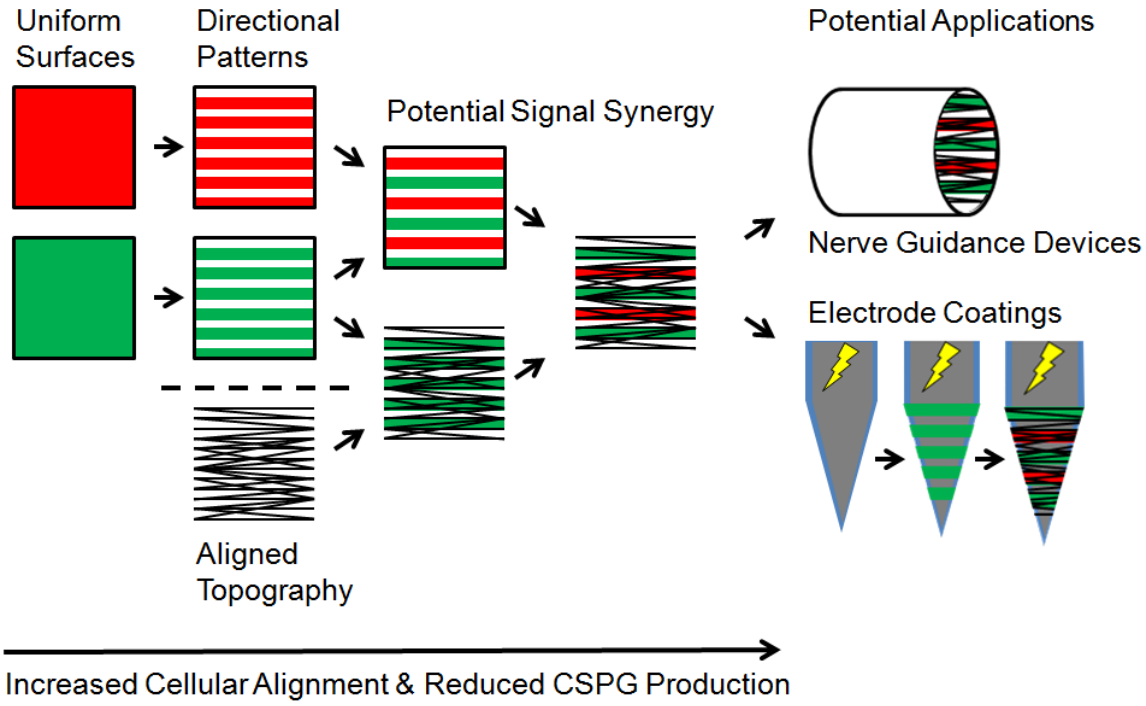

Figure 5.2. Potential benefits of directionally patterned collagen gels. Addition of patterns provides directional cues not present on uniformly coated surfaces. Multicomponent patterning and patterning in conjunction with topographical cues may provide increased alignment accompanied by reduced reactivity in surface contacting cells. Such surface properties may translate to improved outcomes for nerve guidance and signaling devices.

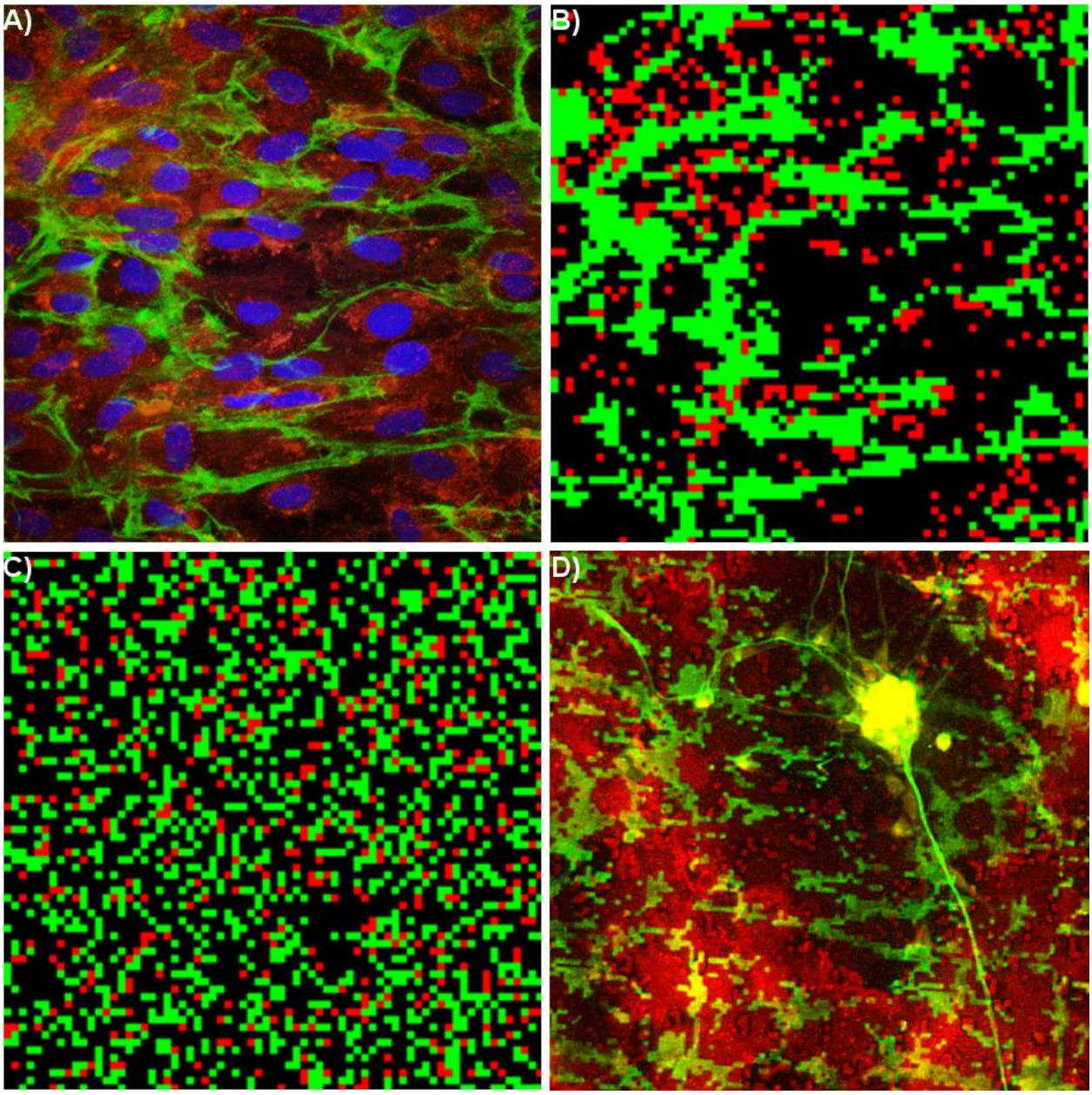

Figure 5.3. Astrocyte-based protein patterns. A) Confocal image of aligned astrocytes labeled for FN (green) and CSPG (red) expression. B) Mimetic pattern template made by thresholding and rastering cell image with minimum feature size of 3 μm. C) Random pattern template with coverage equal to mimetic design. D) DRG (green) on stamped mimetic pattern of FN (green) and AGG (red).

APPENDIX

CELL SUBSTRATE PATTERNING WITH GLYCOSAMINOGLYCANS TO STUDY THEIR BIOLOGICAL ROLES IN THE CENTRAL NERVOUS SYSTEM[*]: RANDOM DOT GRADIENT FABRICATION AND MICROCONTACT PRINTING

A.1. Methods

A.1 Printing Proteoglycan Gradients via Nonspecific Adsorption

1. Generate random pixel distributions using Mathematica (Wolfram) or similar software. In Mathematica, the commands to create a continuous dot gradient are as follow:

Cell 1 - gradientPercolation[n_, m_]:= Module[{p=0}, createRow=(p+=1/(n-1);

h[#, Table[Floor[Random[]+p],{m}]])&

Cell 2 - Apply[List, Flatten[Nest[createRow, Table[0,{m}], n-1], Infinity, h]]]

Show[Graphics[RasterArray[gradientPercolation[1000, 50]/. {0 ->RGBColor[1, 1, 1],1 - RGBColor[0,0,0]}]], AspectRatio->Automatic]

[*] Excerpt reprinted with kind permission from Springer Science+Business Media: Glycosaminoglycans, Cell Substrate Patterning with Glycosaminoglycans to Study Their Biological Roles in the Central Nervous System, vol. 1229, © 2015, pp. 457-467, Tony W. Hsiao et al.

The graphics output can then be copied as a bitmap to lithography patterning software. This command created a 50 unit wide 1,000 unit long gradient.

2. Create a photolithographic template….

3. Cast PDMS stamps … (see Note 2).

4. Adsorb PDMS stamps with proteoglycan solutions for 30 min at room temperature (r.t.) (see Note 3).

5. Rinse the stamp with water and dry with a nitrogen stream.

6. Print the proteoglycans by placing the coated stamp in conformal contact with a coverslip. Allow the stamp to remain in contact with the coverslip for 1–2 min. Carefully remove the stamp from the coverslip. Wash the stamp with detergent and water and store for reuse (see Note 4).

7. To create a pattern made of two macromolecules there are two approaches: precoating the coverslip with the first macromolecule prior to the printing of the second macromolecule, or coating (so-called back-filling) the coverslip with the second macromolecule after it was stamped with the first macromolecule. The approach chosen depends on the desired combination of molecules. For example, coverslips coated with laminin solution (100–500 μg/mL PBS) for 1 h at r.t. can be rinsed with water, dried in nitrogen, and printed with aggrecan solution to create surfaces with laminin and aggrecan-on-laminin features. Substrates with laminin and laminin-on-aggrecan features can be similarly produced by reversing the order of the two macromolecules.

A.2. Notes

1. …

2. For optimal PDMS removal from mask templates, it is best to remove the PDMS from the mask before it is fully cured and rigid. This prevents fracturing of the PDMS. Partial curing is accomplished by placing samples in a 100 °C oven for 30 min, after which the PDMS can be removed from the photoresist surface. The PDMS alone, without the mold, is then placed back into the oven and allowed to fully cure. To control for stamp thickness, the volume of PDMS mix can be adjusted.

3. To facilitate the spreading of solutions and to minimize reagent use, a sterile coverslip can be placed on top of a small volume of solution that has been applied to the top of the PDMS stamp to provide full stamp coverage. If the hydrophobicity of the PDMS is causing difficulties with adsorption of inking proteoglycans, a brief plasma treatment [17], either in oxygen or corona discharge in air, immediately before adsorption can render the surface hydrophilic, although the surface tends to revert to being hydrophobic over time.

4. After use, PDMS stamps should be sonicated in a mild detergent and rinsed with water. The stamps can be stored submerged in water or be dried and sealed in petri-dishes to avoid dust particles and contaminants from adhering to the features.

A.3. References

17. Anderson JR, Chiu DT, Wu H et al (2000) Fabrication of microfluidic systems in poly(dimethylsiloxane). Electrophoresis 21:27–40